Georgia State University
ScholarWorks @ Georgia State University

Biology Dissertations | Department of Biology

5-10-2017

Central Control Of Body Fat And Thermoregulation Through Shared And Separate Sympathetic Circuitries And Sensory Feedback

Ngoc Ly Nguyen

Follow this and additional works at: https://scholarworks.gsu.edu/biology_diss

Recommended Citation
Nguyen, Ngoc Ly, "Central Control Of Body Fat And Thermoregulation Through Shared And Separate Sympathetic Circuitries And Sensory Feedback." Dissertation, Georgia State University, 2017.
https://scholarworks.gsu.edu/biology_diss/188

This Dissertation is brought to you for free and open access by the Department of Biology at ScholarWorks @ Georgia State University. It has been accepted for inclusion in Biology Dissertations by an authorized administrator of ScholarWorks @ Georgia State University. For more information, please contact scholarworks@gsu.edu.

CENTRAL CONTROL OF BODY FAT AND THERMOREGULATION THROUGH SHARED AND SEPARATE SYMPATHETIC CIRCUITRIES AND SENSORY FEEDBACK

by

NGOC LY T. NGUYEN

Under the Directions of Timothy Bartness, PhD and Bingzhong Xue, PhD

ABSTRACT

More than 30% of the population suffers from obesity, which increases the risk of death and secondary health problems. Body fat [white adipose tissue (WAT) and brown adipose tissue (BAT)] are innervated and regulated by the sympathetic nervous system (SNS). WAT stores energy, while BAT generates heat for thermoregulation. Fat also has sensory innervations, but the roles of sensory nerves are still being elucidated. Hence, understanding the neuroanatomy of the SNS innervations of fat and the neural regulation of fat metabolism will be valuable for advancing obesity treatment. Using trans-synaptic tract tracers with unique fluorescent proteins, we defined and compared the SNS innervations of visceral fat [mesenteric WAT (MWAT)] and subcutaneous fat [inguinal WAT (IWAT)] and of IWAT and interscapular BAT (IBAT) in Siberian hamsters. MWAT and IWAT have moderately shared SNS innervations within the

hindbrain, but separate SNS innervations in rostral regions. In contrast, IWAT and IBAT have relatively separate SNS circuitries throughout the brain yet some overlap in SNS nuclei known to regulate thermogenesis. We tested for the presence of functional coordination between IWAT and IBAT defined by overlap in IWAT SNS and IBAT SNS innervations. When IBAT function was impaired by SNS denervation, IWAT SNS drive, thermogenic activity, and beige adipocyte recruitment increased in cold exposed hamsters likely through coordination with IWAT SNS pathways. Conversely, we found that only SNS drive to IWAT increased during acute food deprivation suggesting that populations of SNS neurons singly innervating each fat depot may contribute to differential SNS drive to fat. Lastly, we demonstrated that IWAT sensory nerves mediate the functional coordination between IWAT and IBAT and the regulation of SNS drive to fat. The absence of IWAT sensory feedback via sensory denervation differentially decreased SNS drive to IBAT and IWAT itself, but not to MWAT, retroperitoneal WAT, and epididymal WAT in cold exposed hamsters. Collectively, the studies in this dissertation provide neuroanatomical evidence of separate and shared SNS brain sites likely receiving sensory signaling and regulating SNS drive to fat, and direct evidence of the roles of SNS and sensory nerves innervating fat to energetic homeostasis and thermoregulation.

INDEX WORDS: White fat, Brown fat, Sympathetic drive, Norepinephrine turnover, Pseudorabies virus, Cold exposure

CENTRAL CONTROL OF BODY FAT AND THERMOREGULATION THROUGH SHARED AND SEPARATE SYMPATHETIC CIRCUITRIES AND SENSORY FEEDBACK

by

NGOC LY T. NGUYEN

A Dissertation Submitted in Partial Fulfillment of the Requirements for the Degree of

Doctor of Philosophy

in the College of Arts and Sciences

Georgia State University

2017

Copyright by
Ngoc Ly Thi Nguyen
2017

CENTRAL CONTROL OF BODY FAT AND THERMOREGULATION THROUGH SHARED AND SEPARATE SYMPATHETIC CIRCUITRIES AND SENSORY FEEDBACK

by

NGOC LY T. NGUYEN

Committee Chair: Bingzhong Xue

Committee: Aaron Roseberry

Ruth Harris (Augusta University)

Electronic Version Approved:

Office of Graduate Studies

College of Arts and Sciences

Georgia State University

May 2017

DEDICATION

To loved ones, who have supported and encouraged me during my pursuit of this doctorate degree. Despite the obstacles and disappointments I have encountered, your love and prayers have given me strength to persevere.

ACKNOWLEDGEMENTS

I thank my mentor, Dr. Timothy Bartness, for sharing his time and immense knowledge with me and guiding me throughout my undergraduate and graduate studies. I am utmost grateful for his unfailing support and the moments we had spent discussing science and life. I am appreciative of Dr. Bingzhong Xue for her advisement and support after Dr. Bartness passed and am thankful for her willingness, enthusiasm, and availability. I am especially grateful to my dissertation committee members, Dr. Ruth Harris and Dr. Aaron Roseberry for their time, support, expert guidance, insights, and patience throughout this process – thank you.

I thank past and present Bartness lab members/friends for their support, encouragement, and technical assistance in particular, Dr. Vitaly Ryu, Sierra Williams, Alex Thomas, Dr. Johnny Garretson, Mary Schneider, Dr. Laura Szymanski, Dr. Chris Ehlen, Dr. Cheryl Vaughan, Candace Barr, Yaakov Mitchell, Yang Liu, Vaibhav Maheswari, Fardowsa Robow, Ben Blaschke, Keegan Murphy, Jennifer Mendez, Shasmine Kelly, Eleen Zarebidaki, Bianca Lester, and Daniel Vizcaino. You all have made this process more memorable and enjoyable. I also thank Dr. Xue and Dr. Hang Shi's lab members for their kindness and technical assistance, in particular, Dr. Qiang Cao, Dr. Xin Cui, Dr. Emily Bruggeman, and Fenfen Li.

I am appreciative of Dr. Dabney Dixon, Dr. Kyla Ross, Kathy Rockwell, Dr. Kavita Oommen, Dr. Rebekah Chapman, Dr. Paul Ulrich, Dr. Jeremiah Harden, and Dr. Vincent Rehder for their kindness and continued support and advice. Lastly, I thank Georgia State University for awarding me the 2CI Obesity Reversal Fellowship that has funded my graduate career and the NIH grants awarded to Dr. Bartness for financial support of my dissertation.

TABLE OF CONTENTS

LIST OF TABLES

LIST OF FIGURES

1 INTRODUCTION

1.1 Obesity, the growing epidemic

The incidence of obesity has significantly increased since initial surveys of body mass index several decades ago (53, 84). In 1962, approximately 13 percent of adults were obese and 1 percent were morbidly obese (38, 83). This had grown by 2014, where 31 percent of adults were obese and 5% were morbidly obese (38, 83). Obesity increases risk of death and secondary health problems, such as cardiovascular diseases, hypertension, diabetes mellitus, and stroke (1, 35, 79). It also increases the chances for digestive and liver diseases and colorectal cancer (79). Diet and exercise are commonly proposed treatments for weight loss and are successful for some individuals, but for most do not yield long-term results (41). Presently, there are only five medications for obesity treatment on the market (7). In 1999, the FDA approved the first drug, and 13 years later only approved two more drugs for obesity treatment. In 2014, two additional investigated products were permitted to go on the market. Thus, it is clear that discovery of efficacious and safe medications for weight loss is a long process.

In general, the storage of triacylglycerol and the presence of fat tissues are necessary for homeostasis and survival in mammals including humans, but when there is an over accumulation of fat as in the case of obesity, it becomes detrimental and produces negative effects. The breakdown of fat, lipolysis, can occur through a variety of different processes some of which are circulating hormones (62, 65, 90, 94), but the principal mechanism for lipolysis is through the sympathetic nervous system (SNS) innervation of fat and its release of norepinephrine (NE) (10, 57, 60). For example, *in vitro* data showed epinephrine robustly increases lipolysis in adipocytes (90). However, this was not the case *in vivo* when the adrenal medulla (the source of epinephrine) was removed, lipolysis induced by food deprivation was not prevented (28, 82, 113,

115). Similarly, glucagon stimulates fat breakdown in isolated adipocytes (64-66), but infusion of glucagon into human fat tissue through *in situ* microdialysis did not increase lipolysis (15, 50). The denervation of SNS nerves innervating fat completely blocked lipolysis, which clearly reveals that the SNS is the primary regulator of the hydrolysis of triacylglycerols (8, 9, 12).

Hence, more understanding and knowledge of the central nervous system (CNS) control of fat metabolism and specifically the neuroanatomy of where this SNS innervation takes place will be valuable to discovering optimal target sites (brain sites or population of neurons) for advancing obesity medications. This dissertation aims to investigate the central regions of shared and separate sympathetic outflow to pairs of different fat depots, the pattern of SNS drive across fat pads, and the contribution of fat sensory nerves to the maintenance of energy balance and thermoregulation in the Siberian hamster (*Phodopus sungorus*). This will ultimately deepen the understanding of adipose biology and the neural control of fat regulation.

1.2 The Siberian hamster animal model

Many studies place emphasis on investigating the etiology of obesity and its possible resolution by genetically manipulating genes associated with obesity or the breakdown of fat using mice and rats. Although these studies provide immense knowledge (23), utilizing animal models of natural obesity would be applicable to humans since genetic mutation accounts for less than 5 percent of obesity in people (34). In addition, genetic manipulation to increase lipolysis or energy expenditure often requires a single gene or double gene deletion, which is currently not feasible as a remedy for human obesity. By focusing on animal models that become obese due to environmental influences similar to humans, the reversal of weight gain is a possible reality.

Furthermore, it is advantageous to study the process of natural weight loss rather than ones of genetic manipulations.

Siberian hamsters are an ideal animal model for investigating obesity and its reversal. Unlike rats and mice, they naturally mobilize their fat tissues by interpreting environmental signals of day length (14, 36, 71). More specifically, only a change in photoperiod while keeping all other factors constant can cause severe obesity in Siberian hamsters (14), which decreases potential confounding factors associated with other obesity inducing manipulations. Siberian hamsters housed in long day photoperiod (16 hour light: 8 hour dark) accumulate up to 50% body mass as body fat (14), which would be considered morbidly obese in humans. In short day photoperiod (8 hour light: 16 hour dark), however, they increase mobilization of their fat depots and effortlessly decrease their fat mass to as low as 20% of body mass (14). Thus, these hamsters are a convenient and natural animal model to study the induction and maintenance of obesity and its reversal. Furthermore, the majority of studies investigating the neural innervation of fat have been done using this species (10, 11, 13).

A potential caveat to the use of Siberian hamsters is that although they experience morbid obesity and decreased energy expenditure comparable to humans, unlike humans and other rodent models, they are not insulin resistant nor hyperglycemic (69). Nevertheless, this difference may be worthwhile to investigate since the negative effects of obesity is predominantly due to the emergence of secondary health problems, such as diabetes mellitus and insulin intolerance, which these hamsters are able to avoid despite their massive weight gain.

1.3 Fat depots and their locations

Fat is located in discrete depots across the body and have disparate roles (10, 13, 114). Two widely documented types of fat are white adipose tissue (WAT) and brown adipose tissue

(BAT) (10, 11, 13). WAT is found beneath the skin [inguinal WAT (IWAT)] and within the peritoneal cavity [epididymal WAT (EWAT), retroperitoneal WAT (RWAT), and mesenteric WAT (MWAT)] (Fig. 1.1) (114). Although all WAT store excess triacylglycerols, each WAT depot, in particular visceral and subcutaneous WAT, has a different impact on overall health and energy balance partly due to its anatomical location and likely SNS regulation. Lower body subcutaneous WAT such as IWAT is associated with having protective properties against diabetes and cardiovascular disease (70, 119), because of its preferential storage of free fatty acids and very low-density lipoprotein triglycerides. Consequently, this would prevent ectopic lipid storage in important tissues such as the liver and muscle (42, 72). Conversely, MWAT, a visceral fat depot attached to the intestines, stomach, and pancreas, is regarded as a contributing factor to the metabolic syndrome, because of its high levels of basal lipolysis and drainage into the hepatic portal vein (46). When visceral fat is substantially decreased, the severity of obesity related comorbidities is reduced (56, 86). Given the opposing physiological effects and relevance of 'healthy' subcutaneous WAT (IWAT) and 'harmful' visceral WAT (MWAT), it is unknown whether there are shared or highly separate SNS innervations between these two depots to coordinate or influence their functions. EWAT, found around the testes, and RWAT, located against the back of the peritoneal cavity, are intra-abdominal fat tissues that drain into the vena cava (22).

By contrast, BAT depots are located subcutaneously in the supraclavicular and interscapular regions and within the thoracic cavity (pericardial and para-aortic areas) and perirenal region of the peritoneal cavity (19) (Fig. 1.1). Interscapular BAT (IBAT) is the largest and best-defined BAT in rodent models (19). Investigators have reported the presence of brown-like adipocytes within IWAT, EWAT, and RWAT primarily after SNS activation (Fig. 1.1).

These BAT-like adipocytes are termed ‘brite’ (88) or ‘beige’ (55) cells, because they have both WAT and BAT morphology (26, 68, 121). Here we will use the ‘beige’ terminology. BAT and beige adipocytes primarily maintain body temperature in response to thermoregulatory demands (19, 101). Activation of BAT, in particular, is associated with an increase in total energy expenditure (85).

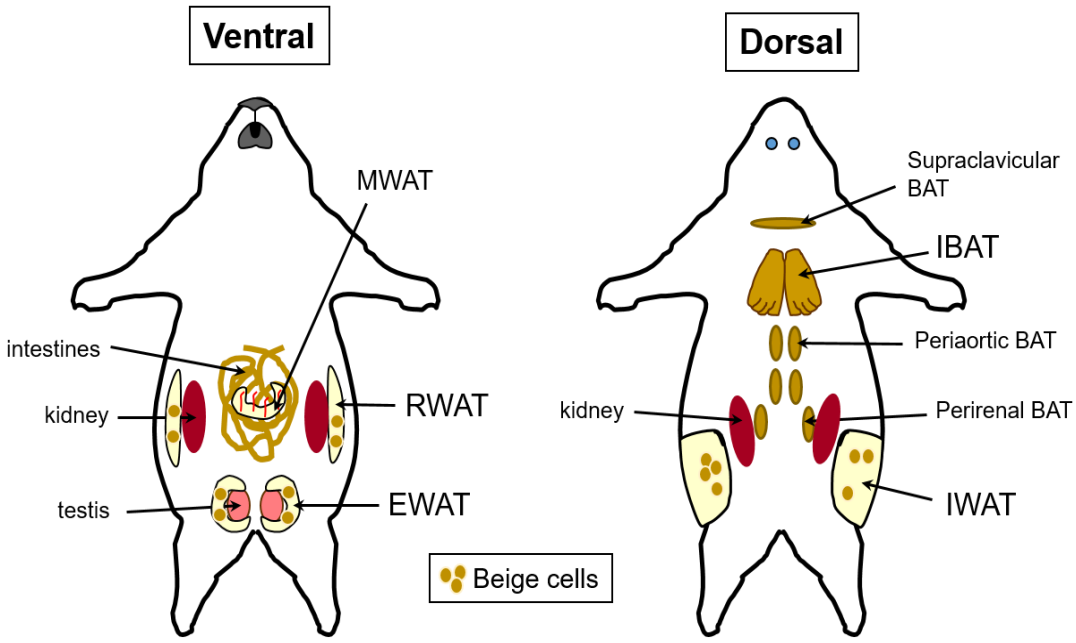

Figure 1.1 Location of fat depots in rodent models.
Schematic depicting the subcutaneous and intra-abdominal locations of white adipose tissue (WAT) and brown adipose tissue (BAT) depots. Mesenteric WAT (MWAT); Retroperitoneal WAT (RWAT); Epididymal WAT (EWAT); Interscapular BAT (IBAT); Inguinal WAT (IWAT). Beige adipocytes are depicted as small, brown circles found in WAT depots.

1.4 The SNS regulation of fat

The SNS is the principal regulator of body fat (10, 11, 13). In times of energy deficit or challenges, the SNS initiates lipolysis. In brief, NE released from SNS postganglionic nerve terminals act as an agonist on adipocyte membrane bound, β adrenergic receptors (βAR) (89) to activate downstream lipolytic enzymes (61) that will hydrolyze stored triacylglycerols. Although BAT and beige adipocytes also undergo lipolysis, they primarily oxidize lipids during β

oxidation and express uncoupling protein 1 (UCP1), which uncouples oxidative phosphorylation and generates heat in a process called nonshivering thermogenesis (19). Because BAT and beige adipocytes robustly oxidize lipids, investigators are exploring ways to increase the activation of these tissues in order to decrease fat mass. In terms of function, when SNS nerves are denervated either surgically or chemically, lipolysis and nonshivering thermogenesis are blocked in WAT depots and IBAT, respectively (20, 28, 32, 51, 73).

Studies using NE turnover (NETO), a direct and dynamic neurochemical measure of SNS activity in fat, revealed the presence of differential SNS drive to fat tissues, which likely influence their function (118). SNS drive to WAT depots and IBAT were measured within the same hamsters given energy challenges of cold exposure, food deprivation, or glucoprivation (18, 44). IWAT NETO was increased in response to all energy challenges, whereas EWAT NETO was particularly unaffected by glucoprivation (18). RWAT NETO was unchanged by acute food deprivation (18). SNS drive to MWAT for these energy challenges, however, is unknown, because MWAT NETO was not measured in these studies. IBAT NETO distinctively remained unchanged during energy deficit *i.e.*, food deprivation and glucoprivation, but significantly increased during cold exposure (18, 44). The presence of differential SNS drive to fat tissues has also been shown in rats and mice (52, 78, 87). The SNS drive to beige adipocytes has not been measured, because likely the isolation of beige adipocytes from WAT is difficult making it unable to reliably extract NE for NETO calculations.

1.5 The emerging role of fat sensory nerves

Sensory nerves innervate body fat, but their functional roles in energy balance are still being elucidated. It is thought that WAT sensory nerves possibly mediate the neural communication among fat depots to maintain energy balance by communicating the status of

energy availability to the CNS. This was suspected when bilateral SNS denervation of either EWAT or IWAT by 6-hydroxydopamine (6OHDA), a neurotoxic compound that destroys noradrenergic neurons, significantly reduced SNS drive to intact fat tissues including IBAT (52), which may be due to a change in EWAT or IWAT sensory input. Data suggest that WAT sensory nerves use leptin, a WAT adipokine that promotes negative energy balance (43, 77), or lipolytic products such as free fatty acids and glycerol to signal energy status (45). Microinjections of leptin into IWAT increased IWAT sensory nerve activity and cFos labeling in the dorsal root ganglia (DRG) (77). The perception that WAT sensory nerves 'sense' lipolysis was supported when glucoprivation not only increased WAT SNS activity and lipolysis (18), but also increased WAT sensory nerve activity (109). Therefore, the existence of non-uniform SNS outflow to different fat tissues and maintenance of energy balance may likely be mediated by WAT afferents providing sensory feedback to the CNS. This explicit role of WAT sensory nerves, however, has not been investigated.

1.6 Central neural circuits to and from fat

The existence of diverse fat tissues and the presence of beige adipocytes raise the question of how fat depots coordinate their functions *i.e.*, lipolysis and nonshivering thermogenesis to maintain overall homeostasis during energy challenges. In order to understand the underlying mechanism behind the functional coordination between different fat depots, compelling evidence of its SNS and sensory innervations are needed. Fat is innervated by the projections of SNS postganglionic neurons from the sympathetic trunk. In contrast, its sensory innervations arise from pseudounipolar neurons of the DRG, which have two processes, one that extends to fat to receive sensory information and one that extends to the dorsal horn of the spinal cord to transmit information.

Current knowledge regarding the SNS and sensory innervations of fat was acquired by neuroanatomical tract tracing, which is a technique that defines synaptic connections between two neurons or an entire chain of neurons (59). The concept of tract tracing is based on the mechanism of macromolecule transport by live neurons (59). In brief, neurons can take up macromolecules at their axon terminals through receptor mediated uptake or vesicular endocytosis (59). When these macromolecules are transported to the soma, it is called retrograde transport (59). However, when macromolecules are taken up by the dendrites and soma and are transported to the axon terminal, it is called anterograde transport (59). Thus, there are two categories of tract tracers, retrograde and anterograde tracers, which are advantageous to use in order to label efferent or afferent nerves selectively and to verify the presence of neural innervation.

Tract tracing has been invaluable to defining the neural communication between fat and the CNS. Classical monosynaptic tract tracers such as Fluoro-Gold and true blue label connections across only one synapse (59) and were initially used to label the SNS and sensory innervations of fat (37, 122). The development of viral trans-synaptic tracers, pseudorabies virus (PRV) and herpes simplex virus-1 (HSV-1) (16, 21, 107), propelled the progression of neuroanatomy studies by making it possible to define entire, hierarchical neural circuits respectively to and from peripheral tissues including muscle (96), pancreas (67), stomach (92, 93), gonads (47, 63), and fat (4, 5, 109, 117). PRV bind to viral attachment protein molecules and are endocytosed at axon terminal membranes (33). Then, they are retrogradely transported to the soma for replication and moved to the dendrites to infect presynaptic neurons (33). HSV-1, however, are taken up by the soma and replicate prior to being transported to the axon terminal, where they infect postsynaptic neurons (33).

1.6.1 SNS NERVES TO FAT

Labeling from monosynaptic tract tracers supported previous observations (30, 31, 91, 104, 120) of the neural innervation of fat from electron microscopy images and directly verified it at the level of the SNS ganglia. Microinjections of Fluoro-Gold, a retrograde tracer, into IWAT revealed labeling within the SNS ganglia (122). Furthermore, microinjections of DiI, an anterograde tracer, into the SNS ganglia labeled SNS nerves innervating adipocytes within IWAT (122), which unambiguously confirmed the SNS innervations of fat. In addition to rodent models, the distribution of SNS postganglionic neurons innervating WAT specifically IWAT, RWAT, and MWAT were also defined in domestic swine (27).

Unlike monosynaptic tracers, PRV identified the central origins of SNS outflow to fat. In several independent studies investigating WAT and BAT SNS innervations, microinjections of PRV into WAT depots or IBAT labeled the central origins of SNS outflow circuits ultimately innervating those tissues (4, 5, 17, 106, 108, 110). PRV labeling was specific to SNS nerves within fat as demonstrated by the absence of PRV labeling when SNS nerves to WAT were chemically denervated by 6OHDA (49). The absence of PRV labeling after SNS denervation also confirmed that fat only has SNS innervations and not parasympathetic (PSNS) ones (49). This was further supported when typical PSNS neurochemical markers, such as vasoactive intestinal peptide, neuronal nitric oxide synthase, and vesicular acetylcholine transporter, were absent in many WAT pads in rats, mice, and hamsters (49).

Across separate studies documenting the origins of SNS outflow to fat specifically IWAT, EWAT, RWAT, and IBAT, there were certain brain sites that were frequently labeled (4, 5, 17, 106, 108, 110). Common areas in the hindbrain are the nucleus of the solitary tract (Sol), rostroventral lateral medulla, gigantocellular regions, noradrenergic group A5, raphe, and

reticular regions. The periaqueductal gray (PAG) is consistently labeled in the midbrain, while the paraventricular, dorsomedial, and lateral hypothalamic nuclei and medial preoptic area (MPA) are regularly defined in the forebrain. These labeled SNS nuclei are known to be involved in the control of thermogenesis (29, 74, 75) and lipolysis (24, 25, 58). For example, direct projections between the raphe region and the MPA have been shown to regulate SNS outflow to IBAT, body temperature, and fever response (76). Other PRV labeled SNS nuclei are known to regulate the control of fat metabolism, food intake, and body mass (3, 25, 40, 116), in addition to contributing to general SNS drive to the periphery (100, 112). For instance, lesions in the paraventricular nucleus of the hypothalamus (PVH) lead to an increase fat accumulation (40), while NE injections into the dorsomedial hypothalamus (DMH) increase plasma free fatty acids and decrease triacylglycerols (125). Among these independent results establishing the SNS circuitries to WAT depots and IBAT, the presence of frequently labeled SNS brain sites found between two different WAT pads and between WAT and BAT strongly suggest the possibility of an overlap in the central origins of SNS outflow circuits to these fat tissues for probable functional coordination during times of energetic demands.

1.6.2 SENSORY NERVES FROM FAT

The sensory innervation of fat was initially implicated by the labeling of sensory nerve associated peptides, such as substance P and calcitonin gene related peptide, in neural fibers innervating fat (39, 48, 54, 103). The sensory innervation of fat was directly revealed when microinjections of true blue, an anterograde monosynaptic tracer, into IWAT resulted in labeling of first order sensory neurons in the DRG (37). Two decades later, the entire sensory projections from fat depots to the brain were independently defined when the H129 strain of HSV-1 was injected into either WAT depots or IBAT (109, 117). H129 labeling is specific to sensory nerves

within fat as shown by the absence of labeled cells when H129 was placed on top of fat tissues instead of local microinjections intra-fat (97, 109). Labeling of afferent projections from WAT depots and IBAT was notably present in the same nuclei as the origins of SNS outflow to fat (109, 117). The pattern of general overlap in PRV labeling of SNS neurons to fat and H129 labeling of sensory neurons from fat suggest the existence of sensory and SNS feedback loops.

1.6.3 INNERVATION OF BEIGE ADIPOCYTES

Unlike WAT and BAT, the SNS and sensory innervation of beige adipocytes is largely unknown (11) and what is known has been inferred from WAT and BAT neuroanatomical studies. Given the overlap in SNS and sensory labeling among fat depots, it is likely that beige adipocytes also have the same central origins of SNS outflow and nuclei receiving sensory feedback.

1.6.4 NEUROANATOMICAL EVIDENCE OF NEURAL CROSSTALK

1.6.4.1 SNS CROSSTALK BETWEEN FAT DEPOTS

The creation of isogenic strains of PRV with unique (green or red) fluorescent reporter protein (6, 105) allows for the labeling of separate and more importantly shared neural circuitries projecting to two different peripheral tissues. For example, isogenic strains of PRV microinjected into the liver and EWAT labeled shared autonomic neurons in the PVH projecting to both metabolically active tissues (111). This study, however, did not control for virulence between the two isogenic strains of PRV and tissue specific differences in viral uptake, which likely contributed to the low proportions of doubly labeled neurons (111). Isogenic strains of PRV were also used to test for sexual dimorphism in SNS innervations of abdominal fat (RWAT) and subcutaneous fat (IWAT) in male and female rats (2). It was found that male rats have more SNS neurons projecting to RWAT, while female rats have more SNS neurons to IWAT (2). These

studies, however, did not extensively document and quantify the level of innervations. Also in both instances, investigators performed phenotyping of PRV labeled neurons by immunostaining (111) or PCR (2), but a caveat to the interpretation of those data is that the viruses corrupt native mRNA machinery within neurons they infect and replace it with viral RNAs (124). Thus, measurement or labeling of proteins other than the fluorescent reporter protein may not reflect the true phenotype. Besides these investigations, isogenic strains of PRV have not been used to label the central origins of SNS outflow to physiologically relevant pairs of fat depots such as true visceral fat (MWAT) and subcutaneous fat (IWAT) or WAT and BAT.

1.6.4.2 SNS AND SENSORY CROSSTALK WITHIN AND BETWEEN FAT DEPOTS

Microinjections of both PRV and H129 into either IWAT (97) or IBAT (98) indeed confirmed the existence of a SNS and sensory crosstalk. Doubly labeled sensory and SNS neurons were found across the brain in nuclei known to regulate lipolysis and nonshivering thermogenesis (97, 98). The presence of colocalized sensory and SNS neurons establish the neuroanatomical reality of bidirectional communication from fat (WAT depots or IBAT) and the CNS. Furthermore, when PRV and H129 were microinjected into IBAT and IWAT, respectively, SNS and sensory crosstalk between IBAT and IWAT was discovered (99). Doubly labeled sensory neurons from IWAT and SNS neurons to IBAT were present throughout the neuroaxis (99), revealing the existence of central neurons that receive sensory signaling from WAT to perhaps influence the SNS drive to IBAT and other WAT depots. Overall, the combinatorial usage of PRV and H129 provides an advantageous method for labeling of SNS and sensory circuits to and from one or two different fat depots.

1.7 Neural communication among fat depots via SNS and sensory crosstalk

Denervation studies have provided tremendous insight into the neural communication among distant and discrete fat depots likely through central sensory and SNS circuitries that were labeled by H129 and PRV, respectively. For example, unilateral denervation of SNS nerves to EWAT by 6OHDA blocked peripheral leptin induced decrease in fat mass not only in the contralateral EWAT, but also IWAT and RWAT (95). This attenuation of leptin induced decrease in fat mass likely resulted from a change in sensory input from EWAT sensory nerves to central brain regions regulating SNS outflow to other WAT depots perhaps to preserve fat stores since SNS denervation blocks lipid mobilization (123). This modification of SNS drive to WAT depots was also seen when SNS nerves to IWAT or EWAT were bilaterally denervated (52).

A recent study from our laboratory functionally tested the signaling between IWAT sensory and IBAT SNS circuitries that was neuroanatomically defined by microinjections of H129 and PRV into IWAT and IBAT, respectively (99). Microinjections of CL316,243, a βAR agonist, into IWAT initiated lipolysis in IWAT and interestingly increased both IWAT sensory nerve activity and IBAT temperature (45). This response was absent when IWAT sensory nerves were surgically denervated (45). The study, however, did not selectively target IWAT afferents and examined the response in conscious animals given a cold challenge. Nevertheless, previous data implicate the involvement of WAT sensory nerves in IBAT thermogenic activity when microinjections of leptin into EWAT stimulated its afferent activity and consequently increased IBAT SNS nerve activity (80, 81). In addition, WAT and BAT coordination was observed in a lipectomy model, where bilateral EWAT lipectomy nearly abolished IBAT NETO (102).

1.8 Dissertation goals

This dissertation targets the neuroanatomical existence of central SNS neurons that are innervating different fat tissues and the necessity of SNS and sensory nerves innervating fat to maintain energetic homeostasis and thermoregulation. Our overarching research question for this dissertation is: are there central SNS neurons that are shared among different WAT depots and IBAT that can influence SNS drive patterns and coordinate lipolysis and thermoregulation, and are WAT afferents necessary to facilitate these processes and regulate SNS drive to WAT depots and IBAT? It is hypothesized that there are CNS nuclei comprising shared SNS outflow to different WAT depots and IBAT to possibly coordinate their functions and that WAT sensory nerves likely feedback to central origins of SNS outflow to facilitate this communication among discrete fat tissues.

The goals of this dissertation focused on testing for convergent SNS outflow circuits to IWAT (subcutaneous fat) and MWAT (visceral fat) and to IBAT and IWAT to obtain insight into the neuroanatomy of the SNS innervations of subcutaneous and visceral fat and the SNS innervations of WAT and BAT. In order to test for the physiological relevance of central sensory and SNS feedback loops or communication, the experiments in this dissertation also included the measurement of SNS drive across WAT depots and IBAT during energy challenges and testing the necessity of SNS or sensory nerves in regulating SNS drive to fat tissues and thermoregulation. Using isogenic strains of PRV with distinct fluorescent reporter proteins, we investigated and extensively quantified the separate and shared SNS innervations of MWAT and IWAT in aim 1 (CHAPTER 2), and the separate and shared SNS innervations of IWAT and IBAT in aim 2 (CHAPTER 3). Additionally, in aim 1, we included MWAT in a NETO study with an acute food deprivation challenge, because SNS drive to MWAT was not previously

tested for this challenge. In aim 2 (CHAPTER 3), we selectively destroyed IBAT SNS nerves via 6OHDA and functionally tested the coordination of IWAT and IBAT SNS pathways for thermoregulation and beige adipocytes recruitment in response to cold exposure. Lastly, in aim 3 (CHAPTER 4), we microinjected capsaicin, the pungent component of red chili peppers that destroys sensory nerves, into IWAT to investigate the necessity of IWAT sensory feedback to the CNS presumably to central SNS brain sites coordinating SNS drive of WAT depots and IBAT during cold exposure.

Collectively, the existence of central SNS neurons shared among different fat tissues as well as WAT sensory signaling to these nuclei likely mediate the complex communication among discrete fat depots to maintain energetic homeostasis and survival during energetic challenges (food deprivation and cold exposure). The research presented in this dissertation provided complementary evidence of brain structures comprising the SNS innervations of different fat depots and the necessity of SNS and sensory nerves to regulate SNS drive and thermoregulation.

Copyright by
American Physiological Society
The American Journal of Physiology – Regulatory, Integrative, Physiology
Nguyen NL, Randall J, Banfield BW, and Bartness TJ
2014

2 CENTRAL SYMPATHETIC INNERVATIONS TO VISCERAL AND SUBCUTANEOUS WHITE ADIPOSE TISSUE

2.1 Abstract

There is a link between visceral white adipose tissue (WAT) and the metabolic syndrome in humans, with health improvements produced with small visceral WAT reduction. By contrast, subcutaneous WAT provides a site for lipid storage that is rather innocuous relative to ectopic lipid storage in muscle or liver. The sympathetic nervous system (SNS) is the principal initiator for lipolysis in WAT by mammals. Nothing is known, however, about the central origins of the SNS circuitry innervating the only true visceral WAT in rodents – mesenteric WAT (MWAT) which drains into the hepatic portal vein. We tested whether the central sympathetic circuits to subcutaneous [inguinal WAT (IWAT)] and visceral WAT (MWAT) are separate or shared and whether they possess differential sympathetic drives with food deprivation in Siberian hamsters. Using two isogenic strains of pseudorabies virus, a retrograde transneuronal viral tract tracer within the same hamsters we found some overlap (~20-55% doubly infected neurons) between the two circuitries across the neural axis with lesser overlap proximal to the depots (spinal cord and sympathetic chain) and with more neurons involved in the innervation of IWAT than MWAT in some brain regions. Food deprivation triggered a greater sympathetic drive to subcutaneous (IWAT) than visceral (MWAT) depots.

2.2 Introduction

Understanding the role of the central control of body fat is important given that obesity is at epidemic proportions with serious secondary health consequences such as Type II diabetes, cardiovascular disease, some cancers and dementias, as well as being a significant economic burden (28; 43; 44; 66). White adipose tissue (WAT) stores energy in the form of triacylglycerol

for mobilization during times of increased energetic demands. By contrast, when there is a surfeit of calories relative to energy expenditure, lipid is stored but depending upon the storage location of the WAT depot, the excess lipid stores can be detrimental. The culprit most often pointed to as being detrimental to health is visceral WAT, which is thought to contribute to comorbidities previously mentioned above [for review see: (10; 24; 32)]. One hypothesis suggests that visceral WAT secretes pro-inflammatory cytokines, such as interleukin-6, that contribute to insulin resistance (33; 40), whereas another hypothesis, the 'hepatic-portal theory', proposes that the visceral WAT has a high lipolytic rate resulting in large amounts of free fatty acids (FFAs) being transported to the liver through the portal vein and ultimately resulting in liver insulin resistance, although visceral WAT as the source of FFAs for this negative response has been questioned [e.g., (32)].

Larger subcutaneous thigh WAT is seen as a potentially beneficial WAT depot because it is associated with the more favorable glucose and lipid profile in humans (51) and provides a potentially enormous location for lipid storage without the more direct organ-associated aspects of visceral WAT (29) or ectopic deposition of lipid in key organs involved in energy homeostasis (e.g., liver, muscle). Subcutaneous WAT also is associated with reductions in plasma insulin concentrations and hepatic steatosis as seen in improved muscle insulin sensitivity of lipodystrophic animal models, which are characterized by the small amount or the lack of body fat (46). Despite a deficit of body fat, some of the same metabolic characteristics associated with obesity are seen in lipodystrophic models because lipids are ectopically deposited in sites where they are typically not stored thus being the hypothesized problem in the lipodystrophic disorders (46).

The central nervous system is now clearly recognized as a participator in the control of peripheral lipid storage and as an activator of the sympathetic nervous system (SNS) innervation of WAT. The SNS initiates lipolysis in humans and other mammals via norepinephrine (NE) release from its postganglionic nerve terminals [for review see: (6; 7)]. Using traditional monosynaptic neuronal and transneuronal viral tract tracers injected into WAT, the sympathetic postganglionic innervation of WAT from the sympathetic chain (64) as well as the origins of the central circuits ultimately terminating in WAT depots have been described in Siberian hamsters, domestic swine and laboratory rats (1; 4; 19; 20; 47; 52; 54; 56). More importantly in terms of function, destruction of the sympathetic nerves innervating WAT by either chemical or surgical denervation significantly blocks lipid mobilization in response to several lipolytic stimuli including food deprivation, short photoperiods, and estradiol replacement in ovariectomized obese rats (9; 14; 21; 62; 65).

Of the WAT depots in rodents, the two that represent visceral and subcutaneous WAT that have analogous counterparts in humans are mesenteric WAT (MWAT) and inguinal WAT (IWAT), respectively (60). MWAT is the only true visceral WAT in rodents, if the definition of visceral WAT is that it drains into the hepatic portal vein because although epididymal WAT (EWAT) and retroperitoneal WAT (RWAT) are intra-abdominal WAT depots, they drain systemically through the inferior vena cava (16). In addition, the often cited EWAT as visceral WAT does not exist in humans [(60); J. G. Kral, personal communication]. The rodent literature, however, is rife with supposed manipulations involving 'visceral fat', which was actually intra-abdominal WAT (e.g., RWAT, EWAT).

In our previous studies testing for changes in the sympathetic drive associated with energy challenges, as measured by a direct neurochemical assessment – norepinephrine turnover

(NETO), we found different sympathetic drives across various WAT depots for each stimulus we tested (i.e., food deprivation, cold exposure, glucoprivation, central melanocortin receptor agonism, short photoperiod exposure) in Siberian hamsters (12; 13). To date, the central circuits defining the SNS outflow to MWAT have not been examined, nor has there been a functional *in vivo* test of sympathetic drive (i.e., NETO) to this WAT depot. In an attempt to understand human WAT depots functioning using non-human rodent animal models, it is important to test whether MWAT and IWAT have similar or separate central SNS outflow circuitries such that, potentially, a therapy could be designed to mobilize lipids from visceral WAT depots while relatively sparing that of subcutaneous WAT depots given that decreases in visceral WAT of as little as 5% has health benefits (16; 41) and the perhaps beneficial aspects of subcutaneous WAT.

Therefore, the purpose of the present investigation was to define the central SNS outflow circuits to MWAT and IWAT and to functionally test the sympathetic drive to these two depots in response to a lipolytic challenge (i.e., food deprivation). We used Siberian hamsters, our model of naturally-occurring obesity that we have employed previously to define the sympathetic outflow to various WAT depots (4; 64) and sensory inflow from WAT depots to the brain (38; 55), in addition to assessing SNS drive using NETO with various energy challenges (12; 13). To define the separate/shared central SNS outflow circuitry, we used isogenic strains of pseudorabies virus (PRV) that have distinct reporters – PRV 152 [green fluorescent protein (GFP) (50)] and PRV 614 [monomeric red fluorescent protein (mRFP) (5)], each injected into one of the two WAT depots. Single- and double-labeled (infected) neurons were quantified across the neuroaxis as well as in the spinal cord and the sympathetic chain. The functional test of differential SNS drive was accomplished by food depriving hamsters for 16 h with ad libitum-fed hamsters as a control and measuring NETO.

2.3 Materials and Methods

2.3.1 ANIMALS

Housing and all experimental procedures were approved by the Georgia State University Institutional Animal Care and Use Committee, in accordance with Public Health Service and United States Department of Agriculture guidelines. Adult male Siberian hamsters ~3.5 mo old (*Phodopus sungorus*) were used. All hamsters (n=41) were kept in individual cages in a vivarium under conditions of controlled lighting (16 h light:8 h dark cycle) and temperature (21 □ 2°C) with ad libitum access to pelleted chow (LabDiet Rodent Chow 5001, St. Louis, MO), unless noted otherwise, and tap water.

2.3.2 EXPERIMENT 1: VIRAL TRACT TRACING THE SNS OF MWAT AND IWAT

2.3.2.1 PRELIMINARY PRV INJECTIONS TESTS

It was necessary to verify that the two isogenic PRV strains infected neurons at a similar rate and that one was not more virulent than the other. As a control to ensure that they were functionally equivalent, a 1:1 mixture of PRV 152 (3 x 108 pfu/mL; generous gift by Lynn Enquist of Princeton University, Princeton, NJ) and PRV 614 [2.2 x 108 pfu/mL (5)] was injected into either MWAT (3 injections) or IWAT (10 injections) at a volume of 150 nl/locus. There was relatively similar single and double labeling of the two PRV strains across the neuroaxis of these hamsters, thereby demonstrating functional equivalence of these doses of PRV 152 and PRV 614 (Nguyen, N. T. and Bartness, T. J., unpublished observations). We have previously demonstrated the specificity of PRV to retrogradely label only sympathetic neurons innervating WAT by chemically denervating the sympathetic nerves to WAT and then injecting PRV into the tissue yielding no infected neurons across the neuroaxis also suggesting specificity and no parasympathetic innervation of this tissue (26).

2.3.2.2 PRV INJECTIONS

Hamsters (n=6) were single housed 1 wk before PRV injections, which were performed according to Biosafety Level II conditions. They were anesthetized with 2-3% isoflurane (Baxter Healthcare, Deerfield, IL), the fur around the haunch of their right leg was shaved and the skin was alternatively wiped with povidone iodine (Ricca Chemical Company, Arlington, TX) and alcohol, then with povidone iodine last. The hamsters were placed in lateral recumbency and a subcutaneous incision was made to reveal IWAT. Using a 1.0 µl syringe, 150 nl of PRV 152 (3 x 108 pfu/mL) was injected at each of 10 loci across IWAT to evenly distribute the virus. The syringe was held in place for 1 min after each injection to prevent reflux up the outside of the needle and to allow time for the virus to disperse at each locus. The skin was closed with sterile wound clips (Stoelting, Wood Dale, IL) and nitrofurozone powder (nfz Puffer, Hess & Clark, Lexington, KY) was applied to minimize infection. The hamsters were then transferred to clean biohazard cages. All hamsters received subcutaneous injections of ketofen (5 mg/kg, Fort Dodge Animal Health, Fort Dodge, IA), an analgesic, for 3 d post virus injections and apple slices to supply readily consumed calories and water. We previously tested the transit times of PRV 152 and PRV 614 to reach the brain from the two WAT depots and concluded that 24 h after PRV 152 injections into IWAT was the optimal time point to inject PRV 614 into MWAT (Nguyen, N. T. and Bartness, T. J., unpublished observations). Therefore, the same hamsters were re-anesthetized, shaved on the ventral side, and placed supine. A horizontal incision was made through the skin and the peritoneum in order to expose the abdominal cavity. The intestines were gently pulled out onto an isotonic saline-soaked sterile surgical drape to reveal MWAT and to prevent desiccation. Using a 1.0 µl syringe, l50 nl of PRV 614 (2.2 x 108 pfu/mL) was injected at each of 3 loci to distribute the virus evenly across MWAT. The peritoneum and skin was

closed with sterile sutures (Ethicon, Johnson & Johnson, Somerville, NJ) and sterile wound clips, respectively. Nitrofurozone powder was applied, and the hamsters continued to receive ketofen and apple slices as a part of post operational care. As an additional control for WAT depot specific differences in viral uptake, in another group of hamsters, the WAT depots into which the viruses were injected were reversed (i.e., PRV 614 and PRV 152 were injected into IWAT and MWAT, respectively).

2.3.2.3 HISTOLOGY

The hamsters were euthanized by overdose with an intraperitoneal (i.p.) injection of pentobarbital sodium (300 mg/kg) 6 d post virus injections into IWAT and transcardial perfusion was performed with heparinized 0.02% saline (75 ml), followed by 4% paraformaldehyde (150 mL) solution. The brains were removed and placed in the same fixative for overnight, and then immersed in a cryoprotectant solution of 30% sucrose. The brains were sectioned at 30 µm on a freezing stage sliding microtome and every 4th brain section was processed for double fluorescent immunohistochemistry (IHC) against GFP and mRFP. The ipsilateral and contralateral sympathetic ganglia associated with vertebral segment thoracic 5 (T5) to lumbar 3 (L3) level of the spinal cord as well as the spinal cords themselves were harvested and sliced at 16 µm and 40 µm, respectively, also on a freezing stage sliding microtome. The sympathetic ganglia were collected onto slides (Superfrost Plus, VWR International, West Chester, PA) in a series of three. Every 4th ganglia and spinal cord sections were processed for double-fluorescent IHC against GFP and mRFP similar to the brain sections.

2.3.2.4 IMMUNOHISTOCHEMISTRY

We tested the primary and secondary antibodies against GFP and mRFP with positive and negative controls to ensure specificity and no cross reactivity of the antibodies before

performing the double fluorescent IHC. Then, the brain and spinal cord sections were incubated in 0.1 M PBS (pH 7.4) x 3 rinses for 5 min each, followed by 20 % normal goat serum (NGS; Vector Laboratories, Inc., Burlingame, CA) in 0.4 % Triton X-100 for 30 min. The sections were incubated in a cocktail of primary antibodies consisting of mouse anti-GFP (1:500, Abcam, Cambridge, MA) and rabbit anti-RFP (1:2000, Rockland Immunochemicals Inc., Gilbertsville, PA) in 0.1 M PBS with 2 % NGS and 0.4 % Triton X-100 for 1 d at room temperature. They then were rinsed with 0.1 M PBS x 3 for 5 min each, and the sections were subsequently incubated in a cocktail of secondary antibodies consisting of goat anti-mouse Alexa 488 (1:500, Jackson ImmunoResearch, West Grove, PA) and goat anti-rabbit CY3 (1:800, Jackson ImmunoResearch, West Grove, PA) in 0.1 M PBS with 2 % NGS and 0.4 % Triton X-100 for 2 h at room temperature. The sections were mounted onto gelatin subbed slides and coverslipped with ProLong Gold Antifade reagent (Life Technologies, Grand Island, NY). The double fluorescent IHC for the sympathetic ganglia followed the same protocol as the free floating brain sections and spinal cords except the primary antibodies concentrations of mouse anti-GFP and rabbit anti-RFP were increased to 1:400 and 1:600, respectively, and the incubation times increased to 2 d because the sympathetic ganglia sections were slide-mounted. The concentrations of the secondary antibodies of goat anti-mouse Alexa 488 and goat anti-rabbit CY3 were also increased to 1:350 and 1:550, respectively.

2.3.3 EXPERIMENT 2: TESTS OF THE SNS DRIVE TO MWAT AND TO IWAT AFTER 16 H FOOD DEPRIVATION

Hamsters (n=35) used for NETO were handled daily to adapt them to the handling associated with the test and their body mass were monitored for 2 wks. They then were matched for absolute body mass and percent body mass change and were divided into experimental

groups. The food deprivation length used was based on a robust increase in NETO by Siberian hamsters previously in our laboratory (13). Hamsters were divided into 2 groups: a) ad libitum-fed (n=17) and b) food-deprived for 16 h (n=18). On the day of the food deprivation, all hamsters had food removed from their cheek pouches and body weight was measured after which hamsters were transferred into clean cages. Food was removed for the food-deprived groups, but tap water was freely available. At the end of the 16 h food deprivation, body mass was measured for all hamsters.

2.3.3.1 NETO AND TISSUE PREPARATION

Before tissue harvesting, hamsters were transferred to the laboratory and were acclimated for 2 h in a quiet environment to prevent unnecessary stress that can affect catecholamine release. Ad libitum-fed (n=10) and food-deprived (n=10) hamsters were terminated by rapid decapitation to obtain baseline values of NE for between group calculation of NETO as we have done previously (12; 13; 48; 64). In brief, the interscapular brown adipose tissue (IBAT), IWAT, EWAT, RWAT, and MWAT were quickly harvested, weighed, frozen in liquid nitrogen, and stored in -80° C until NE extraction. NETO was assayed using the α-methyl-p-tyrosine (α-MPT; M3281, Sigma-Aldrich, St. Louis, MO) method during the last 4 h of the food deprivation. Alpha-MPT is an active competitive inhibitor for tyrosine hydroxylase, thereby preventing the synthesis of catecholamines (57). The remaining hamsters were given i.p. injections of α-MPT (250 mg α-MPT/kg) 4 h before the completion of the food deprivation and a supplemental dose (125 mg/kg) was given 2 h after the initial dose to ensure the inhibition of catecholamine synthesis. The same procedures for termination and WAT depots harvesting were carried out for these hamsters. The adipose tissues were processed and extracted for NE with dihydroxybenzylamine as an internal control to ensure extraction efficiency. The NE content was

measured following our methods [for review see: (61)] and modifications (64) of the method of Mefford (35).

2.3.3.2 QUANTIFICATION ANALYSES

PRV-labeled neurons were considered positive based on cell size, shape and fluorescent intensity. They were analyzed and quantified using an Olympus BX41 microscope. Images were acquired at 4x and 10x magnifications using an Olympus DP73 camera and were adjusted for brightness, contrast, sharpness, and overlaying of double-labeled neurons using Adobe Photoshop CS5 (Adobe Systems, San Jose, CA, USA). A mouse brain atlas (42) was used as reference to identify brain sites, because no commercially available Siberian hamster brain atlas exists and the size and shape of most hamster brain areas are comparable to that of mouse rather than the Syrian hamster. Absolute values of positively-labeled neurons in the brains were collapsed across each bilateral nucleus/region within each hamster and converted into total percentage of PRV-labeled neurons, and then averaged across the number of hamsters. The percentages of double-labeled (infected) neurons are represented as the mean percentage of total PRV single- and double-labeled neurons. There was bilateral labeling from MWAT within the spinal cords and sympathetic chains, whereas IWAT had largely ipsilateral labeling with some trivial labeling on the contralateral side. Therefore, in the spinal cord and sympathetic chains, we quantified the labeling from the ipsilateral side of PRV injections into IWAT and that same ipsilateral side for MWAT also and presenting the data as total percentage of PRV-labeled neurons as well.

2.3.3.3 STATISTICAL ANALYSES

All statistical analyses were carried out using NCSS (version 2007, Kaysville, UT). A one-way ANOVA with Duncan's New Multiple Range post hoc test was used to compare the

percentage of double-labeled neurons to single-labeled neurons either projecting to MWAT or to IWAT. The same analyses were performed for the quantifications of labeled neurons in the spinal cords and sympathetic chains. The student's t-tests were performed comparing NETO values of ad libitum-fed and food-deprived hamsters. Exact probabilities and test values were omitted for simplicity and clarity of presentation, and statistical significance was considered if $p<0.05$.

2.4 Results

2.4.1 EXPERIMENT 1: VIRAL TRACT TRACING THE SNS OF MWAT AND IWAT

The PRV-injected hamsters showed signs of viral infection such as unkempt coats, but no overwhelming symptoms of illness before termination. We compared the sympathetic innervations of MWAT and IWAT at the levels of the sympathetic chain, spinal cord, and brain.

2.4.1.1 SYMPATHETIC CHAIN

Labeled neurons projecting to MWAT and IWAT that were single-labeled as well as those that were double-labeled projecting to both WAT depots were found in the sympathetic ganglia associated with the T5 to L3 spinal levels (Fig. 2.1, A). The majority of single-labeled neurons that projected to either MWAT or IWAT were distributed at T13, L1, and L2 (Fig. 2.1, A). The mean absolute number of PRV-labeled neurons projecting to either WAT depot did not reach statistical significance (Fig. 2.1, A); however, when expressed as the percentage of the total number of PRV-labeled neurons from T5 to L3, there were statistically significantly more PRV-infected neurons projecting to MWAT at T13 compared with IWAT ($p<0.05$; Fig. 2.1, B). The regional specificity of single-labeled PRV labeling in the sympathetic ganglia was most notably seen at T13-L1 ($p<0.05$; Fig. 2.1, B; Fig. 2.2). These ganglia are physically fused (64), but they can be easily discriminated because T13 is round and similar in shape to the other

thoracic sympathetic ganglia, whereas L1 is long and cylindrically-shaped similar to the other lumbar sympathetic ganglia (Fig. 2.2). Unlike the other sympathetic ganglia that had relatively similar percentages of both single- and double-labeled neurons (~30-50%), T13 had a statistically significantly lower percentage of double-labeled neurons (~10%) compared with the single-labeled neurons innervating MWAT or IWAT, while L1 only had lower percentage of double-labeled neurons when compared with single-labeled neurons projecting to IWAT ($p<0.05$; Fig. 2.1, B). When the data were collapsed across the thoracic sympathetic ganglia (T5-T13), there was a significantly greater percentage of labeled neurons projecting to MWAT than to IWAT ($p<0.05$; Fig. 2.1, C), but a similar analysis for the data collapsed across the lumbar sympathetic ganglia (L1-L3) revealed no such difference (Fig. 2.1, C). The double-labeled neurons projecting to both MWAT and IWAT were statistically significantly lower compared with the single-labeled neurons when the thoracic and lumbar sympathetic ganglia data were collapsed ($p<0.05$; Fig. 2.1, C). When all of the sympathetic ganglia (T5-L3) were collapsed across all hamsters, the single-labeled neurons projecting to MWAT and IWAT were statistically greater than the double-labeled neurons, and MWAT had an overall greater percentage of single-labeled neurons compared with IWAT (data not shown).

2.4.1.2 SPINAL CORD

PRV 152 and PRV 614 labeled the spinal cord as the viruses moved transneuronally and retrogradely toward the brain. There was positive labeling across the cervical, thoracic, and lumbar portions of the spinal cord (Fig. 2.3, A). The intermediolateral (IML) nucleus of the spinal cord, home of the sympathetic preganglionic neurons, had few doubly-infected cells and this sparse double-labeling was similar to the labeling observed in the sympathetic ganglia (Fig.

2.3, B-D). The percentage of double-labeled neurons was significantly lower as compared to that of singe-labeled neurons projecting to either MWAT or IWAT ($p<0.05$; Fig. 2.3, A).

2.4.1.3 BRAIN

There was bilateral infection in the hindbrain, midbrain, and forebrain as a result of the PRVs infecting high order neurons retrogradely from MWAT and IWAT. Overall, this general pattern of infection was similar to previous PRV labeling of EWAT (4; 54; 64), RWAT (1) and IWAT (4; 54) in earlier studies. The percentages of neurons ultimately projecting to MWAT and to IWAT were quite similar to each other with an exception of some nuclei in the hindbrain, midbrain, and forebrain (see Table 2.1).

For some of the hindbrain regions such as the ambiguus nucleus (Amb), area postrema (AP), dorsal paragigantocellular nucleus (DPGi), linear nucleus of the medulla (Li), peripyramidal nucleus (Ppy), dorsal raphe nucleus (DR), caudal/rostral linear nucleus of the raphe (CLi/RLi), lateral/parvicellular part of reticular nucleus (LRt/-PC), nucleus of the solitary tract (Sol; Fig. 2.4, A-B), and ventral spinocerebellar tract (vsc; Fig. 2.4, A) they had significantly more labeled sympathetic circuit neurons projecting to IWAT than to MWAT ($p<0.05$; Table 2.1). There were exceptions however, such as the hypoglossal nucleus, A5 region, facial regions, gigantocellular areas (Fig. 2.4, A), parabrachial areas, the dorsal and ventral parts of the subcoeruleus nucleus, (Fig. 2.5, A and C), locus coeruleus (Fig. 2.5, A), raphe magnus nucleus (RMg; Fig. 2.4, A; Fig. 2.5, A-B), raphe obscurus nucleus (Fig. 2.4, A), raphe pallidus (RPa; Fig. 2.4, A and C), rubrospinal tract (Fig. 2.5, A), and trigeminal areas, where there were similar percentages of single-labeled neurons projecting to MWAT and to IWAT that did not reach statistical significance. For the other remaining quantified hindbrain regions, though statistical significance was not reached, there was a tendency for IWAT to have

a greater percentage of single-labeled neurons than MWAT. It appears that in the hindbrain IWAT (~30-45%; subcutaneous WAT) has a greater percentage of sympathetic circuit neurons than MWAT (~20-35%; visceral WAT) with ~20-40% of double-labeled neurons projecting to both WAT depots.

Nuclei within the midbrain had ~20-50% of double-labeled neurons (Table 2.1). PRV labeling of neurons ultimately projecting to IWAT were statistically greater in the posterior commissure, cuneiform nucleus (CnF), Edinger-Westphal nucleus (EW), medial longitudinal fasciculus (mlf), dorsolateral periaqueductal gray (DLPAG), dorsomedial periaqueductal gray (DMPAG), lateral periaqueductal gray (LPAG), ventral lateral periaqueductal gray (VLPAG), rubral areas, laterodorsal tegmental nucleus ventral part (LDTg/-V), and pedunculopontine tegmental nucleus (PPTg) than neurons that comprise the circuit ultimately innervating MWAT ($p<0.05$; Table 2.1). Similar to the hindbrain, there also were regions where we observed no statistical difference between the numbers of single- and double-labeled neurons.

Heavy PRV labeling from MWAT and IWAT were seen in the forebrain. There was not a significant difference between the percentage of neurons comprising the circuits ultimately innervating MWAT and IWAT in the large majority of forebrain regions such as the dorsomedial hypothalamic nucleus (Fig. 2.6, A-B), sub-zona incerta, posterior hypothalamic area, the majority of the subnuclei of the preoptic area, the paraventricular nucleus of the hypothalamus (PVH; Fig. 2.7, A-B), the suprachiasmatic nucleus, and thalamic regions. There were, however, a statistically significantly greater percentage of neurons ultimately projecting to IWAT than to MWAT in only a few areas such as the medial preoptic area (MPA; Fig. 2.8, A-B), and lateral hypothalamic area proper (LH proper; $p<0.05$; Table 2.1). We only found differences in these two areas (LH proper and MPA) within the forebrain, whereas the midbrain and hindbrain had

many brain regions that showed differences between the innervation to MWAT and IWAT. The percentage of double-labeled neurons was ~20-40% in forebrain brain regions whereas the percentage of single-labeled neurons was similar (~20-45%; Table 2.1). Thus, we did not detect many distinct differences between the circuits ultimately innervating MWAT (visceral WAT) and IWAT (subcutaneous WAT) in the forebrain compared with more numerous differences in the midbrain and hindbrain.

2.4.2 EXPERIMENT 2: TESTS OF THE SNS DRIVE TO MWAT AND TO IWAT AFTER 16 H FOOD DEPRIVATION

Utilizing the NETO tests, we compared the sympathetic drives of MWAT and IWAT, as well as other WAT depots in response to standard energy challenge that stimulates the SNS drive to WAT – food deprivation (13; 36).

2.4.2.1 BODY MASS

The mean absolute body mass from pre- to post-food deprivation was statistically significantly decreased after the 16 h food deprivation ($p<0.05$; Table 2.2), but not surprisingly for the ad libitum-fed group. When the change in body mass was examined, the average change in body mass from pre- to post-food deprivation was significantly decreased compared with that of the corresponding ad libitum-fed groups ($p<0.05$; Table 2.2).

2.4.2.2 NETO

MWAT in the 16 h food deprivation group often had negative NETO values because the basal levels of NETO (0 h) were lower than at the time of NETO testing (4 h) which contradicts physiological reality. Therefore, for those cases of negative NETO values, the values were set to zero as we have done previously (12; 13; 37; 39; 48; 64). This can happen in some sample by chance when basal levels of NE are initially low due to low sympathetic drive (12; 13; 39).

We included IBAT as a negative control for the NETO tests, and we expected that the food-deprived hamsters would decrease their IBAT utilization when energy is not available (i.e., food deprivation) given that BAT thermogenesis is energetically costly as we have seen previously [e.g., (13)] and therefore have low NETO. This also was the case here. Food deprivation of 16 h produced differential NETO that was WAT depot-specific. Specifically, IWAT NETO from food deprived-hamsters was significantly greater than IWAT from ad libitum-fed hamsters whereas MWAT had negligible NETO for both the ad libitum-fed and the 16 h food-deprived groups. We previously found a small, but significant EWAT NETO increase with food deprivation (13), whereas here there was a tendency ($p=0.06$) for a similar small increase, but not a difference between RWAT and IBAT NETO between ad libitum-fed and food-deprived animals (Fig. 2.9).

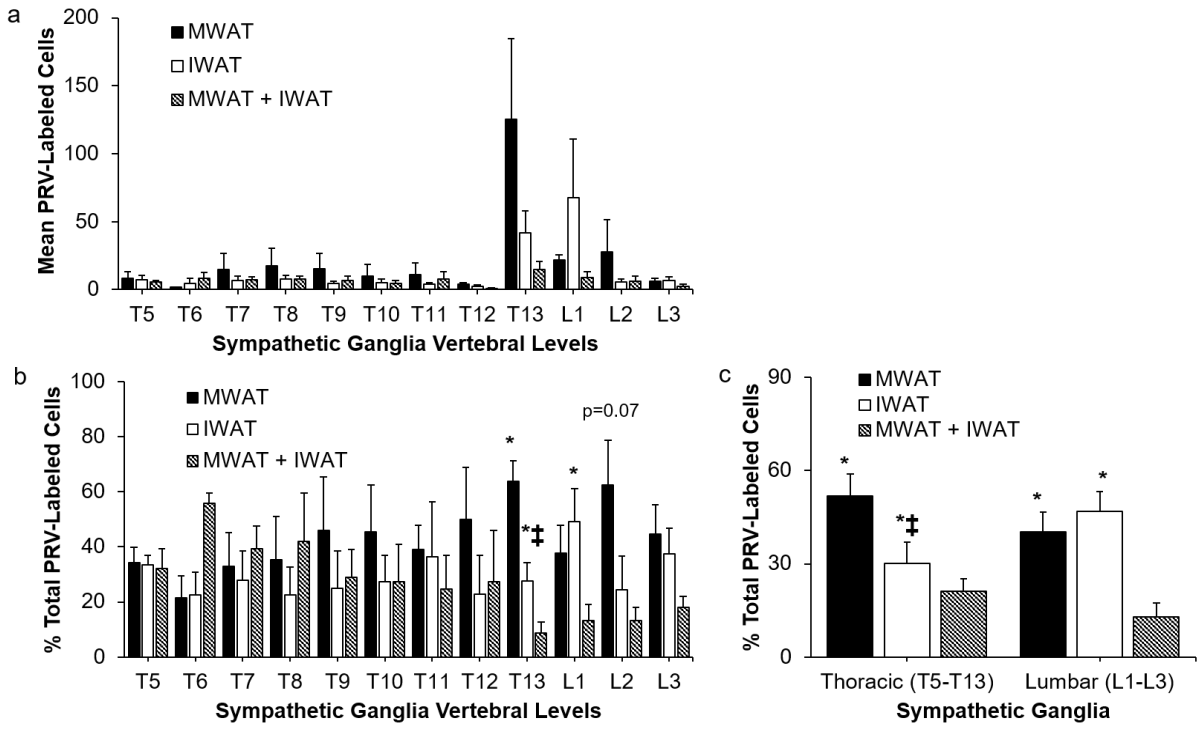

Figure 2.1 Sympathetic innervations of MWAT and IWAT at the T5-L3 sympathetic chain levels.
(a) Distribution of PRV-labeled cells across vertebral levels. (b) Total percentage of PRV-labeled cells. (c) Total percentage of PRV-labeled cells in collapsed thoracic (T5-T13) and lumbar (L1-L3) sympathetic ganglia. ‡$p<0.05$ vs. MWAT; *$p<0.05$ vs. MWAT + IWAT.

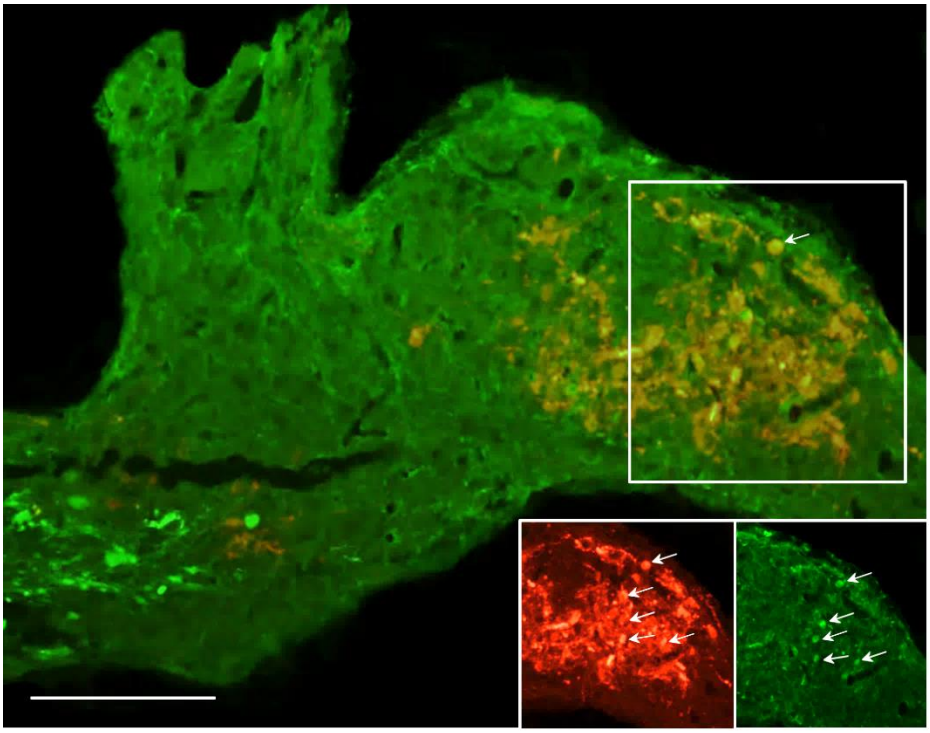

Figure 2.2 Photomicrographs illustrating isogenic strains of PRV labeling the sympathetic innervation of MWAT, IWAT, and of both WAT depots.
MWAT (red), IWAT (green), both WAT depots (yellow; white arrows) at the vertebral level of T13-L1. Scale bar = 100 μm.

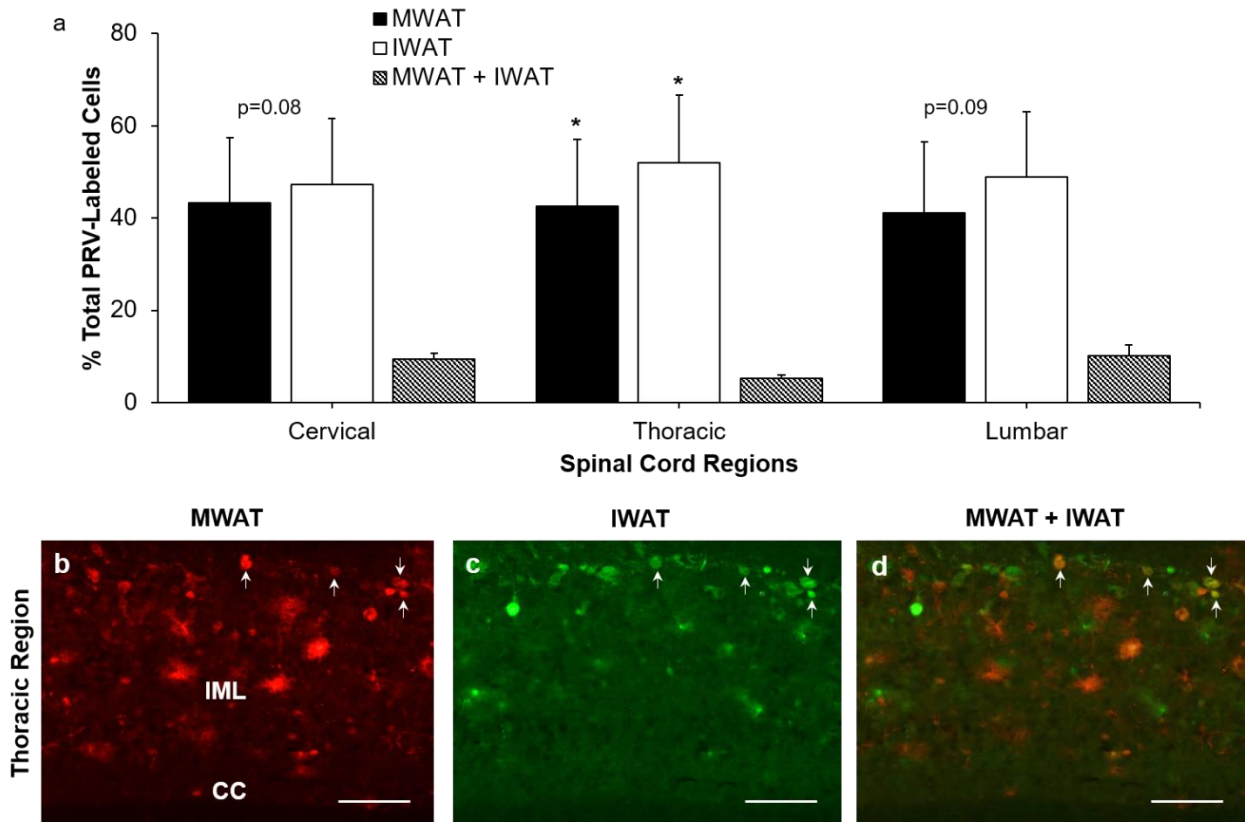

Figure 2.3 Distribution of PRV-labeled cells in the spinal cord.
(a) Quantification of positively labeled PRV cells across the cervical, thoracic, and lumbar regions. (b-d) Photomicrographs of sympathetic neurons projecting to MWAT (red), to IWAT (green), and to both WAT depots (yellow; white arrows) at the thoracic region of the spinal cord. *$p<0.05$ vs. MWAT + IWAT. CC, central canal; IML, intermediolateral nucleus. Scale bar = 100 μm.

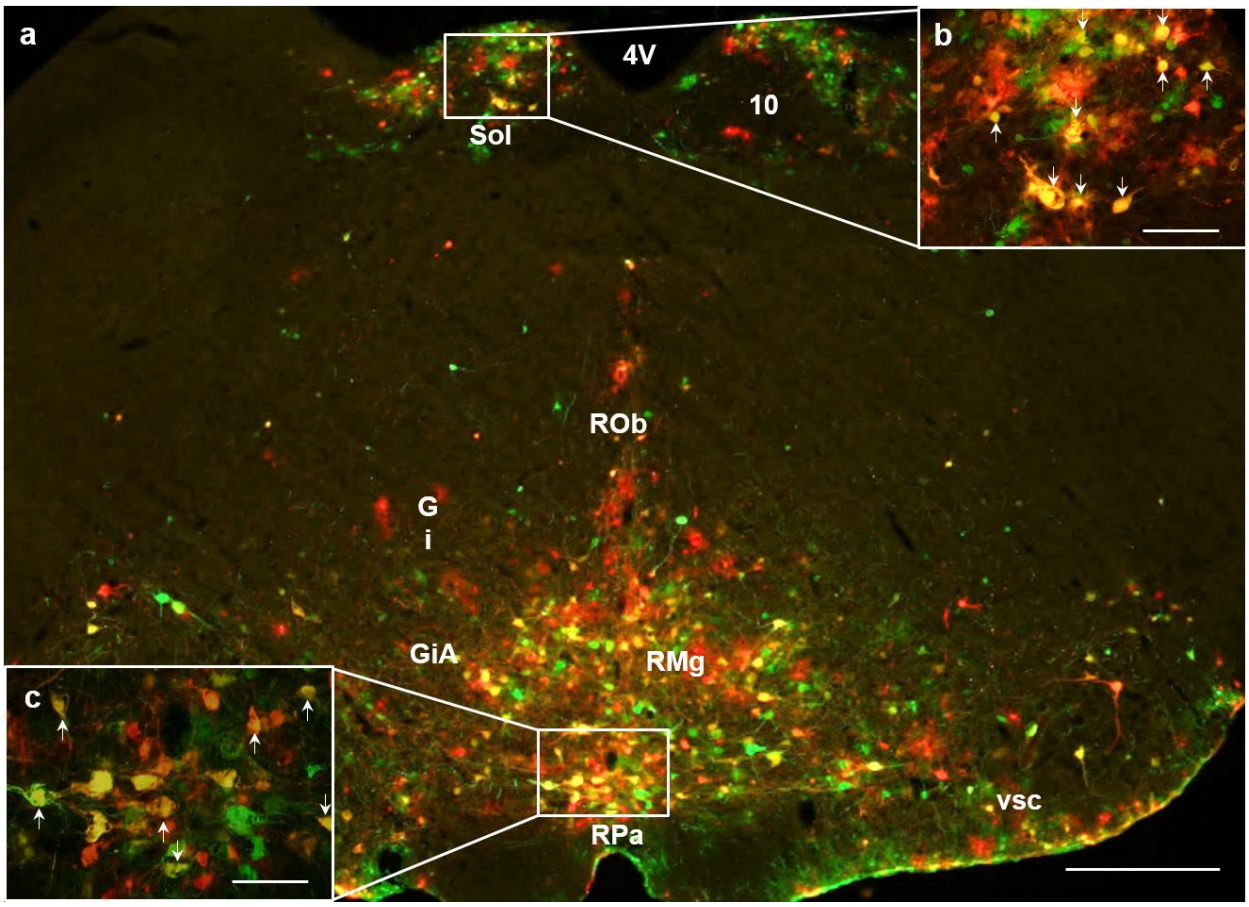

Figure 2.4 Photomicrographs illustrating PRV labeling in the hindbrain.
(a) Low magnification (4x) photomicrograph illustrating PRV labeling in the hindbrain. High magnification (10x) photomicrograph illustrating PRV labeling in the Sol (b) and RPa (c). (a-c) Sympathetic neurons projecting to MWAT (red), to IWAT (green), and to both WAT depots (yellow; white arrows). 4V, fourth ventricle; 10, dorsal motor nucleus of the vagus; Gi, gigantocellular reticular nucleus; GiA, gigantocellular reticular nucleus, alpha part; RMg, raphe magnus nucleus; ROb, raphe obscurus nucleus; RPa, raphe pallidus nucleus; Sol, nucleus of the solitary tract; vsc, ventral spinocerebellar tract. (a) scale bar = 500 µm, (b,c) scale bar = 200 µm.

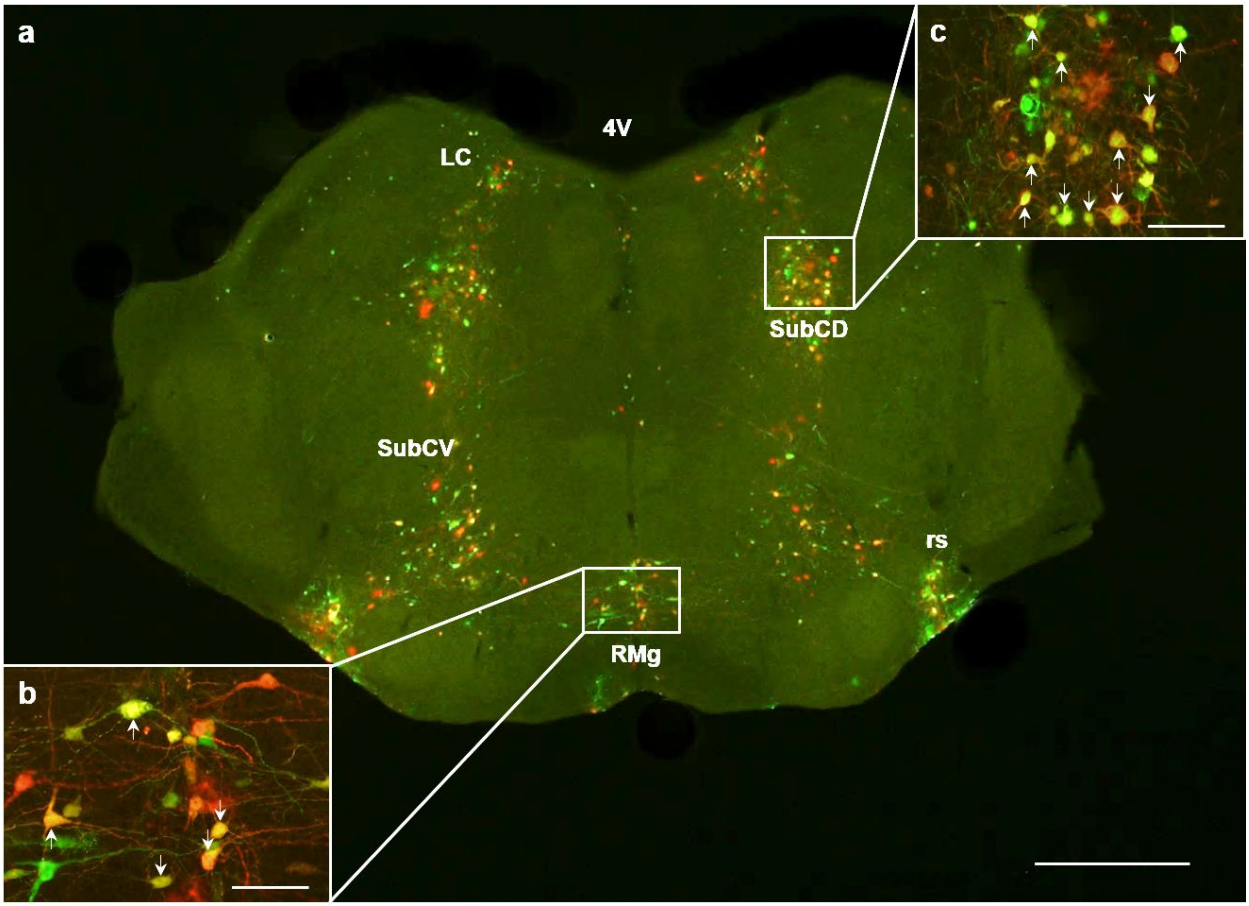

Figure 2.5 Photomicrographs illustrating PRV labeling in the midbrain.
(a) Low magnification (4x) photomicrograph illustrating PRV labeling in the midbrain. High magnification (10x) photomicrograph illustrating PRV labeling in the RMg (b) and SubCD (c). (a-c) Sympathetic neurons projecting to MWAT (red), to IWAT (green), and to both WAT depots (yellow; white arrows). 4V, fourth ventricle; LC, locus coeruleus; RMg, raphe magnus nucleus; rs, rubrospinal tract; SubCD, subcoeruleus nucleus, dorsal part; SubCV, subcoeruleus nucleus, ventral part. (a) scale bar = 500 µm, (b,c) scale bar = 200 µm.

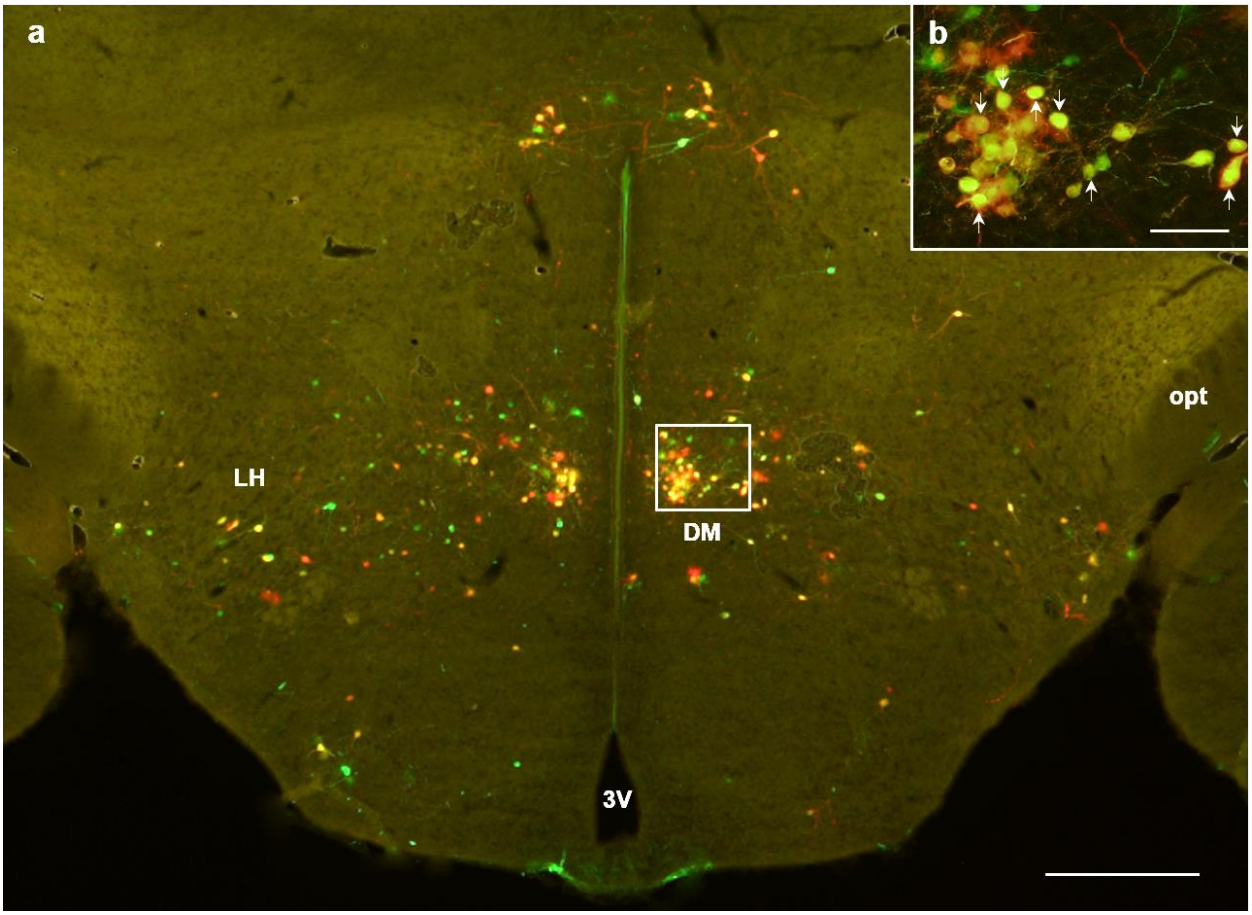

Figure 2.6 Photomicrographs illustrating PRV labeling in the DMH.
(a) Low magnification (4x) photomicrograph illustrating PRV labeling in the DMH. High magnification (10x) photomicrograph illustrating PRV labeling in the DMH (b). (a-b) Sympathetic neurons projecting to MWAT (red), to IWAT (green), and to both WAT depots (yellow; white arrows). 3V, third ventricle; DM, dorsomedial hypothalamic nucleus; LH, lateral hypothalamic area; opt, optic tract. (a) scale bar = 500 µm, (b) scale bar = 200 µm.

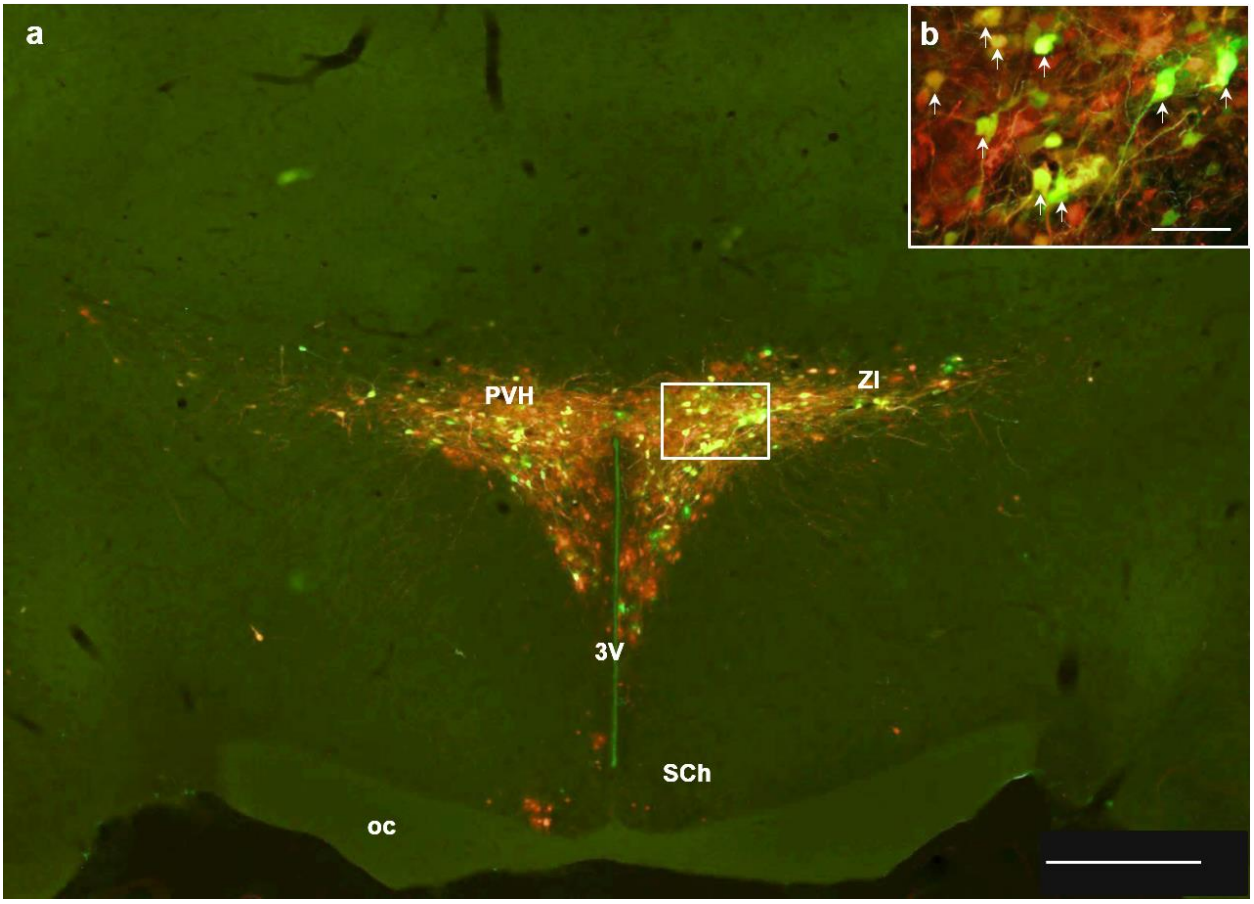

Figure 2.7 Photomicrographs illustrating PRV labeling in the PVH.
(a) Low magnification (4x) photomicrograph illustrating PRV labeling in the PVH. High magnification (10x) photomicrograph of PRV labeling in the PVH (b). (a-b) Sympathetic neurons projecting to MWAT (red), to IWAT (green), and to both WAT depots (yellow; white arrows). 3V, third ventricle; oc, optic chiasm; PVH, paraventricular nucleus of the hypothalamus; SCh, suprachiasmatic nucleus; ZI, zona incerta. (a) scale bar = 500 µm, (b) scale bar = 200 µm.

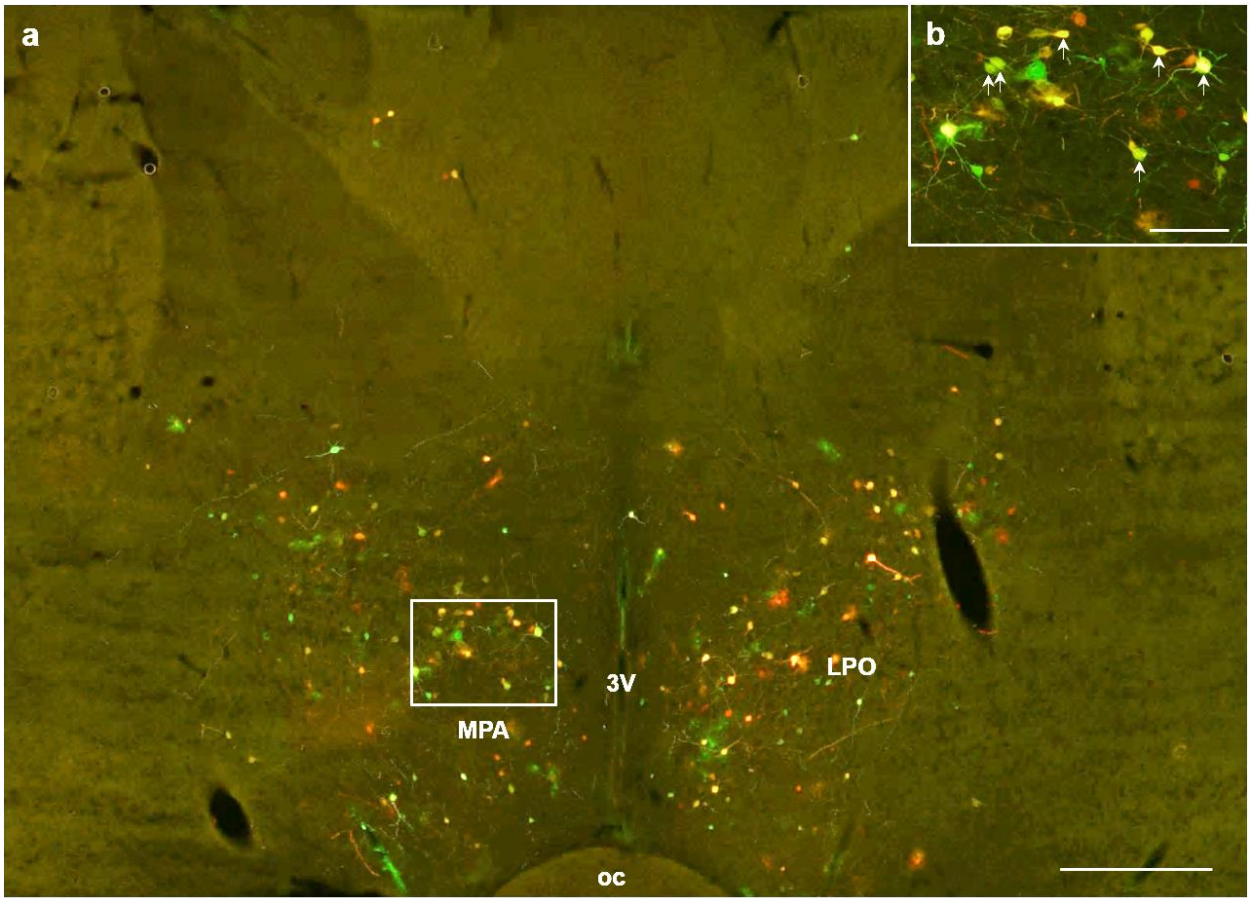

Figure 2.8 Photomicrographs illustrating PRV labeling in the POA.
(a) Low magnification (4x) photomicrograph illustrating PRV labeling in the POA. High magnification (10x) photomicrograph of PRV labeling in the MPA, a subregion of the POA (b). (a-b) Sympathetic neurons projecting to MWAT (red), to IWAT (green), and to both WAT depots (yellow; white arrows). 3V, third ventricle; LPO, lateral preoptic area; MPA, medial preoptic area; oc, optic chiasm. (a) scale bar = 500 µm, (b) scale bar = 200 µm.

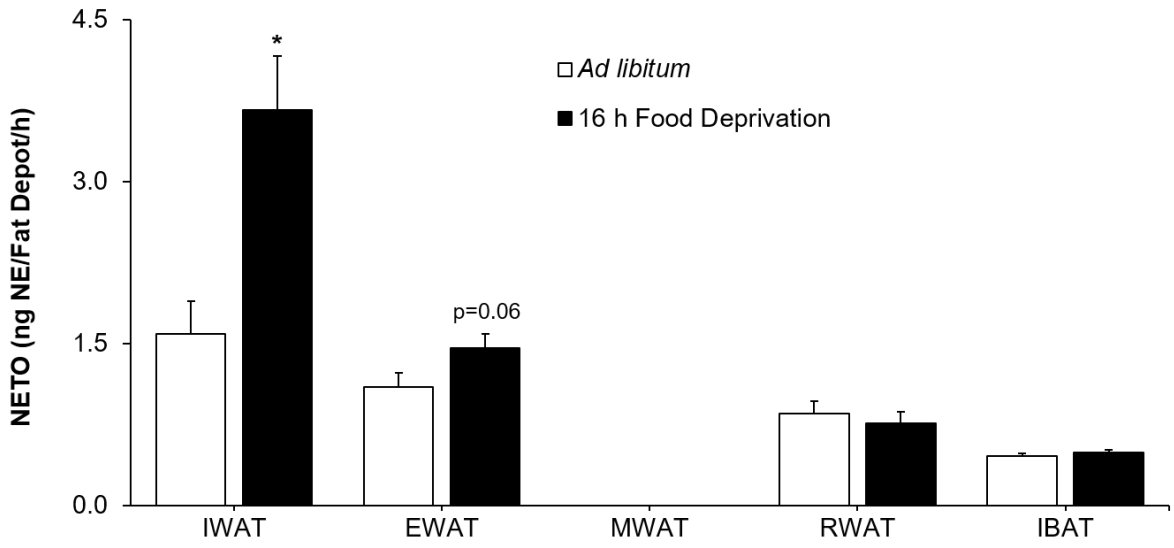

Figure 2.9 Mean ± SE NETO expressed per fat depot in Siberian hamsters subjected to 16 h food deprivation.
*p<0.05 vs. *ad libitum*-fed.

Table 2.1 Total percentage of PRV-labeled cells innervating MWAT, IWAT, and both WAT depots.

The percentage values were averaged across hamsters (n=6) and presented in tabular form as means ± SE. ‡p<0.05 vs. MWAT; *p<0.05 vs. MWAT + IWAT.

	% MWAT	% IWAT	% MWAT + IWAT	Total Mean of All PRV-Labeled Cells
Hindbrain				
12/12N	34.27 ± 3.10	37.85 ± 4.96	27.88 ± 5.90	280.00 ± 46.15
10 (DMV)	35.90 ± 2.33*	37.96 ± 2.56*	26.14 ± 2.47	652.67 ± 124.12
A5	26.20 ± 3.09	37.41 ± 2.74	36.39 ± 3.64	99.50 ± 32.53
Amb	28.61 ± 2.61	40.08 ± 2.97*‡	31.31 ± 2.75	387.33 ± 78.86
AP	30.11 ± 1.29	44.04 ± 3.75*‡	25.85 ± 3.06	447.33 ± 104.61
Bar	28.99 ± 4.66	37.43 ± 5.93	33.58 ± 8.76	51.20 ± 5.63
C3	16.46 ± 2.71	28.74 ± 12.21	54.80 ± 12.44	35.00 ± 12.64
Cu/Ecu	35.91 ± 3.50*	41.28 ± 3.29*	22.81 ± 2.05	198.00 ± 38.78
Facial regions	29.00 ± 3.00	37.17 ± 1.67	33.83 ± 4.59	739.83 ± 211.68
Gigantocellular areas				
DPGi	24.70 ± 1.89	42.00 ± 4.27‡	33.29 ± 3.06	432.17 ± 49.63
Gi	31.77 ± 2.93	36.83 ± 3.27	31.40 ± 1.60	1006.50 ± 168.33
GiA	29.94 ± 3.66	36.56 ± 2.77	33.49 ± 3.12	216.00 ± 71.19
GiV	35.72 ± 3.52	33.81 ± 1.15	30.47 ± 3.68	1061.33 ± 126.57
LPGi	31.80 ± 2.76	35.12 ± 3.42	33.09 ± 2.88	1150.33 ± 184.46
In/InM	34.60 ± 4.22	40.77 ± 4.04*	24.62 ± 4.61	78.50 ± 14.28
LC	35.63 ± 7.39	37.98 ± 5.41	26.39 ± 6.26	126.80 ± 26.59
Li	26.66 ± 3.88	42.12 ± 5.02‡	31.22 ± 2.52	365.50 ± 108.57

Table 1 (cont).

	% MWAT	% IWAT	% MWAT + IWAT	Total Mean of All PRV-Labeled Cells
Parabrachial areas				
LPB	26.88 ± 4.00	35.41 ± 6.14	37.71 ± 3.72	202.80 ± 87.89
MPB	26.08 ± 4.70	36.44 ± 6.86	37.48 ± 5.23	101.80 ± 35.98
Ppy	34.36 ± 2.71*	46.39 ± 2.78*‡	19.25 ± 1.44	191.50 ± 32.40
Pr	27.63 ± 2.73	38.88 ± 2.88‡	33.49 ± 1.36	209.50 ± 32.75
Raphe areas				
DR	28.59 ± 3.04	42.87 ± 5.25‡	28.54 ± 3.54	192.33 ± 36.27
RC	35.66 ± 4.19	25.65 ± 8.95	38.69 ± 5.17	183.50 ± 34.86
CLi/RLi	29.76 ± 3.63	45.21 ± 4.23*‡	25.03 ± 2.12	63.67 ± 9.77
MnR	31.76 ± 4.06	39.90 ± 3.80	28.34 ± 5.52	29.33 ± 4.81
PMnR	35.57 ± 4.79	38.20 ± 5.87	26.23 ± 5.24	48.67 ± 6.46
RMg	25.90 ± 4.58	36.11 ± 2.39	37.80 ± 4.66	163.17 ± 39.32
ROb	33.60 ± 3.04	35.23 ± 1.66	31.17 ± 3.80	660.83 ± 121.82
RPa	31.38 ± 1.60*	29.93 ± 2.09*	38.69 ± 2.74	269.67 ± 71.49
Reticular regions				
IRt	28.60 ± 2.55	39.96 ± 3.06	31.44 ± 3.84	1094.83 ± 195.38
LRt/-PC	28.68 ± 2.60	46.22 ± 2.32*‡	25.10 ± 2.64	714.17 ± 334.06
Md-D/V	29.36 ± 2.73	39.40 ± 3.39	31.24 ± 2.92	992.00 ± 180.27
PCRt/-A	32.45 ± 3.86	40.70 ± 3.17*	26.84 ± 3.22	505.83 ± 113.70
PMn	34.34 ± 5.07	40.54 ± 0.96	25.12 ± 4.67	380.50 ± 148.36

Table 1 (cont).

	% MWAT	% IWAT	% MWAT + IWAT	Total Mean of All PRV-Labeled Cells
RVL/C1	29.32 ± 4.43	39.23 ± 5.70	31.45 ± 1.80	566.83 ± 97.08
RO	42.90 ± 8.41	37.32 ± 6.54	19.78 ± 2.89	61.33 ± 10.41
rs	28.39 ± 1.19	36.29 ± 3.06	35.31 ± 2.56	471.33 ± 109.74
Sol	26.42 ± 2.06	42.32 ± 3.32*‡	31.26 ± 2.59	3533.83 ± 586.94
Sub-CD/V	24.04 ± 2.12	35.17 ± 5.91	40.79 ± 6.01	301.50 ± 109.35
Trigeminal areas	32.10 ± 4.02	38.48 ± 2.68	29.43 ± 4.25	758.00 ± 205.03
Vestibular areas	32.01 ± 3.81	41.99 ± 2.21*‡	26.00 ± 2.56	552.00 ± 163.80
vsc	31.28 ± 2.63	40.57 ± 2.46*‡	28.15 ± 2.39	1002.50 ± 166.14
Midbrain				
Posterior commissure	29.46 ± 3.50	46.68 ± 4.56*‡	23.86 ± 3.74	69.67 ± 23.34
CnF	25.97 ± 2.93*	36.27 ± 3.31‡	37.76 ± 3.22	120.83 ± 29.82
Dk	15.78 ± 12.06	45.01 ± 5.49	39.21 ± 8.13	84.50 ± 30.85
DpMe	27.39 ± 4.23	39.65 ± 3.86	32.96 ± 4.88	160.33 ± 36.88
EW	24.66 ± 2.75	44.24 ± 3.89*‡	31.10 ± 3.63	52.83 ± 14.48
InC	40.67 ± 6.45	34.02 ± 4.25	25.31 ± 6.31	95.67 ± 28.42
InCo	25.19 ± 12.51	28.95 ± 4.70	45.86 ± 15.48	28.83 ± 10.53
Lemniscus	28.28 ± 6.13	36.99 ± 3.71	34.73 ± 2.70	19.40 ± 5.07
mlf	29.12 ± 2.79	39.04 ± 2.93‡	31.84 ± 2.18	435.67 ± 71.00
Oculomotor	29.95 ± 3.26	36.07 ± 3.65	33.97 ± 2.06	291.67 ± 76.58
Peri Olivary	28.26 ± 5.51	34.66 ± 3.36	37.08 ± 6.28	65.17 ± 24.31
PAG				

Table 1 (cont).

	% MWAT	% IWAT	% MWAT + IWAT	Total Mean of All PRV-Labeled Cells
PAG anterior	25.88 ± 2.85	37.39 ± 4.69	36.72 ± 5.56	124.00 ± 28.56
DLPAG	29.59 ± 2.69	45.23 ± 3.17*‡	25.17 ± 4.00	117.00 ± 20.56
DMPAG	26.21 ± 2.85	36.76 ± 3.50‡	37.02 ± 4.19	197.50 ± 33.87
LPAG	24.16 ± 2.96*	38.37 ± 2.67‡	37.46 ± 3.78	445.33 ± 83.26
VLPAG	26.82 ± 2.32	37.75 ± 3.58‡	35.44 ± 3.25	282.50 ± 55.14
pn				
PnC	29.04 ± 5.33	42.80 ± 5.04	28.16 ± 3.19	77.17 ± 30.03
PnO	29.93 ± 4.65	30.87 ± 4.55	39.20 ± 6.10	135.33 ± 10.43
PnR	27.50 ± 8.96	52.50 ± 13.58	20.00 ± 13.07	9.00 ± 3.70
PnV	21.03 ± 1.34	57.67 ± 9.56	21.30 ± 8.54	23.75 ± 14.82
pv	27.86 ± 4.87	35.63 ± 2.68	36.51 ± 3.83	68.50 ± 13.42
R	30.01 ± 2.17	36.00 ± 3.23	33.98 ± 3.74	188.17 ± 32.98
Rubral areas	23.60 ± 4.09*	38.28 ± 2.96‡	38.12 ± 4.70	165.00 ± 46.53
scp	28.07 ± 4.59	36.80 ± 4.17	35.13 ± 3.28	157.40 ± 50.52
SN	30.62 ± 6.34	41.20 ± 5.24	28.18 ± 3.77	134.50 ± 36.58
Tegmental areas				
ATg	18.89 ± 10.08	54.19 ± 8.75	26.93 ± 10.97	12.25 ± 3.90
DMTg	28.39 ± 3.01	43.15 ± 5.48	28.45 ± 4.82	97.75 ± 35.97
DTg-C/P	28.12 ± 8.37	52.56 ± 4.19	19.32 ± 6.12	32.20 ± 12.13
LDTg/-V	22.63 ± 4.30*	42.96 ± 3.80‡	34.41 ± 2.87	215.67 ± 84.31
MiTg	23.16 ± 4.56	40.70 ± 10.12	36.13 ± 5.56	22.75 ± 3.92

Table 1 (cont).

	% MWAT	% IWAT	% MWAT + IWAT	Total Mean of All PRV-Labeled Cells
PDTg	38.35 ± 5.85	41.00 ± 2.84	20.65 ± 5.81	30.33 ± 6.06
PPTg	25.88 ± 2.07*	33.37 ± 2.73‡	40.75 ± 2.40	219.17 ± 44.23
RtTg/-P	29.18 ± 5.05	41.58 ± 8.97	29.24 ± 11.21	38.33 ± 10.55
SPTg	27.28 ± 4.10	37.45 ± 3.50	35.27 ± 4.42	44.40 ± 14.77
VLTg	21.39 ± 2.18	29.70 ± 4.65	48.92 ± 6.53‡	61.75 ± 7.60
VTg	23.30 ± 10.33	27.94 ± 9.90	48.77 ± 15.56	27.83 ± 8.32
VTA	25.56 ± 2.95	31.21 ± 6.14	43.22 ± 4.68	159.33 ± 41.45
Forebrain				
Hypothalamic				
AH	38.92 ± 2.83*	41.53 ± 2.48*	19.54 ± 1.56	298.33 ± 74.58
Arc	33.09 ± 2.78	41.90 ± 3.50*	25.00 ± 3.20‡	200. 00 ± 51.94
DM	19.77 ± 7.01	35.67 ± 6.62	44.56 ± 12.71	288.83 ± 63.52
DTM	24.44 ± 5.67	42.16 ± 9.34	33.40 ± 11.43	43.60 ± 5.26
LA	35.45 ± 3.18*	45.28 ± 1.24*	19.27 ± 4.02	74.33 ± 15.67
LH				
LH proper	28.42 ± 2.67	38.65 ± 2.60‡	32.94 ± 2.67	617.83 ± 148.17
subZI	33.63 ± 1.35	30.33 ± 2.33	36.04 ± 2.09	241.50 ± 37.07
Pe/AVPe	39.56 ± 1.82*	39.00 ± 2.45*	21.44 ± 1.59	490.50 ± 76.94
PH	28.45 ± 3.08	37.36 ± 4.42	34.19 ± 2.92	198.83 ± 92.70
ADP	34.93 ± 3.03	36.68 ± 4.13	28.39 ± 3.41	66.17 ± 14.60

Table 1 (cont).

	% MWAT	% IWAT	% MWAT + IWAT	Total Mean of All PRV-Labeled Cells
POA				
LPO	29.40 ± 3.97	32.82 ± 4.23	37.78 ± 3.10	244.50 ± 44.24
MnPO	29.17 ± 8.11	36.75 ± 11.72	34.08 ± 9.19	38.40 ± 11.82
MPA	27.28 ± 2.67	38.85 ± 3.62‡	33.87 ± 1.89	473.00 ± 83.49
MPO-C/L/M	31.09 ± 4.03	40.10 ± 3.82*	28.81 ± 1.62	443.83 ± 59.65
StA	46.43 ± 3.57*	33.93 ± 8.93	19.64 ± 5.36	5.50 ± 1.50
VLPO	29.17 ± 2.93	39.28 ± 6.10	31.55 ± 4.17	43.60 ± 15.42
VMPO	39.35 ± 17.11	29.12 ± 10.01	31.54 ± 8.27	14.80 ± 5.89
VOLT	37.00 ± 3.07*	45.71 ± 5.24*	17.29 ± 7.47	16.80 ± 3.85
PVH				
PaAP	39.41 ± 4.29	34.81 ± 6.26	25.77 ± 2.99	76.67 ± 16.75
PaDC	32.54 ± 3.60	32.16 ± 4.90	35.29 ± 6.80	50.67 ± 13.68
PaLM	33.84 ± 3.10	31.95 ± 2.66	34.21 ± 3.11	171.33 ± 29.47
PaMM	38.58 ± 3.21*	34.40 ± 2.00*	27.02 ± 1.88	227.67 ± 34.84
PaMP	36.08 ± 2.58*	36.57 ± 2.45*	27.35 ± 2.05	213.33 ± 34.90
PaPo	30.79 ± 3.44	38.94 ± 3.81	30.28 ± 3.93	112.83 ± 28.14
PaV	37.62 ± 6.31	36.17 ± 8.51	26.21 ± 3.54	69.17 ± 12.77
SPa	42.69 ± 3.18*	37.77 ± 3.86*	19.54 ± 3.64	48.83 ± 9.67
SCh				
SCh anterior	39.88 ± 8.94*	41.44 ± 7.49	18.68 ± 3.73	83.67 ± 16.31

Table 1 (cont).

	% MWAT	% IWAT	% MWAT + IWAT	Total Mean of All PRV-Labeled Cells
SChDM	38.60 ± 9.56	43.72 ± 5.48*	17.68 ± 6.20	36.83 ± 8.40
SChVL	33.74 ± 5.34	42.07 ± 6.49	24.19 ± 5.27	35.67 ± 11.39
VMH	31.20 ± 1.96	42.15 ± 4.64*	26.65 ± 3.54	142.83 ± 36.24
Thalamic				
PF	27.77 ± 5.22	35.06 ± 5.42	37.18 ± 5.71	80.33 ± 31.15
Re/VRe/Xi	36.27 ± 1.81*	37.66 ± 1.62*	26.07 ± 2.71	222.00 ± 46.41
Other forebrain areas				
BST	35.88 ± 2.92*	38.06 ± 3.08*	26.07 ± 3.31	499.50 ± 151.57
Fascicular	29.66 ± 4.52	40.53 ± 3.06	29.81 ± 5.74	74.00 ± 20.36
LS	35.48 ± 5.37	37.69 ± 7.86	26.83 ± 3.05	31.67 ± 6.69
Mammillary bodies	32.23 ± 6.88	35.97 ± 7.72	31.79 ± 8.40	119.33 ± 38.30
PeF	23.10 ± 3.83	45.39 ± 7.20	31.51 ± 8.47	49.00 ± 10.56
PSTh	24.78 ± 5.14	35.98 ± 4.74	39.24 ± 6.17	131.20 ± 49.05
SI	34.04 ± 3.43	39.08 ± 2.89	26.88 ± 3.95	123.67 ± 27.05
TC	32.60 ± 4.39	44.93 ± 7.21*	22.47 ± 5.03	43.00 ± 13.88
VP	31.51 ± 2.94*	45.51 ± 2.51*	22.97 ± 1.61	100.00 ± 65.13
ZI	35.29 ± 1.92	36.03 ± 2.51	28.67 ± 3.22	215.00 ± 52.44

Hindbrain: 12/12N, hypoglossal nucleus; 10 (DMV), dorsal motor nucleus of vagus; A5, A5 noradrenaline cells; Amb, ambiguus nucleus; AP, area postrema; Bar, Barrington's nucleus; C3, C3 adrenaline cells; Cu/Ecu, cuneate nucleus/external cuneate nucleus; DPGi, dorsal paragigantocellular nucleus; Gi, gigantocellular reticular nucleus; GiA, gigantocellular reticular nucleus, alpha part; GiV, gigantocellular reticular nucleus, ventral part; LPGi, lateral paragigantocellular nucleus; In/InM, intercalated nucleus of the medulla/intermedius nucleus of the medulla; LC, locus coeruleus; Li, linear nucleus of the medulla; LPB, lateral parabrachial

nucleus; MPB, medial parabrachial nucleus; Ppy, peripyramidal nucleus; Pr, prepositus nucleus; DR, dorsal raphe nucleus; RC, raphe cap; CLi/RLi, caudal linear nucleus of the raphe/rostral linear nucleus of the raphe; MnR, median raphe nucleus; PMnR, paramedian raphe nucleus; RMg, raphe magnus nucleus; ROb, raphe obscurus nucleus; RPa, raphe pallidus nucleus; IRt, intermediate reticular nucleus; LRt/-PC, lateral reticular nucleus/-parvicellular part; Md-D/V, medullary reticular nucleus-dorsal/ventral parts; PCRt/-A, parvicellular reticular nucleus/-alpha part; PMn, paramedian reticular nucleus; RVL/C1, rostroventrolateral reticular nucleus/C1 adrenaline cells; Ro, nucleus of Roller; rs, rubrospinal tract; Sol, nucleus of the solitary tract; Sub-CD/V, subcoeruleus nucleus-dorsal/ventral parts; vsc, ventral spinocerebellar tract.

Midbrain: CnF, cuneiform nucleus; Dk, nucleus of Darkschewitsch; DpMe, deep mesencephalic nucleus; EW, Edinger-Westphal nucleus; InC, interstitial nucleus of Cajal; InCo, intercollicular nucleus; mlf, medial longitudinal fasciculus; PAG, periaqueductal gray; PAG anterior, periaqueductal gray anterior; DLPAG, dorsolateral periaqueductal gray; DMPAG, dorsomedial periaqueductal gray; LPAG, lateral periaqueductal gray; VLPAG, ventrolateral periaqueductal gray; Pn, pontine nuclei; PnC, pontine reticular nucleus nucleus, caudal part; PnO, pontine reticular nucleus, oral part; PnR, pontine raphe nucleus; PnV, pontine reticular nucleus, ventral part; pv, periventricular fiber system; R, red nucleus; scp, superior cerebellar peduncle; SN, substantia nigra; ATg, anterior tegmental nucleus; DMTg, dorsomedial tegmental area; DTg-C/P, dorsal tegmental nucleus -central/pericentral parts; LDTg/-V, laterodorsal tegmental nucleus/-ventral part; MiTg, microcellular tegmental nucleus; PDTg, posterodorsal tegmental nucleus; PPTg, pedunculopontine tegmental nucleus; RtTg/-P, reticulotegmental nucleus of the pons/-pericentral part; SPTg, subpedencular tegmental nucleus; VLTg, ventrolateral tegmental area; VTg, ventral tegmental nucleus; VTA, ventral tegmental area.

Forebrain: AH, anterior hypothalamus; Arc, arcuate nucleus; DM, dorsomedial hypothalamic nucleus; DTM, dorsal tuberomammillary nucleus; LA, lateroanterior hypothalamic nucleus; LH, lateral hypothalamic area; LH proper, lateral hypothalamic area proper; subZI, sub-zona incerta; Pe/AVPe, periventricular hypothalamic nucleus/anteroventral periventricular nucleus; PH, posterior hypothalamic area; ADP, anterodorsal preoptic nucleus; POA, preoptic area; LPO, lateral preoptic area; MnPO, median preoptic nucleus; MPA, medial preoptic area; MPO-C/L/M, medial preoptic nucleus-central/lateral/medial parts; StA, strial part of the preoptic area; VLPO, ventrolateral preoptic nucleus; VMPO, ventromedial preoptic nucleus; VOLT, vascular organ of the lamina terminalis; PVH, paraventricular nucleus of the hypothalamus; PaAP, paraventricular hypothalamic nucleus, anterior parvicellular part; PaDC, paraventricular hypothalamic nucleus, dorsal cap; PaLM, paraventricular hypothalamic nucleus, lateral magnocellular part; PaMM, paraventricular hypothalamic nucleus, medial magnocellular part; PaMP, paraventricular hypothalamic nucleus, medial parvicellular part; PaPo, paraventricular hypothalamic nucleus, posterior part; PaV, paraventricular hypothalamic nucleus, ventral part; SPa, subparaventricular zone of the hypothalamus; SCh, suprachiasmatic nucleus; SCh, anterior, suprachiasmatic nucleus, anterior; SChDM, suprachiasmatic nucleus, dorsomedial part; SChVL, suprachiasmatic nucleus, ventrolateral part; VMH, ventromedial hypothalamic nucleus; PF, parafascicular thalamic nucleus; Re/VRe/Xi, reuniens thalamic nucleus/ventral reuniens thalamic nucleus/xiphoid thalamic nucleus; BST, bed nucleus of the stria terminalis; LS, lateral septal nucleus; PeF, perifornical nucleus; PSTh, parasubthalamic nucleus; SI, substantia innominata; TC, tuber cinereum area; VP, ventral pallidum; ZI, zona incerta.

Table 2.2 Body weight changes before and after 16 h food deprivation.
Data are presented as means ± SE. *p<0.05 vs. *ad libitum*-fed.

Condition	Initial Body Mass (g)	Final Body Mass (g)	Δ Body Mass (g)
Ad libitum-Fed	39.30 ± 1.00	39.29 ± 1.01	-0.01 ± 0.22
16 h Food Deprivation	38.91 ± 0.97	36.82 ± 0.85*	-2.10 ± 0.18*

2.5 Discussion

The present study used isogenic strains of PRV that have a distinct fluorescent reporters of either GFP or mRFP to reveal, for the first time, both separate and shared SNS outflow circuitries between true visceral WAT (MWAT) and subcutaneous WAT (IWAT) in a rodent species and to our knowledge any species. The labeled central outflow circuits to MWAT and IWAT from the present study are reminiscent of the general overall pattern of viral infections labeling the SNS outflow from the brain to WAT seen previously for IWAT (4; 4; 54; 64), EWAT (4; 64), and RWAT (1) using PRV.

We performed extensive histological analyses across the neuroaxis. We previously demonstrated the distribution of the postganglionic SNS innervation of IWAT and EWAT (64) using a fluorescent monosynaptic retrograde tract tracer (Fluorogold) and demonstrated largely differential innervation of this subcutaneous and intra-abdominal WAT depot, respectively (64). Here we found largely separate SNS innervation between MWAT and IWAT with a greater percentage of single-labeled neurons to IWAT as compared to MWAT and ~20-55% of shared neurons between the two WAT depots within the brain. Such separation of the SNS outflow from brain to WAT depots such as these allows for the relative unique patterns of sympathetic drive to WAT depots with various lipolytic challenges [for review see: (6; 7)]. This peripheral delineation of innervation between MWAT and IWAT makes it plausible to support the contribution of MWAT to hepatic insulin resistance and overall the metabolic syndrome with IWAT

contributing as a relatively safe repository of excess lipid energy (25; 46). We found a higher percentage of single-labeled neurons from the T5-T13 for MWAT than IWAT when we collapsed the labeled cells for each sympathetic ganglia from the thoracic (T5-T13) and lumbar (L1-L3) sympathetic ganglia, suggesting that MWAT has a greater thoracic SNS innervation as well, perhaps, contributing to a higher level of basal lipolysis and, as a result, increases in FFA release to the hepatic portal vein (2). As noted however, this apparent increase in postganglionic sympathetic innervation of MWAT did not translate into a greater NETO with food deprivation to this depot relative to the other WAT pads. The differences between innervation of MWAT and IWAT in the IML of the spinal cord were not observed suggesting that differential SNS drive to MWAT and WAT may originate from the sympathetic chain (~60% of single-labeled neurons for each WAT depot).

The arrangement of preganglionic neurons of the IML innervating several postganglionic neurons within the sympathetic chain before that final projection to the target tissue permits a single sympathetic neuron within the IML nucleus of the spinal cord to synapse on many excitatory or inhibitory postganglionic neurons or in other cases to have a single or few projections to postganglionic neurons (30). Therefore, this aspect of the SNS allows for both convergence and divergence for target tissue innervation resulting in possible coordination of sympathetic outflow to multiple WAT depots as well as control of outflow to individual WAT depots. This divergence is perhaps exemplified not only by the increased NETO to IWAT versus MWAT in the present study, but also by the unique patterns of sympathetic drive (NETO) across WAT and BAT pads for each lipolytic stimulus [food deprivation (13), short day photoperiod (64), central melanocortin 4-receptor agonism (12), food deprivation (13), cold exposure (13), and glucoprivation (13)]. Thus, it is not surprising that there are low percentages of double-

labeled neurons in the sympathetic chain (~10-30%), because if they were plentiful or completely overlapping, then such nearly unique patterns of sympathetic drive for each stimulus would be rare or not even possible.

More centrally across the brain, we found an overlap (~20-55% of doubly-infected neurons) between the two SNS outflow circuitries to MWAT and to IWAT. IWAT had significantly more single-labeled neurons than MWAT for several hindbrain regions: Amb, AP, DPGi, Li, Ppy, Pr, DR, CLi/RLi, LRt/-PC, Sol, vestibular areas, and vsc, some midbrain regions: posterior commissure, CnF, EW, mlf, DLPAG, DMPAG, LPAG, VLPAG, rubral areas, LDTg/-V, and PPTg, and a few forebrain sites: LH proper and MPA. The remaining brain regions had roughly equal percentages of single-labeled neurons across the brain for the outflow circuitries to IWAT and to MWAT. The regions that are typically known to be involved in energy metabolism and of sympathetic outflow were labeled by both PRVs as seen in our earlier work (4; 11; 54) and always include the original five areas noted by Strack et al. (59) – the PVH, A5 noradrenergic cell group, caudal raphe region (including the NTS, raphe pallidus, RMg, RPa,), rostral ventrolateral medulla, and ventromedial medulla. Though there are these distinct differences across these brain regions, many of the brain areas ultimately innervating these two WAT depots were more similar than different.

There are caveats with utilization of two isogenic viral tract tracers (PRVs), including but not limited to the issue of one PRV infecting a neuron first and preventing the second PRV from doing so – the so-called ‘principle of exclusion’ in virology, as well as the virulence of one PRV dominating the infection if they do reach the neurons at approximately the same time [for review see: (15; 53)]. We have decreased the likelihood of these problems by conducting preliminary studies, however, as discussed in the Methods section. It should be noted that it is not possible to

design the timing of the injections from two peripheral sites to assure nearly simultaneous reaching of the two viruses for every area of interest in the brain. Because of these potential difficulties, even though we attempted to minimize them, it is always assumed that the percentage of double-labeled neurons may actually be much greater (53).

We functionally tested this differential (but also shared) SNS innervation of IWAT and MWAT depots through the energetic challenge of food deprivation (16 h), which we previously significantly increased IWAT and EWAT NETO (the latter a small but significant increase) with food deprivation, but no change for RWAT or IBAT (13). Here IWAT NETO more than doubled and EWAT NETO showed a small but non-significant increase ($p=0.06$), with no change in NETO for RWAT or IBAT as seen previously (13). This is the first time we assayed MWAT NETO. The finding of differential sympathetic drives to MWAT and to IWAT in this study may have, as its neuroanatomical basis, some of the differences we found in the PRV-induced labeling of the sympathetic outflow circuits from the brain to these WAT depots across the neuroaxis. At most, only ~20-55 % of PRV-infected neurons were doubly-labeled indicating participation in the SNS outflow to both depots, and much less when approaching the final common pathways in the IML (~10%) and sympathetic chain (~10-30%). Human visceral WAT has higher lipolytic rates than subcutaneous WAT (see Perspectives directly below), but unlike humans, this is a MWAT relatively small intra-abdominal WAT depot in rodents in general (18) and in our hamsters specifically. In humans, there are clear distinctions between substances produced and possible contributions of MWAT versus the normally greater mass of omental WAT (60). Omental WAT is absent in rodents or perhaps may be present as an almost imperceptible white ‘spot’ or ‘stripe’ on the stomach fundus of laboratory rats, mice and Syrian and Siberian hamsters (T. J. Bartness, R. S. Harris and P. Scherer, independent unpublished

observations). IWAT, given its larger capacity to store lipid and its non-association with an organ that can have local physiological functions (17), in principle, is in a better position to supply lipid energy fuels with food deprivation than other WAT pads. Indeed, with the exception of short winter-like photoperiod exposure in Siberian hamsters where NETO is greater in EWAT than IWAT (64), NETO in IWAT is increased more than in any of the other WAT pads with cold exposure (13), food deprivation [shown previously (13) and here], glucoprivation (13) and central melanocortin receptor agonism (12).

Here we have demonstrated that MWAT (visceral WAT) and IWAT (subcutaneous WAT) have relatively separate SNS circuitries in the periphery with moderately shared but more substantial separate circuitries across the brain. We demonstrated that subcutaneous WAT (IWAT) has a greater sympathetic drive with food deprivation when compared with visceral WAT (MWAT).

2.6 Perspectives and Significance

Several studies demonstrated that visceral WAT has a higher rate of basal (i.e., non-SNS/NE-stimulated lipolysis), lipolysis and that in general, human visceral white adipocytes have higher basal lipolytic rates than do subcutaneous adipocytes [e.g., (45; 63); c.f. (3)]. The role of adrenoceptor stimulation in basal lipolysis also may be somewhat independent of β-adrenoceptor stimulation with factors affecting adipose triglyceride lipase (ATGL; a.k.a. desnutrin) being more important for basal lipolysis (27). Clearly, however, as we have shown here and previously, there is sympathetic drive occurring in the *in vivo* non-energetically challenged situation that also should be important for basal lipolysis via the adenylyl cyclase/cAMP/protein kinase A phosphorylation/hormone sensitive lipase and perilipin A phosphorylation intracellular signaling pathway (8).

Regarding SNS/NE- stimulated lipolysis, however, the data are mixed with subcutaneous WAT having greater stimulated lipolysis than MWAT *in vitro* (63). *In vivo*, using phosphorylated HSL and perilipin A as markers of lipolysis in WAT pads, central melanocortin 4-receptor-stimulated lipolysis that increases SNS drive (NETO) to subcutaneous WAT (IWAT and dorsosubcutaneous WAT), but not intra-abdominal WAT [EWAT, RWAT; (12)], only increases phosphorylated HSL and phosphorylated perilipin A in these subcutaneous WAT pads with increases in NETO, but not the intra-abdominal ones (49) demonstrating the *in vivo* physiological coupling of increases in SNS drive to lipolysis. Thus, it is difficult to unequivocally unify *in vitro* tests of β-adrenoceptor stimulated lipolysis to the *in vivo* physiological condition.

The conventional wisdom for the involvement of lipolysis/FFAs in the metabolic syndrome is that it is the result of excess systemic FFA coming from visceral WAT that would include mesenteric and omental WAT depots in humans that drain into the hepatic-portal vein [reviewed in: (32)]. It is now clear, however, that upper body non-splanchnic draining WAT instead of visceral hepatic-portal vein draining WAT is the main source of FFAs and thus, the likely culprit for the adverse health consequences in humans [for review see (31; 32)]. Most non-human animal studies that purport to study the effects of or differences in visceral versus subcutaneous WAT do not use hepatic-portal draining WAT which, as noted above, is only MWAT in rodents. The negligible/undetectable sympathetic drive (NETO) to MWAT with food deprivation in the present studies casts some doubt as to whether, although visceral WAT by definition, this WAT depot is the human equivalent of visceral WAT and therefore, even actual visceral WAT in rodents may not mimic the human condition. In humans, distinctions between the functions and pathophysiology of MWAT and omental WAT are emerging, with MWAT

seen as having independent effects on the metabolic syndrome from omental WAT (34). For example, omental WAT has greater adrenoceptor-stimulated lipolysis than MWAT *in vitro* (23). Thus, for human and non-human animals it seems evident that WAT depots should not be thought of as uniform in any sense of the word including innervation and sympathetic drive, along with cytokine and other substance production (60). This begs for a more thorough understanding of why the depots are associated with nearby organs and whether this is just by chance, or as with EWAT and the testes in frogs, laboratory rats and mice, and Syrian hamsters, is necessary for functions of the adjacent organ, in this example spermatogenesis (17; 22; 22; 58).

2.7 Acknowledgements

The authors thank Yaakov G. Mitchell for assistance with virus injections, Keegan T. Murphy and Danni Liu for assistance with tissue harvesting and Eleen Zarebidaki and Benjamin Blaschke with norepinephrine extractions. The authors also thank Dr. Vitaly Ryu for helpful discussions on the manuscript. This work was funded by NIH DK35254 to TJB.

2.8 References

1. **Adler ES, Hollis JH, Clarke IJ, Grattan DR and Oldfield BJ.** Neurochemical characterization and sexual dimorphism of projections from the brain to abdominal and subcutaneous white adipose tissue in the rat. J Neurosci 32: 15913-15921, 2012.

2. **Arner P.** Insulin resistance in type 2 diabetes: role of fatty acids. Diabetes Metab Res Rev 18 Suppl 2: S5-S9, 2002.

3. **Arner P.** Human fat cell lipolysis: biochemistry, regulation and clinical role. Best Pract Res Clin Endocrinol Metab 19: 471-482, 2005.

4. **Bamshad M, Aoki VT, Adkison MG, Warren WS and Bartness TJ.** Central nervous system origins of the sympathetic nervous system outflow to white adipose tissue. Am J Physiol 275: R291-R299, 1998.

5. **Banfield BW, Kaufman JD, Randall JA and Pickard GE.** Development of pseudorabies virus strains expressing red fluorescent proteins: new tools for multisynaptic labeling applications. J Virol 77: 10106-10112, 2003.

6. **Bartness TJ and Bamshad M.** Innervation of mammalian white adipose tissue: Implications for the regulation of total body fat. Am J Physiol 275: R1399-R1411, 1998.

7. **Bartness TJ, Shrestha YB, Vaughan CH, Schwartz GJ and Song CK.** Sensory and sympathetic nervous system control of white adipose tissue lipolysis. Mol Cell Endocrinol 318: 34-43, 2010.

8. **Bezaire V and Langin D.** Regulation of adipose tissue lipolysis revisited. Proc Nutr Soc 68: 350-360, 2009.

9. **Beznak ABL and Hasch Z.** The effect of sympathectomy on the fatty deposit in connective tissue. Quart J Exptl Physiol 27: 1-15, 1937.

10. **Bjorntorp P.** Adipose tissue distribution and function. Int J Obesity 15: 67-81, 1991.

11. **Bowers RR, Festuccia WTL, Song CK, Shi H, Migliorini RH and Bartness TJ.** Sympathetic innervation of white adipose tissue and its regulation of fat cell number. Am J Physiol 286: R1167-R1175, 2004.

12. **Brito MN, Brito NA, Baro DJ, Song CK and Bartness TJ.** Differential activation of the sympathetic innervation of adipose tissues by melanocortin receptor stimulation. Endocrinology 148: 5339-53347, 2007.

13. **Brito NA, Brito MN and Bartness TJ.** Differential sympathetic drive to adipose tissues after food deprivation, cold exposure or glucoprivation. Am J Physiol Regul Integr Comp Physiol 294: R1445-R1452, 2008.

14. **Cantu RC and Goodman HM.** Effects of denervation and fasting on white adipose tissue. Am J Physiol 212: 207-212, 1967.

15. **Card JP.** Practical considerations for the use of pseudorabies virus in transneuronal studies of neural circuitry. Neurosci Biobehav Rev 22: 685-694, 1998.

16. **Catalano KJ, Stefanovski D and Bergman RN.** Critical role of the mesenteric depot versus other intra-abdominal adipose depots in the development of insulin resistance in young rats. Diabetes 59: 1416-1423, 2010.

17. **Chu Y, Huddleston GG, Clancy AN, Harris RB and Bartness TJ.** Epididymal fat is necessary for spermatogenesis, but not testosterone production or copulatory behavior. Endocrinology 151: 5669-5779, 2010.

18. **Cinti S.** The Adipose Organ. Milano: Editrice Kurtis, 1999.

19. **Czaja K, Barb CR and Kraeling RR.** Hypothalamic neurons innervating fat tissue in the pig express leptin receptor immunoreactivity. Neurosci Lett 425: 6-11, 2007.

20. **Czaja K, Kraeling RR and Barb CR.** Are hypothalamic neurons transsynaptically connected to porcine adipose tissue? Biochem Biophys Res Commun 311: 482-485, 2003.

21. **Demas GE and Bartness TJ.** Direct innervation of white fat and adrenal medullary catecholamines mediate photoperiodic changes in body fat. Am J Physiol 281: R1499-R1505, 2001.

22. **Faust IM, Johnson PR and Hirsch J.** Noncompensation of adipose mass in partially lipectomized mice and rats. Am J Physiol 231: 538-544, 1976.

23. **Fried SK, Leibel RL, Edens NK and Kral JG.** Lipolysis in intraabdominal adipose tissues of obese women and men. Obes Res 1: 443-448, 1993.

24. **Gasteyger C and Tremblay A.** Metabolic impact of body fat distribution. J Endocrinol Invest 25: 876-883, 2002.

25. **Gavrilova O, Marcus-Samuels B, Graham D, Kim JK, Shulman GI, Castle AL, Vinson C, Eckhaus M and Reitman ML.** Surgical implantation of adipose tissue reverses diabetes in lipoatrophic mice. J Clin Invest 105: 271-278, 2000.

26. **Giordano A, Song CK, Bowers RR, Ehlen JC, Frontini A, Cinti S and Bartness TJ.** White adipose tissue lacks significant vagal innervation and immunohistochemical evidence of parasympathetic innervation. Am J Physiol 291: R1243-R1255, 2006.

27. **Girousse A and Langin D.** Adipocyte lipases and lipid droplet-associated proteins: insight from transgenic mouse models. Int J Obes (Lond) 36: 581-594, 2012.

28. **Goldstein LB, Bushnell CD, Adams RJ, Appel LJ, Braun LT, Chaturvedi S, Creager MA, Culebras A, Eckel RH, Hart RG, Hinchey JA, Howard VJ, Jauch EC, Levine SR, Meschia JF, Moore WS, Nixon JV and Pearson TA.** Guidelines for the primary prevention of stroke: a guideline for healthcare professionals from the American Heart Association/American Stroke Association. Stroke 42: 517-584, 2011.

29. **Heilbronn L, Smith SR and Ravussin E.** Failure of fat cell proliferation, mitochondrial function and fat oxidation results in ectopic fat storage, insulin resistance and type II diabetes mellitus. Int J Obes Relat Metab Disord 28 Suppl 4: S12-S21, 2004.

30. **Janig W and McLachlan EM.** Characteristics of function-specific pathways in the sympathetic nervous system. TINS 15: 475-481, 1992.

31. **Jensen MD.** Lipolysis: contribution from regional fat. Annu Rev Nutr 17: 127-139, 1997.

32. **Jensen MD.** Is visceral fat involved in the pathogenesis of the metabolic syndrome? Human model. Obesity (Silver Spring) 14 Suppl 1: 20S-24S, 2006.

33. **Li Y, Bujo H, Takahashi K, Shibasaki M, Zhu Y, Yoshida Y, Otsuka Y, Hashimoto N and Saito Y.** Visceral fat: higher responsiveness of fat mass and gene expression to calorie restriction than subcutaneous fat. Exp Biol Med (Maywood) 228: 1118-1123, 2003.

34. **Liu KH, Chan YL, Chan WB, Chan JC and Chu CW.** Mesenteric fat thickness is an independent determinant of metabolic syndrome and identifies subjects with increased carotid intima-media thickness. Diabetes Care 29: 379-384, 2006.

35. **Mefford IN.** Application of high performance liquid chromatography with electrochemical detection to neurochemical analysis: measurement of catecholamines, serotonin and metabolites in rat brain. J Neurosci Methods 3: 207-224, 1981.

36. **Migliorini RH, Garofalo MAR and Kettelhut IC.** Increased sympathetic activity in rat white adipose tissue during prolonged fasting. Am J Physiol 272: R656-R661, 1997.

37. **Mul JD, O'Duibhir E, Shrestha YB, Koppen A, Vargovic P, Toonen PW, Zarebidaki E, Kvetnansky R, Kalkhoven E, Cuppen E and Bartness TJ.** Pmch-deficiency in rats is associated with normal adipocyte differentiation and lower sympathetic adipose drive. PLoS ONE 8: e60214, 2013.

38. **Murphy KT, Schwartz GJ, Nguyen NL, Mendez JM, Ryu V and Bartness TJ.** Leptin-sensitive sensory nerves innervate white fat. Am J Physiol Endocrinol Metab 304: E1338-E1347, 2013.

39. **Nautiyal KM, Dailey MJ, Brito NA, Brito MN, Harris RBS, Bartness TJ and Grill HJ.** Energetic responses to cold temperatures in rats lacking forebrain-caudal brainstem connections. Am J Physiol 295: R789-R798, 2008.

40. **Ohman MK, Shen Y, Obimba CI, Wright AP, Warnock M, Lawrence DA and Eitzman DT.** Visceral adipose tissue inflammation accelerates atherosclerosis in apolipoprotein E-deficient mice. Circulation 117: 798-805, 2008.

41. **Pasanisi F, Contaldo F, de Simone G and Mancini M.** Benefits of sustained moderate weight loss in obesity. Nutr Metab Cardiovasc Dis 11: 401-406, 2001.

42. **Paxinos G and Franklin KBJ.** The mouse brain in stereotaxic coordinates. San Diego: Academic Press, 2001.

43. **Rao GH, Thethi I and Fareed J.** Vascular disease: obesity and excess weight as modulators of risk. Expert Rev Cardiovasc Ther 9: 525-534, 2011.

44. **Reaven GM.** Insulin resistance: the link between obesity and cardiovascular disease. Med Clin North Am 95: 875-892, 2011.

45. **Rebuffe-Scrive M, Andersson B, Olbe L and Bjorntorp P.** Metabolism of adipose tissue in intraabdominal depots of nonobese men and women. Metabolism 38: 453-458, 1989.

46. **Reitman ML, Mason MM, Moitra J, Gavrilova O, Marcus-Samuels B, Eckhaus M and Vinson C.** Transgenic mice lacking white fat: models for understanding human lipoatrophic diabetes. Ann NY Acad Sci 892: 289-296, 1999.

47. **Shi H and Bartness TJ.** Neurochemical phenotype of sympathetic nervous system outflow from brain to white fat. Brain Res Bull 54: 375-385, 2001.

48. **Shi H, Bowers RR and Bartness TJ.** Norepinephrine turnover in brown and white adipose tissue after partial lipectomy. Physiol Behav 81: 535-543, 2004.

49. **Shrestha YB, Vaughan CH, Smith BJ, Jr., Song CK, Baro DJ and Bartness TJ.** Central melanocortin stimulation increases phosphorylated perilipin A and hormone-sensitive lipase in adipose tissues. Am J Physiol Regul Integr Comp Physiol 299: R140-R149, 2010.

50. **Smith BN, Banfield BW, Smeraski CA, Wilcox CL, Dudek FE, Enquist LW and Pickard GE.** Pseudorabies virus expressing enhanced green fluorescent protein: A tool for in vitro electrophysiological analysis of transsynaptically labeled neurons in identified central nervous system circuits. Proc Natl Acad Sci U S A 97: 9264-9269, 2000.

51. **Snijder MB, Dekker JM, Visser M, Bouter LM, Stehouwer CD, Kostense PJ, Yudkin JS, Heine RJ, Nijpels G and Seidell JC.** Associations of hip and thigh circumferences independent of waist circumference with the incidence of type 2 diabetes: the Hoorn Study. Am J Clin Nutr 77: 1192-1197, 2003.

52. **Song CK and Bartness TJ.** CNS sympathetic outflow neurons to white fat that express melatonin receptors may mediate seasonal adiposity. Am J Physiol 281: R666-R672, 2001.

53. **Song CK, Enquist LW and Bartness TJ.** New developments in tracing neural circuits with herpesviruses. Virus Res 111: 235-249, 2005.

54. **Song CK, Jackson RM, Harris RB, Richard D and Bartness TJ.** Melanocortin-4 receptor mRNA is expressed in sympathetic nervous system outflow neurons to white adipose tissue. Am J Physiol Regul Integr Comp Physiol 289: R1467-R1476, 2005.

55. **Song CK, Schwartz GJ and Bartness TJ.** Anterograde transneuronal viral tract tracing reveals central sensory circuits from white adipose tissue. Am J Physiol Regul Integr Comp Physiol 296: R501-R511, 2009.

56. **Song CK, Vaughan CH, Keen-Rhinehart E, Harris RB, Richard D and Bartness TJ.** Melanocortin-4 receptor mRNA expressed in sympathetic outflow neurons to brown adipose tissue: Neuroanatomical and functional evidence. Am J Physiol 295: R417-R428, 2008.

57. **Spector S, Sjoerdsma A and Udenfriend S.** Blockade of endogenous norepinephrine synthis by alpha-methyl-tyrosine, an inhibitor of tyrosine hydroxylase. J Pharmacol Exp Ther 147: 86-95, 1965.

58. **Srinivasan V, Thombre DP, Lakshmanan S and Chakrabarty AS.** Effect of removal of epididymal fat on spermatogenesis in albino rats. Indian J Exp Biol 24 : 487-488, 1986.

59. **Strack AM, Sawyer WB, Hughes JH, Platt KB and Loewy AD.** A general pattern of CNS innervation of the sympathetic outflow demonstrated by transneuronal pseudorabies viral infections. Brain Res 491: 156-162, 1989.

60. **Tchkonia T, Thomou T, Zhu Y, Karagiannides I, Pothoulakis C, Jensen MD and Kirkland JL.** Mechanisms and metabolic implications of regional differences among fat depots. Cell Metab 17: 644-656, 2013.

61. **Vaughan, C. H., Zarebidaki, E., Ehlen, J. C., and Bartness, T. J.** Analysis and measurement of the sympathetic and sensory innervation of white and brown adipose tissue. Methods in Enzymology. 2013. Ref Type: In Press

62. **Wertheimer E. Stoffwechselregulationen. I.** Regulation des Fettstoffwechsels. Die zentrale Regulierung der Fettmobilisierung. Pflugers Arch ges Physiol 213: 262-298, 1926.

63. **Yang YK, Chen M, Clements RH, Abrams GA, Aprahamian CJ and Harmon CM.** Human mesenteric adipose tissue plays unique role versus subcutaneous and omental fat in obesity related diabetes. Cell Physiol Biochem 22: 531-538, 2008.

64. **Youngstrom TG and Bartness TJ.** Catecholaminergic innervation of white adipose tissue in the Siberian hamster. Am J Physiol 268: R744-R751, 1995.

65. **Youngstrom TG and Bartness TJ.** White adipose tissue sympathetic nervous system denervation increases fat pad mass and fat cell number. Am J Physiol 275: R1488-R1493, 1998.

66. **Zalesin KC, Franklin BA, Miller WM, Peterson ED and McCullough PA.** Impact of obesity on cardiovascular disease. Med Clin North Am 95: 919-937, 2011.

Copyright by
American Physiological Society
The American Journal of Physiology – Regulatory, Integrative, Physiology
Nguyen NL, Barr CL, Ryu V, Cao Q, Xue B, and Bartness TJ
2017

3 SEPARATE AND SHARED SYMPATHETIC OUTFLOW TO WHITE AND BROWN FAT COORDINATELY REGULATE THERMOREGULATION AND BEIGE ADIPOCYTE RECRUITMENT

3.1 Abstract

White adipose tissue (WAT) and brown adipose tissue (BAT) are innervated and regulated by the sympathetic nervous system (SNS). It is not clear, however, whether there are shared or separate central SNS outflows to WAT and BAT that regulate their function. We injected two isogenic strains of pseudorabies virus, a retrograde transneuronal viral tract tracer, with unique fluorescent reporters into interscapular BAT (IBAT) and inguinal WAT (IWAT) of the same Siberian hamsters to define SNS pathways to both. To test the functional importance of SNS coordinated control of BAT and WAT, we exposed hamsters with denervated SNS nerves to IBAT to 4°C for 16-24 hours, and measured core and fat temperatures, and norepinephrine turnover (NETO) and uncoupling protein 1 (UCP1) expression in fat tissues. Overall, there were more SNS neurons innervating IBAT than IWAT across the neuroaxis. However, there was a greater percentage of singly labeled IWAT neurons in midbrain reticular nuclei than singly labeled IBAT neurons. The hindbrain had ~30-40% of doubly labeled neurons while the forebrain had ~25% suggesting shared SNS circuitry to BAT and WAT across the brain. The raphe nucleus, a key region in thermoregulation, had ~40% doubly labeled neurons. Hamsters with IBAT SNS denervation maintained core body temperature during acute cold challenge and had increased beige adipocyte formation in IWAT. They also had increased IWAT NETO, temperature, and UCP1 expression compared with intact hamsters. These data provide strong neuroanatomical and functional evidence of WAT and BAT SNS crosstalk for thermoregulation and beige adipocyte formation.

3.2 Introduction

The brain regulates body fat through sympathetic nervous system (SNS) nerves directly innervating peripheral fat depots. In humans and rodent models, fat is stored in white adipose tissue (WAT) and brown adipose tissue (BAT). WAT stores energy, while BAT oxidizes fatty acids and generates heat through nonshivering thermogenesis, which decreases fat mass and maintains core body temperature [for reviews see: (27, 30, 60)]. When stimulated SNS nerve terminals will release norepinephrine (NE) and initiate lipolysis in WAT and nonshivering thermogenesis in BAT [for reviews see: (5, 7, 8)]. When SNS nerves projecting to WAT and BAT are either chemically or surgically denervated, lipid mobilization (9, 16, 20, 72) and nonshivering thermogenesis (21, 28, 43) are respectively blocked. Uncoupling protein 1 (UCP1) in BAT mitochondria uncouples the electron transport during ATP synthesis and generates heat when SNS outflow to BAT is increased (14, 51). UCP1-dependent nonshivering thermogenesis is necessary for thermoregulation as demonstrated by the cold intolerance of UCP1 knockout (KO) mice during acute (18-24 hour) cold exposure without previous cold acclimation (22, 31).

Although WAT and BAT have distinct functional differences, it has been observed that WAT can remodel itself to possess BAT-like characteristics (18, 32, 39, 54, 74). BAT-like or beige adipocytes express functional UCP1 in WAT and have BAT-like multilocular lipid droplet morphology when stimulated by β adrenergic agonism (18, 39, 74). Interestingly, while UCP1 KO mice are unable to perform BAT nonshivering thermogenesis, their inguinal WAT (IWAT) shows recruitment of multilocular brown-like adipocytes (38, 65) and increased expression of the BAT marker cell death-inducing DFFA-like effector A and cytochrome c oxidase activity (41). These data are indicative of WAT remodeling in the absence of functional BAT, thus suggesting a potential crosstalk that is an interaction between WAT and BAT SNS for coordinated

thermoregulatory responses. However, the specific contribution of induced beige adipocytes in WAT to whole body thermoregulation and fat metabolism has not been tested. In addition, the neuroanatomical basis of the functional crosstalk between WAT and BAT in thermoregulation is unclear.

In previous studies investigating the SNS outflow to WAT and BAT, the central SNS neurons projecting to WAT (58, 62, 63) or to BAT were independently labeled (3, 59, 64) with pseudorabies virus (PRV), a retrograde trans-synaptic tract tracer. Similarly labeled brain regions were observed in independent WAT and BAT neuroanatomical studies suggestive of shared SNS outflow to both BAT and WAT. However, a specific neuroanatomical investigation of whether WAT and BAT have shared or separate SNS circuitries that may potentially participate in the coordinated control of thermoregulation has not been made. The use of isogenic strains of PRV each with unique fluorescent reporter protein provides an advantage to define the presence of separate or more importantly shared central SNS innervations across the neuroaxis from two fat depots within the same animal (1, 50).

Thus, the present study is designed to investigate whether there are shared or separate central SNS outflows to WAT and BAT that may coordinately regulate their functions. We have labeled the central SNS circuitries between WAT and BAT for the first time using isogenic strains of PRVs tagged with unique fluorescent reporter proteins [either green fluorescent protein (GFP) or red fluorescent protein (RFP)]. We have also tested whether there is coordinated SNS control of WAT and BAT thermogenic function in acute (16-24 hour) cold exposed hamsters with SNS denervation of BAT. For those hamsters, we assessed WAT beigeing with physiological, molecular, and histological parameters of temperature measurements, UCP1 expression, and adipocyte morphology, respectively.

3.3 Materials and Methods

3.3.1 ANIMALS

Adult male Siberian hamsters (*Phodopus sungorus*, 3 months old) were singly housed under a long day photoperiod light cycle (16 hour light:8 hour dark) and an ambient temperature of 22 ± 2°C. Hamsters were given ad libitum regular rodent chow (Purina Rodent Chow, St. Louis, MO) and tap water for all studies. We used Siberian hamsters, because they are a natural model of obesity reversal due to their seasonal obesity in long day photoperiod and its reversal in short day photoperiod (20). The adiposity of long day Siberian hamsters is comparable to rats and mice genetically manipulated for obesity or given a high fat diet and this adiposity can be manipulated without dietary intervention, but simply with photoperiod. In addition, the SNS outflow to WAT and BAT in Siberian hamsters has been extensively characterized (5, 8) and the SNS innervation of their fat tissues is comparable to other mammals with more similarities than differences in the general pattern (2, 42). All procedures were approved by the Georgia State University Institutional Animal Care and Use Committee and were in accordance with Public Health Service and United States Department of Agriculture guidelines.

3.3.2 EXPERIMENT 1: DOES IWAT AND IBAT HAVE SHARED OR SEPARATE CENTRAL SNS INNERVATIONS?

3.3.2.1 PRELIMINARY PRV INJECTIONS TESTS

It was necessary to verify that the two isogenic PRV strains infected neurons at a similar rate and that one was not more virulent than the other. As a control to ensure that they were functionally equivalent a 1:1 equal volume mix (50) of PRV 152 (3x108 pfu/mL) with GFP and PRV 614 (1.8x108 pfu/mL) with RFP were unilaterally injected into either IWAT (0.15 µl/locus, total volume of 1.5 µl) or IBAT (0.15 µl/locus, total volume of 0.75 µl) to ensure similar

virulence between the two viruses and to decrease the possibility for the phenomenon of exclusion, which occurs in a dual virus tract tracing study when a virus infects a neuron and consequently decreases the ability of another virus from infecting it (34). There were similar percentages of PRV 152 and PRV 614 SNS labeled neurons in the brains of these hamsters, thereby demonstrating functional equivalence of PRV 152 at 3x108 pfu/mL and PRV 614 at 1.8x108 pfu/mL (Nguyen, N.T. and Bartness, T.J., unpublished observations). Therefore, we used these PRV 152 and 614 titers in our dual tract tracing study with IWAT and IBAT.

3.3.2.2 DUAL PRV TRACT TRACING OF IWAT AND IBAT

All virus injections were executed according to Biosafety Level 2 standards. Based on the proximity of IWAT and IBAT to the brain, we injected PRV into IWAT first and injected isogenic PRV with a different reporter tag into IBAT 24 hours later in order to obtain the optimal time for the progression of both viruses across the neuroaxis (Nguyen, N.T. and Bartness, T.J., unpublished observations). In another cohort, the fat depots in which the isogenic PRVs were injected were reversed to account for fat depot differences in viral uptake. The number of fluorescently labeled SNS neurons across the neuroaxis (i.e., SNS ganglia, spinal cord, and brain) from the two cohorts were averaged for the calculation of singly and doubly labeled neurons. Because it was not technically possible to ensure that the PRVs simultaneously reached every brain site to label SNS outflow to IWAT and IBAT, there may be more doubly labeled neurons than we quantified despite our controls to minimize this risk.

In brief for PRV injections into IWAT, hamsters (n=7) were anesthetized. An incision was made around the inguinal region to expose the right IWAT. Hamsters were unilaterally injected with 0.15 µl of PRV 152 or PRV 614 at 10 loci along the fat depot to evenly distribute the virus. As we previously observed no side preference of PRV infection between right and left

fat depots (Song, C.K. and Bartness, T.J., unpublished observations), we performed unilateral injections of the PRV into the right IWAT depot. The Hamilton syringe was held in place for 1 minute after each injection to prevent efflux when removing the syringe. The incision site was closed with sterile wound clips, and hamsters were given subcutaneous injections of Ketofen (5 mg/kg, Fort Dodge Animal Health, Fort Dodge, IA), an analgesic, daily for 3 days post-surgery. Hamsters were transferred to clean cages. For PRV injections into IBAT, the same hamsters were re-anesthetized and shaved followed by a small interscapular incision. A unilateral injection of isogenic PRV counterpart with a different reporter tag was made into the right IBAT at 5 loci for a total of 0.75 µl 24 hours after IWAT injections. A reduced volume of PRV was injected into IBAT to accommodate its smaller size (36, 59). We followed the same surgical procedures previously used for closing the incision site and Ketofen administration. We have previously tested PRV injections for potential viral leakage by placing the virus on the surface of an exposed fat depot and found no positive labeling in the SNS ganglia, spinal cord, and brain as opposed to intra-fat injections of the virus (59). We have also examined the specificity of viral transport by injecting PRV into a SNS denervated fat depot and observed no labeling, confirming that PRV requires SNS nerves from fat for trans-synaptic labeling (26).

3.3.2.3 TISSUE FIXATION

Hamsters were euthanized 6 days after PRV injections into IWAT and perfused with 0.9% heparin saline (100 mL) followed by 4% paraformaldehyde (150 mL). Brains, spinal cords, and SNS ganglia were harvested and post-fixed in the same fixative for 4 hours (brains and spinal cords) or 15 minutes (SNS ganglia) at 4°C after which brains and spinal cords were transferred to a 30% sucrose in 0.1 M phosphate buffered saline (PBS, pH 7.4) solution and SNS ganglia to an 18% sucrose solution. Brains were sectioned at 35 µm thickness on a freezing stage

sliding microtome. Spinal cords and SNS ganglia (T1-T3, T12-L3) were sectioned at 40 µm and 16 µm, respectively, on a Leica cryostat and directly transferred to slides (Superfrost Plus, VWR International, Arlington, IL). Sections of brains, spinal cords, and SNS ganglia were stored in 0.1 M PBS with 0.1% sodium azide (NaN3) at 4ºC until double fluorescent immunohistochemistry (IHC) was performed.

3.3.2.4 DOUBLE FLUORESCENT IHC

Double fluorescent IHC was used to amplify GFP and RFP labeling in every 4th brain, spinal cord, and SNS ganglia section to eliminate counting neurons twice as we previously described (50). We have previously tested the primary and secondary antibodies used in this protocol to ensure specificity and absence of cross reactivity (50). All steps were performed at room temperature. Sections were blocked in 20% normal goat serum (NGS, Vector Laboratories, Burlingame, CA) in 0.4% PBS Triton (PBTx) for 30 minutes followed by incubation in rabbit anti-RFP (1:2000, Rockland Immunochemicals Inc., Gilbertsville, PA) and mouse anti-GFP (1:500, Abcam, Cambridge, MA) antibodies in 0.4% PBTx with 2% NGS and 0.1% NaN3 for 24 hours. Then sections were incubated with goat anti-rabbit CY3 (1:800, Jackson Immunoresearch, West Grove, PA) and goat anti-mouse Alexa 488 (1:500, Jackson Immunoresearch West Grove, PA) antibodies in 0.4% PBTx with 2% NGS for 2 hours. Double fluorescent IHC for spinal cords and SNS ganglia followed the same steps except the mouse anti-GFP and rabbit anti-RFP antibody concentrations were increased to 1:400 and 1:600, respectively, and the incubation times increased to 2 days because the sections were slide-mounted. The concentrations of goat anti-mouse Alexa 488 and goat anti-rabbit CY3 antibodies were also increased to 1:350 and 1:550, respectively. For negative controls, primary antibodies were omitted resulting in a notable absence of amplified staining.

3.3.2.5 QUANTIFICATION ANALYSIS

Quantification of PRV labeled SNS neurons was performed as previously described (50). PRV labeled SNS neurons were considered positive based on cell size, morphology, and fluorescent intensity. They were analyzed using an Olympus BX41 microscope with appropriate filters for GFP and RFP. Images were acquired at 10x and 20x magnifications using an Olympus DP73 camera and were adjusted for brightness and contrast using Adobe Photoshop CS5 (Adobe Systems, San Jose, CA, USA). Adobe Photoshop was also used to merge GFP and RFP images to visualize yellow-orange doubly labeled neurons. Positively labeled neurons singly or doubly projecting to IWAT and IBAT were quantified using the manual tag feature of Adobe Photoshop thus ensuring each neuron was counted once. A mouse brain atlas (53) was used to identify brain sites as we and others have previously done (10, 50, 58, 59, 63, 64), because no commercially available Siberian hamster brain atlas exists. Absolute values of PRV labeled SNS neurons found in each nucleus or region were either kept as absolute values or converted into a percentage of total PRV labeled SNS neurons. We also collapsed quantifications of PRV labeled neurons across the whole brain and in nuclei found in the hindbrain, midbrain, or forebrain in order to better examine the distribution of labeled SNS neurons to IWAT and/or IBAT across these large brain divisions. Distinct and collapsed neuronal quantifications were averaged across the number of hamsters. The absolute values or percentages of singly labeled IWAT and IBAT and doubly labeled neurons are represented as the mean absolute or percentage of total PRV labeled SNS neurons. For emphasis of their potential contribution and importance to thermoregulation and beigeing, we compared labeled SNS neurons across hypothalamic nuclei and classic SNS and thermoregulatory nuclei in bar graphs in addition to our table of labeled cell counts. We

quantified the labeling from the ipsilateral side of PRV injections into IWAT and IBAT in all spinal cords and SNS ganglia and presented the data in the same manner as the brain sections.

3.3.3 EXPERIMENT 2: DOES SNS DENERVATION OF IBAT INCREASE SNS DRIVE TO AND BEIGE ADIPOCYTE FORMATION IN IWAT?

3.3.3.1 NOREPINEPHRINE TURNOVER (NETO) DURING 16 HOUR COLD CHALLENGE

IBAT SNS denervation was performed using a modified method described in previous publications for IWAT SNS denervation (23, 29, 55). Briefly, age and weight matched male hamsters (n=52) were divided into two groups: vehicle control (VC) group and IBAT SNS denervated group for NETO, a direct neurochemical measure of SNS drive, in IBAT and WAT tissues. IBAT SNS denervation was achieved by microinjections of 6-hydroxydopamine (6OHDA), a selective neurotoxin to SNS nerves (55). Hamsters were anesthetized and an incision was made around the interscapular region to expose the lobes of IBAT. Saline or 6OHDA (10 mg/mL, 2 µl/locus for a total of 30 µl per IBAT lobe; Sigma-Aldrich, St. Louis, MO) was bilaterally injected into IBAT using a Hamilton syringe. The syringe was held in place for 1 minute to prevent efflux. The skin was closed with sterile wound clips and Ketofen was administered.

NETO was measured two weeks after intra-IBAT injections of 6OHDA or saline in hamsters housed either room temperature (RT) or 4ºC as described (12). In brief, hamsters were handled daily for two weeks before NETO measures to adapt them to the handling associated with the procedure and to decrease stress-induced NE release. On the day that NETO was measured, hamsters were placed either in 4ºC or RT for 16 hours and NETO was measured during the last 4 hours of the experiment (12). Hamsters were injected i.p. with α-methyl-p-tyrosine (250 mg/kg α-MPT; Sigma-Aldrich, St. Louis, MO), an active competitive inhibitor for

TH, which is the rate limiting enzyme for NE production; thus, preventing the synthesis of catecholamine. A supplemental dose of α-MPT (125 mg/kg) was given 2 hours after the initial dose to ensure the inhibition of catecholamine synthesis. Four hours after the first α-MPT injection, hamsters were weighed, then decapitated. IBAT, IWAT, epididymal WAT (EWAT), and retroperitoneal WAT (RWAT) were quickly harvested, weighed, frozen in liquid nitrogen, and stored at -80° C until NE extraction. To obtain baseline NE values for between animal calculations of NETO, one half of hamsters from each treatment and temperature groups were euthanized without receiving α-MPT injections 4 hours before the conclusion of the study (12, 70). The adipose tissues were processed and extracted for NE with dihydroxybenzylamine (Sigma-Aldrich, St. Louis, MO) as an internal control for extraction efficiency. NE content and NETO were measured as described previously [for review see: (70)] and following our methods and the modification of the method of Mefford (40). Calculations were made according to the following formula: $k = (\lg[NE]0 - \lg[NE]4)/(0.434 \times 4)$ and $K = k[NE]0$, where k is the constant rate of NE efflux, [NE]0 is the initial NE concentration, [NE]4 is the final NE concentration, and K = NETO.

3.3.3.2 IBAT SNS DENERVATION AND IBUTTON AND TRANSPONDERS IMPLANTATION

VC or 6OHDA were injected into the IBAT of a separate cohort of hamsters (n=32). IBAT and IWAT temperatures of those same hamsters were measured using implantable programmable temperature transponders (IPTT) 300 (serial no. 2144251, Bio Medic Data Systems, Seaford, DE) placed under the fat depot as previously described (11, 36, 59, 64, 68, 69). In brief, an IPTT was carefully placed under IBAT and was secured with sterile sutures (Ethicon, Johnson & Johnson, Somerville, NJ) after intra-IBAT injections of 6OHDA or saline. A small incision was made at the inguinal region to expose IWAT and another IPTT was placed

and secured under it similarly to IBAT. Temperature readings on IPTTs were detected with a portable hand-held reader programmer (model no. DAS-1001R, Bio Medic Data Systems, Seaford, DE). The portable hand-held reader for IPTTs was placed on the ventral side around the inguinal region of IWAT to detect IWAT temperature and on the dorsal side above the interscapular region to detect IBAT temperature (36, 64, 68). Each IPTT had a unique ID number and was programmed with the reader such that when the reader was placed on either ventral or dorsal side, it only read the corresponding IPTT placed under IWAT or IBAT, respectively. Core temperature was measured in the same hamsters using iButton data loggers (Maxim Integrated, DS1922L, 8KB) placed intraperitoneally as previously described (68). iButtons were calibrated using One Wire Viewer (Version 3.17.44) and programmed to automatically record core body temperature every 30 minutes during the 24 hour cold challenge. iButtons were first dipped in paraffin wax and gas sterilized. A small lateral incision was made on the ventral side of the hamster through the skin and peritoneal wall for iButton insertion into the abdominal cavity. The peritoneal wall was closed with sterile sutures and skin incision sites were closed with sterile wound clips and Ketofen was administered.

3.3.3.3 24 HOUR COLD CHALLENGE

Two weeks post surgeries, hamsters in VC and 6OHDA groups were further divided into either 4ºC or RT groups. Body mass was recorded before and after the challenge. IWAT and IBAT temperatures were recorded every hour, and core temperature was also recorded with the iButton data logger system every 30 minutes during 24 hours of the cold challenge. At the end of the 24 hour cold challenge hamsters were decapitated. IBAT, IWAT, EWAT, and RWAT were quickly dissected, weighed, frozen in liquid nitrogen, and subsequently stored at -80°C until further analysis by western blot for tyrosine hydroxylase (TH), a marker of SNS nerves, and

UCP1, a marker of brown and beige adipocytes. Portions of IWAT and IBAT were placed into tissue cassettes and stored in neutral buffered 10% formalin for fixation before paraffin embedding for fat UCP1 IHC. Remaining portions of IBAT and IWAT were used to measure calcitonin gene related peptide (CGRP), a marker of sensory nerves, to verify 6OHDA chemical specificity for SNS nerves and to measure the degree of sensory innervation in IBAT and IWAT.

3.3.3.4 WESTERN BLOT AND FAT UCP1 IHC

TH and UCP1 protein expression in IWAT and IBAT were measured by western blot as described previously (19). Primary antibodies used were rabbit anti-UCP1 (1:500; Abcam, Cambridge, MA), rabbit anti-TH (1:500, EMD Millipore, Temecula, CA), and rabbit anti-α tubulin (1:500, Cell Signaling, Danvers, MA) as a loading control. Membranes were blocked with 5% non-fat dry milk in tris buffered saline (TBS), then incubated with primary antibodies at 4°C for 24 hours. They were washed with TBS with 0.1% tween 20 followed by 2 hour incubation with goat anti-rabbit Alexa Fluor 680 nm antibody (ThermoFisher Scientific, Carlsbad, CA) at room temperature before visualization of protein bands using Odyssey FC Imaging System (Li Cor Biotechnology, Lincoln, NE). TH and UCP1 protein expression was normalized to α tubulin.

Paraffin embedded IWAT and IBAT tissues of 24 hour cold exposed hamsters were sliced at 6 μm on a rotary microtome, mounted onto slides, and dried on a warming plate (37 ˚C). Sections were deparaffinized and rehydrated followed by an antigen retrieval step with target retrieval solution (Dako, Carpinteria, CA). They were then incubated with rabbit anti-UCP1 antibody (1:150; Abcam, Cambridge, MA) overnight at 4°C followed by 20 minutes incubation with biotinylated donkey anti-rabbit antibody (1:100; Jackson Immunoresearch, West Grove, PA), then avidin-biotin complex (Vector Laboratories, Burlingame, CA) for 30 minutes per kit

direction. Lastly, 10 minute exposure to diaminobenzidine (Vector Laboratories, Burlingame, CA) was used for visualization of fat UCP1. Bright field photomicrographs were acquired at 20x and 40x magnification using an Olympus DP73 camera on an Olympus BX41 microscope.

3.3.3.5 CGRP ENZYME IMMUNOASSAY

CGRP levels in IBAT and IWAT were measured using an enzyme linked immunosorbent assay kit (SPI Bio, Massy, France) according to the manufacturer's directions as we have previously done (68). The correlation coefficient was 99.9% for CGRP assays.

3.3.3.6 STATISTICAL ANALYSES

Results are expressed as means ± SE. Statistical analyses were carried out using Systat Software (version 11.0, San Jose, CA). The percentage of PRV labeled SNS neurons projecting to IWAT and/or IBAT were transformed for analysis using square root transformation and tested for normality with Shapiro-Wilk test. A one way ANOVA with Student Newman Keuls post hoc test was used to compare the absolute values and percentages of doubly labeled neurons with singly labeled IWAT and IBAT neurons. Percentage data of labeled neurons that did not fit normal distribution and violated equal variance test were analyzed using Kruskal-Wallis test for nonparametric data. Placement of transponders under IBAT and IWAT were visually verified during fat tissue extraction post cold challenge. Fat temperature recordings of hamsters that had misplaced transponders were omitted from analysis. IBAT and IWAT temperatures were analyzed by one way repeated measures ANOVA. NETO and protein values were statistically analyzed by two way ANOVA (treatment x temperature) and core temperature data were analyzed by two way repeated measure ANOVA. The Student Newman Keuls post hoc test was used when differences within or between groups were obtained.

3.4 Results

3.4.1 EXPERIMENT 1: DOES IWAT AND IBAT HAVE SHARED OR SEPARATE CENTRAL SNS INNERVATIONS?

3.4.1.1 SNS GANGLIA

A regional distribution of PRV labeled SNS neurons to IWAT and IBAT was found across T1-T3 and T12-L3 vertebral levels of the SNS ganglia (Fig. 3.1, A-D). There was a higher percentage of singly labeled IBAT neurons at the thoracic level compared with singly labeled IWAT and doubly labeled neurons ($p<0.05$), and this pattern was reversed at the lumbar level (Fig. 3.1, C-D). T3 SNS ganglion had the highest percentage of singly labeled IBAT neurons (~60%) compared with other vertebral levels (~30%) though these values did not reach statistical differences (Fig. 3.1, A and C). The SNS ganglia from T13-L2 had a higher percentage of PRV labeled neurons projecting to IWAT compared with doubly labeled neurons ($p<0.05$; Fig. 3.1, C). This is consistent with our previous observation that there is a pattern for SNS ganglia at the lumbar level to innervate IWAT (Fig. 1, D) (58, 59).

3.4.1.2 SPINAL CORD

There was a higher percentage of singly labeled SNS neurons projecting to IBAT (~40%) and to IWAT (~50%) compared with the population of doubly labeled neurons (~10%) at all levels of the spinal cord, particularly the lumbar region ($p<0.05$; Fig. 3.2, A-D). When PRV labeled neurons in the spinal regions were collapsed the numbers of singly labeled IWAT and singly labeled IBAT neurons were greater than doubly labeled ones ($p<0.05$; Fig. 3.2, E). However, unlike the SNS ganglia, there was no difference in the percentage of singly labeled neurons projecting to either IBAT or IWAT in the spinal cord (Fig. 3.1, C-D).

3.4.1.3 BRAIN

The central SNS neurons ultimately projecting to IBAT and IWAT were labeled in a caudal to rostral manner in the brain (Figs. 3.3-3.6). Bilateral infection in the hindbrain, midbrain, and forebrain was observed when isogenic PRVs labeled SNS neurons bilaterally innervating IWAT (63) and IBAT (64). Within the whole brain and in the hindbrain, midbrain, and forebrain, there was a consistent pattern for a higher percentage of singly labeled IBAT neurons compared with singly labeled IWAT and doubly labeled neurons (Figs. 3.3-3.5; Fig. 3.6, A-B). Percentages of doubly labeled neurons vary across many distinct areas in the hindbrain, midbrain, and forebrain demonstrating evidence of greater separate SNS circuitry in some brain sites, but greater shared SNS circuitry in others (Figs. 3.3-3.5; Fig. 3.6, D-E; Table 3.1).

The hindbrain consistently had more PRV labeled SNS neurons (i.e., singly and doubly labeled neurons) than the midbrain and forebrain regions ($p<0.05$; Fig. 3.6, C). The percentage of singly labeled IBAT neurons tended to be higher than that of singly labeled IWAT and doubly labeled neurons within the hindbrain (Fig. 3.6, B). The raphe pallidus nucleus (RPa) was the only hindbrain nucleus that had a greater percentage of singly labeled IBAT neurons (~40%) compared with IWAT neurons (~20%; $p<0.05$) (Fig. 3.3, H; Fig. 3.6. E; Table 3.1). It was also the only nucleus we observed that had a higher percentage of doubly labeled neurons (~40%) compared with singly labeled IWAT neurons ($p<0.05$; Fig. 3.3, H; Fig. 3.6, E; Table 3.1). Other hindbrain sites such as the lateral paragigantocellular nucleus (LPGi), Kolliker-Fuse nucleus (KF), medullary reticular nucleus dorsal part (MdD), motor trigeminal nucleus (Mo5), solitary nucleus ventrolateral part (SolVL), and ventral spinocerebellar tract (vsc) had a general tendency to have higher percentages of singly labeled IBAT neurons compared with IWAT neurons (Fig. 3, C-D; Table 3.1). There was a higher percentage of singly labeled IWAT and IBAT neurons

than doubly labeled ones in several hindbrain regions, including the hypoglossal nucleus (12N), gigantocellular reticular nucleus (Gi), dorsal paragigantocellular nucleus (DPGi), intermediate reticular nucleus (IRt), linear nucleus of the medulla (Li), medullary reticular nucleus ventral part (MdV), and parvicellular reticular nucleus/-alpha part (PCRt/A) ($p<0.05$; Table 3.1).

The midbrain had ~60% fewer singly and doubly labeled neurons compared with the hindbrain ($p<0.05$; Fig. 3.6, C). The number of singly labeled neurons innervating either IWAT or IBAT was greater than that of doubly labeled neurons in many midbrain sites including dorsomedial tegmental area (DMTg), pontine reticular nucleus caudal oral, and ventral parts (PnC, PnO, PnV), red nucleus magnocellular part/superior cerebellar peduncle (brachium conjunctivum) (RMC/scp), red nucleus parvicellular part/scp (RPC/scp), retroparafascicular nucleus (RPF), reticulotegmental nucleus of the pons (RtTg), supraoculomotor periaqueductal gray/supraoculomotor cap (Su3/C), and supratrigeminal nucleus (Su5) ($p<0.05$; Table 3.1). There was a higher percentage of singly labeled IBAT than IWAT neurons in the DMTg and Su5 ($p<0.05$; Table 3.1). The medial longitudinal fasciculus (mlf) and ventral tegmental area (VTA) had tendencies for greater percentages of singly labeled IBAT neurons than IWAT neurons as well (Table 3.1). In contrast, the PnC and RtTg had ~20-40% more singly labeled IWAT neurons than IBAT neurons ($p<0.05$; Table 3.1).

Similar to the midbrain, the forebrain had less singly and doubly labeled neurons than the hindbrain ($p<0.05$; Fig. 3.6, C). There was a greater percentage of singly labeled neurons to either IBAT or IWAT than doubly labeled ones in the posterior hypothalamic area (PH), paraventricular nucleus of the hypothalamus (PVH) medial magnocellular part (PaMM), PVH posterior part (PaPo), PVH ventral part (PaV), subparaventricular zone of the hypothalamus (SPa), parasubthalamic nucleus (PSTh), xiphoid thalamic nucleus (Xi), and zona incerta (ZI)

($p<0.05$; Fig. 3.5, F; Table 3.1). Brain sites such as the arcuate nucleus (Arc), dorsomedial hypothalamic nucleus (DM), lateral hypothalamus (LH), medial preoptic area (MPA), medial preoptic nucleus medial part (MPOM), and PVH anterior parvicellular part (PaAP) had tendencies for higher percentages of singly labeled IBAT neurons compared with IWAT neurons, but this did not reach statistical significance (Fig. 3.5, B-C, F, H, and L; Table 3.1). The hypothalamus, located within the forebrain, has a large population of SNS neurons involved in the control of fat metabolism. We found a pattern of more singly labeled SNS neurons projecting to IBAT and IWAT in caudal hypothalamic nuclei than rostral ones such as the anterior and paraventricular hypothalamus (Fig. 3.5, B, D, F, H and K; Fig. 3.6, D).

We also examined brain sites that are classically involved in SNS outflow and essential for thermoregulation to determine if there were differences in SNS circuitries in those sites (Fig. 3.6, E). There were similar percentages of singly labeled IWAT and IBAT neurons in most of those regions except for the RPa, which had a higher percentage of singly labeled IBAT and doubly labeled neurons compared with singly labeled IWAT neurons ($p<0.05$; Fig. 3.6, E). The RPa in addition to the raphe obscurus nucleus (ROb) and A5 region (A5) had a greater percentage of doubly labeled neurons compared with the nucleus of the solitary tract (NTS), PVH, and preoptic area (POA) ($p<0.05$; Fig. 3.3, B, G, and H; Fig. 3.6, E).

3.4.2 EXPERIMENT 2: DOES SNS DENERVATION OF IBAT INCREASE SNS DRIVE TO AND BEIGE ADIPOCYTE FORMATION IN IWAT?

3.4.2.1 IBAT SNS DENERVATION IMPAIRED BAT NONSHIVERING THERMOGENESIS

All hamsters survived the acute cold challenge. There were no differences in body mass across groups before the cold challenge, nor were there differences in body mass between VC and 6OHDA treated groups at either RT or after cold exposure (Fig. 3.7, A). All cold exposed

hamsters lost weight during the challenge ($p<0.05$; Fig. 3.7, A). There were no changes in IBAT CGRP levels between VC and 6OHDA treated hamsters (Fig. 3.7, B). IBAT NETO tended to decrease in 6OHDA treated hamsters compared with VC treated ones at RT (Fig. 3.7, C). Acute cold exposure significantly increased IBAT NETO in VC hamsters, but not in 6OHDA treated hamsters ($p<0.05$; Fig. 3.7, C). Consistent with this, IBAT TH expression was lower in 6OHDA treated hamsters compared with their VCs in both cold and RT conditions ($p<0.05$; Fig. 3.7, D-E). In addition, UCP1 protein levels were reduced in IBAT of 6OHDA treated hamsters even at RT ($p<0.05$; Fig. 3.7, D and F). Twenty four hour cold exposure up-regulated UCP1 expression in IBAT of VC, but not of 6OHDA hamsters ($p<0.05$; Fig. 3.7, D and F). As expected, IBAT temperature of 6OHDA treated hamsters did not increase during cold exposure as it did in VC hamsters ($p<0.05$; Fig. 3.7, G). Specifically, IBAT temperature was lower in 6OHDA treated than VC hamsters after 4, 7-8, 11, 13, 18, and 21-22 hours of cold exposure ($p<0.05$) while there were no differences in IBAT temperatures between 6OHDA and VC treated hamsters at RT (Fig. 3.7, G-H). IBAT from 6OHDA treated hamsters in both cold and RT conditions had a WAT-like unilocular appearance with lower UCP1 immunoreactive (ir) staining compared with VC hamsters (Fig. 3.7, I). These data and the absence of change in IBAT CGRP levels in 6OHDA treated hamsters (Fig. 3.7, B) demonstrated that SNS denervation of IBAT with 6OHDA selectively impaired IBAT SNS activity without affecting sensory innervation.

3.4.2.2 THERMOREGULATORY FUNCTION AND BEIGEING IN IWAT OF IBAT SNS DENERVATED HAMSTERS

There was no difference in IWAT NETO between 6OHDA and VC treated hamsters at RT. As expected, cold exposure significantly increased IWAT NETO in VC hamsters, but the increase was exaggerated in 6OHDA treated hamsters ($p<0.05$; Fig. 3.8, A). Cold exposure also

increased NETO in EWAT and RWAT of VC hamsters ($p<0.05$), confirming previous observations (12); however, this response was absent in EWAT and attenuated in RWAT of cold exposed 6OHDA hamsters (Fig. 3.8, A). There were no differences in IWAT UCP1 expression for cold exposed VC hamsters or in either treatment group housed at RT (Fig. 3.8, B). IWAT UCP1 was increased in cold exposed 6OHDA treated hamsters, and this was significantly different ($p<0.05$) from cold exposed VC hamsters, but did not reach significance compared with hamsters housed at RT (Fig. 3.8, B). There were no differences in UCP1 protein expression in EWAT and RWAT for any of the groups (data not shown).

IBAT SNS denervated hamsters were able to maintain their core body temperatures despite impaired IBAT thermogenic function, as there were largely no differences in core body temperatures across groups either at RT or during 24 hour cold exposure (Fig. 3.8, C). By contrast, there was a consistent trend for IWAT temperatures of cold exposed IBAT SNS denervated hamsters to be increased compared with VC treated hamsters (Fig. 3.8, D). This reached significance after 5 and 8 hours ($p<0.05$) and tended to be increased after 6 ($p=0.069$) and 23 ($p=0.071$) hours of cold exposure (Fig. 3.8, D). There were no differences in IWAT temperatures between 6OHDA and VC treated groups housed at RT except at the 13th hour during the experiment, when IWAT temperature was higher in 6OHDA than VC hamsters ($p<0.05$; Fig. 3.8, E). Adipocytes in IWAT from 6OHDA treated hamsters were small and had UCP1-positive, BAT-like multilocular lipid droplet morphology (Fig. 3.8, F). 6OHDA cold exposed hamsters had the greatest amount of UCP1 ir staining compared with other groups (Fig. 3.8, F).

Finally, CGRP, a marker of sensory nerves, was increased in IWAT of 6OHDA treated hamsters versus VC treated hamsters at RT ($p<0.05$). A similar difference was observed in cold exposed hamsters, but did not reach statistical significance ($p=0.069$; Fig. 3.8, G).

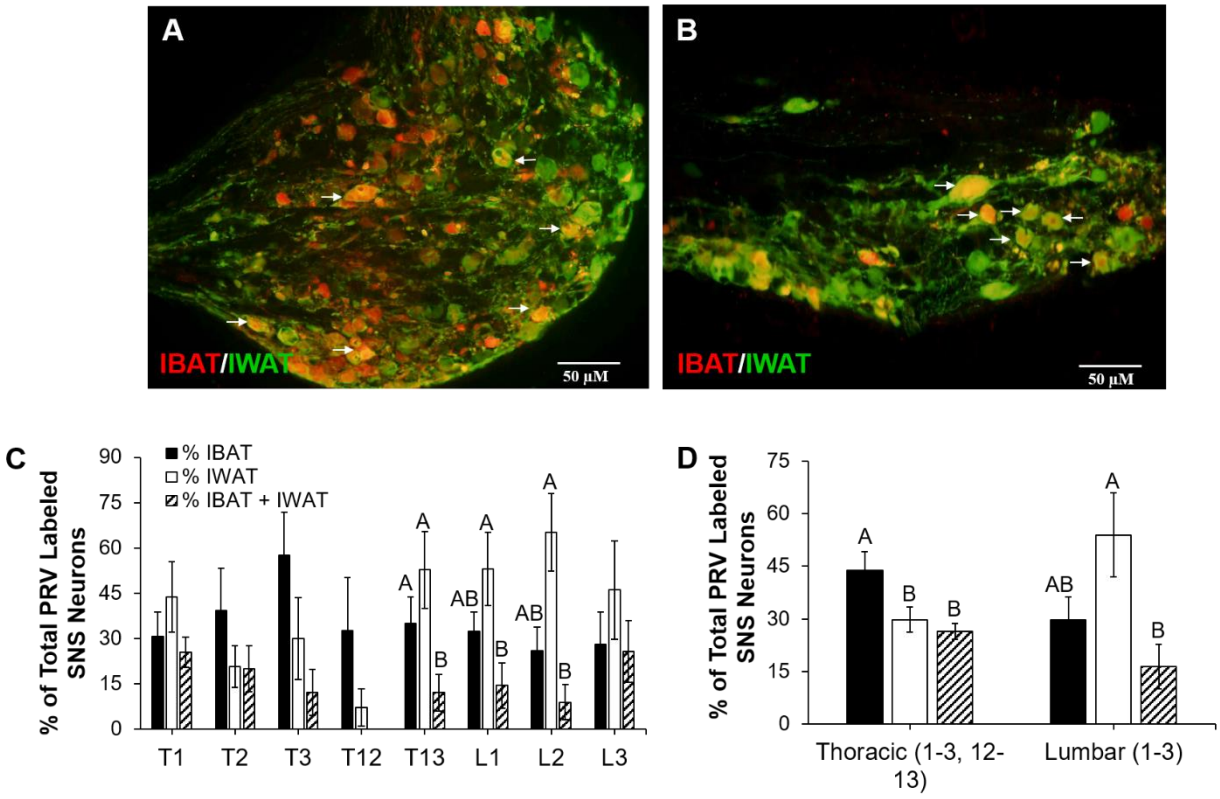

Figure 3.1 Distribution of SNS neurons to IBAT and IWAT across thoracic and lumbar regions of the SNS ganglia.
(A-B) Representative PRV labeling of SNS neurons to IBAT (red) and IWAT (green) in T3 (A) and L3 (B) SNS ganglia. Doubly labeled neurons are indicated by white arrows. (C) Percentage of total 834 PRV labeled SNS neurons across each thoracic (T1-3, 12-13) and lumbar (L1-3) regions. (D) Percentage of total PRV labeled SNS neurons across collapsed thoracic and lumbar regions. Scale bar = 50 µm. Values that do not share a common superscript are significantly different at $p<0.05$.

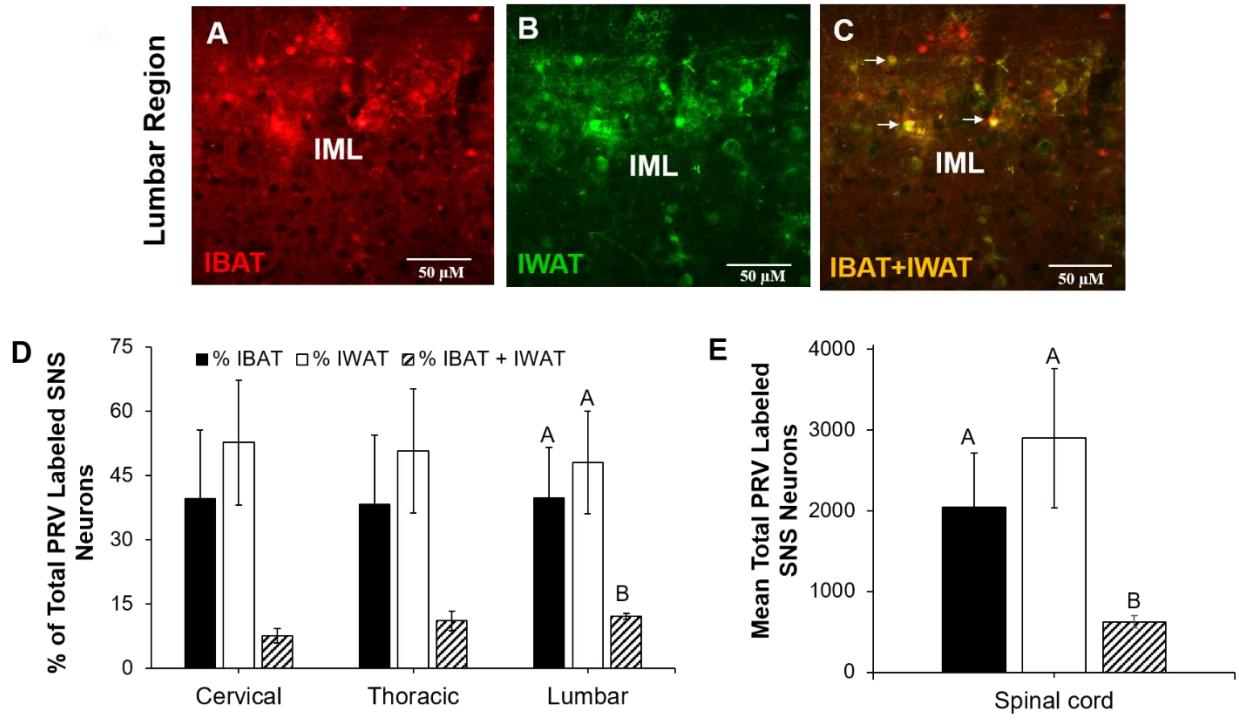

Figure 3.2 Distribution of SNS neurons to IBAT and IWAT in the spinal cord.
(A-C) Representative PRV labeling of SNS neurons to IBAT (red) and IWAT (green) in lumbar region. Doubly labeled neurons are indicated by white arrows. (D) Percentage of total PRV labeled SNS neurons across cervical, thoracic, and lumbar regions. (E) Mean total PRV labeled SNS neurons in whole spinal cord. Scale bar = 50 µm. Values that do not share a common superscript are significantly different at $p<0.05$. CC, central canal.

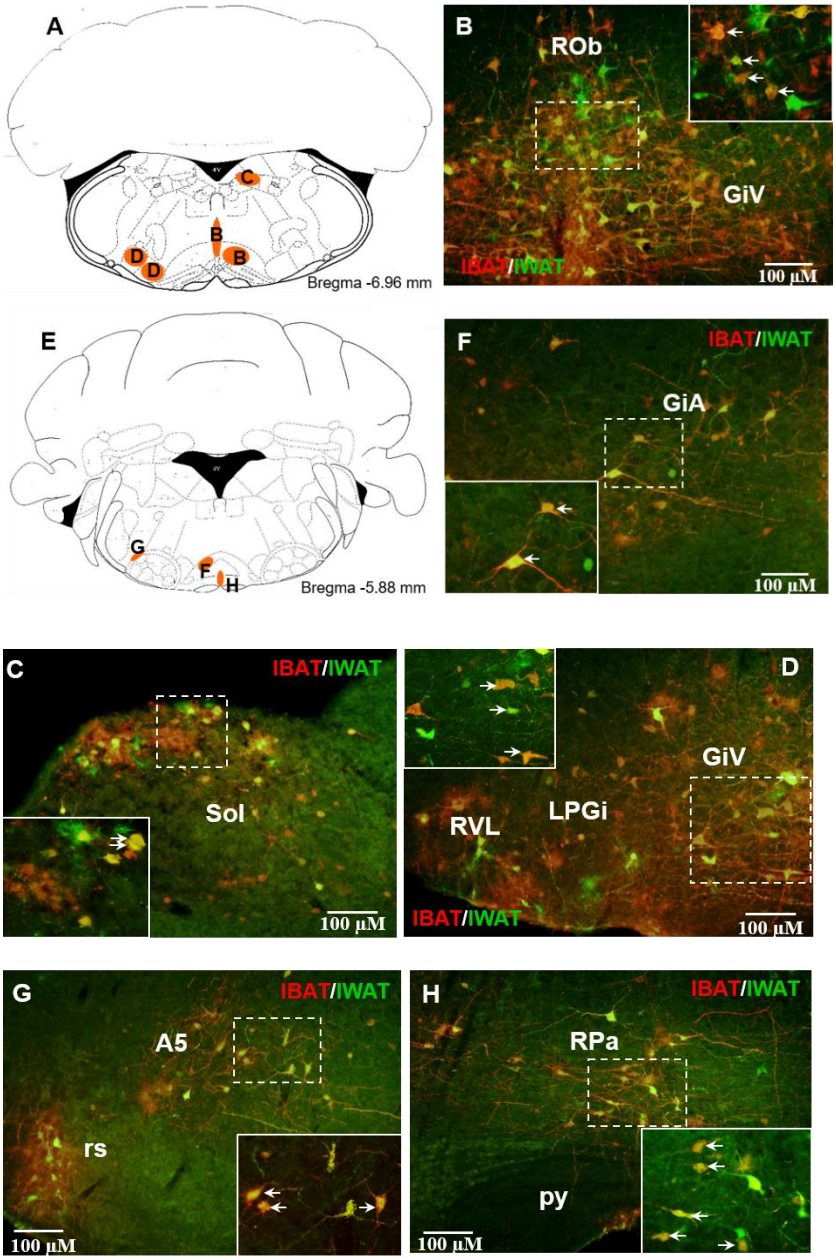

Figure 3.3 Photomicrographs illustrating central SNS neurons to IBAT and IWAT in the hindbrain.
(A, E) Schematics (adapted from Paxinos and Franklin 2001, 2nd edition) illustrating areas of PRV labeling highlighted in orange (B-D, F-H). Low (10x) magnification images of PRV labeled SNS neurons in ROb and GiV (B), Sol (C), RVL and LPGi (D), GiA (F), A5 and rs (G), and RPa (H). Dashed lines indicate regions of high magnification (20x). SNS neurons projecting to IBAT (red), to IWAT (green), and to both fat depots (yellow-orange; white arrows). Scale bar = 100 µm. 4V, fourth ventricle; A5, A5 noradrenaline cells; GiA, gigantocellular reticular nucleus, anterior part; GiV, gigantocellular reticular nucleus, ventral part; LPGi, lateral paragigantocellular nucleus; py, pyramidal tract; ROb, raphe obscurus nucleus; RPa, raphe

pallidus nucleus; rs, rubrospinal tract; RVL, rostroventrolateral reticular nucleus; Sol, nucleus of the solitary tract.

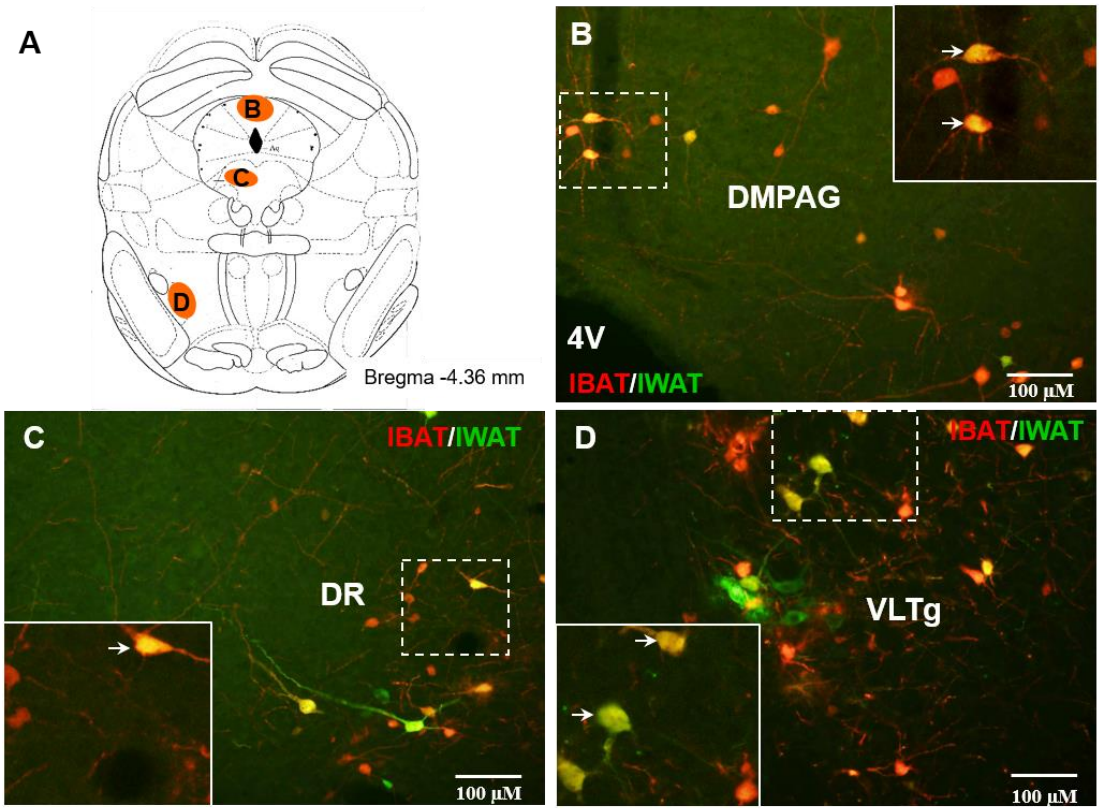

Figure 3.4 Photomicrographs illustrating central SNS neurons to IBAT and IWAT in the midbrain.
(A) Schematic (adapted from Paxinos and Franklin 2001, 2nd edition) illustrating areas of PRV labeling highlighted in orange (B-D). Low (10x) magnification images of PRV labeled SNS neurons in DMPAG (B), DR (C), and VLTg (D). Dashed lines indicate regions of high magnification (20x). SNS neurons projecting to IBAT (red), to IWAT (green), and to both fat depots (yellow-orange; white arrows). Scale bar = 100 µm. 4V, fourth ventricle; DMPAG, dorsomedial periaqueductal gray; DR, dorsal raphe; VLTg; ventral lateral tegmental area.

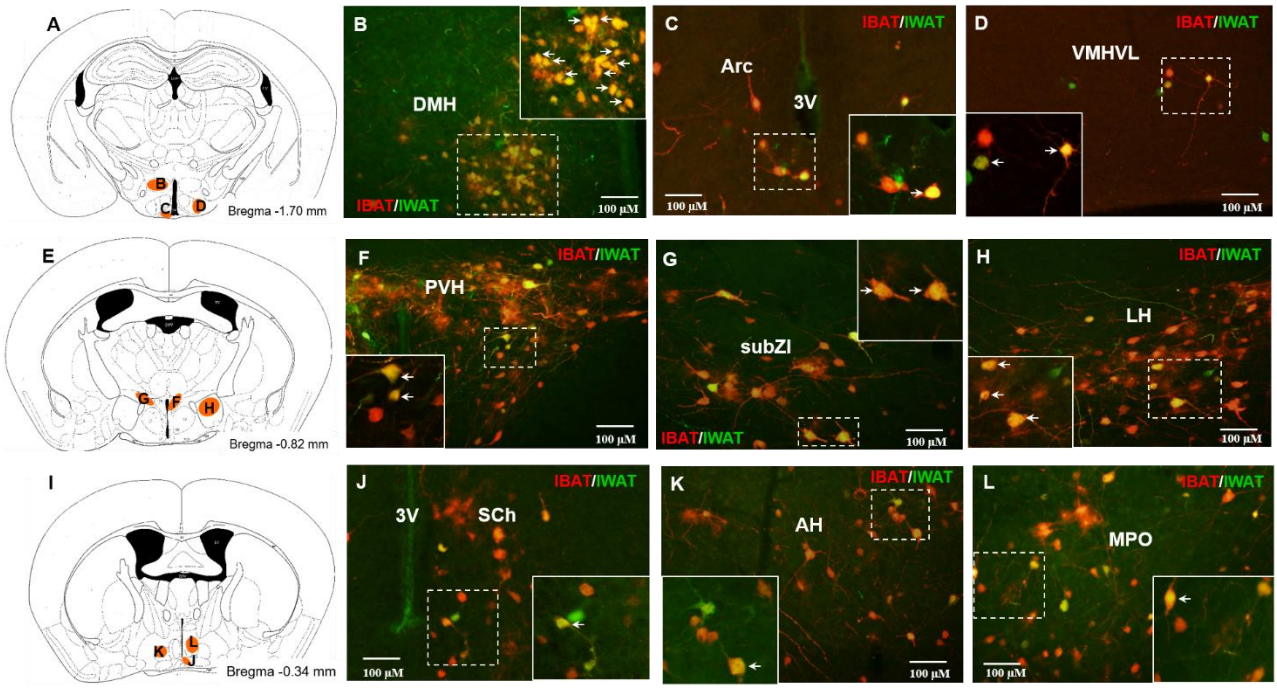

Figure 3.5 Photomicrographs illustrating central SNS neurons to IBAT and IWAT in the forebrain.
(A, E, I) Schematics (adapted from Paxinos and Franklin 2001, 2nd edition) illustrating areas of PRV labeling highlighted in orange (B-D, F-H, J-L). Low (10x) magnification images of PRV labeled SNS neurons in DMH (B), Arc (C), VMHVL (D) , PVH (F), subZI (G), LH (H), SCh (J), AH (K), and MPO (L). Dashed lines indicate regions of high magnification (20x). SNS neurons projecting to IBAT (red), to IWAT (green), and to both fat depots (yellow-orange; white arrows). Scale bar = 100 µm. 3V, third ventricle; AH, anterior hypothalamus; Arc, arcuate nucleus; DMH, dorsomedial hypothalamic nucleus; LH, lateral hypothalamus; MPO, medial preopotic nucleus; opt, optic tract; PVH, paraventricular nucleus of the hypothalamus; SCh, suprachiasmatic nucleus; subZI, sub zona incerta; VMHVL, ventromedial hypothalamic nucleus, ventral lateral part.

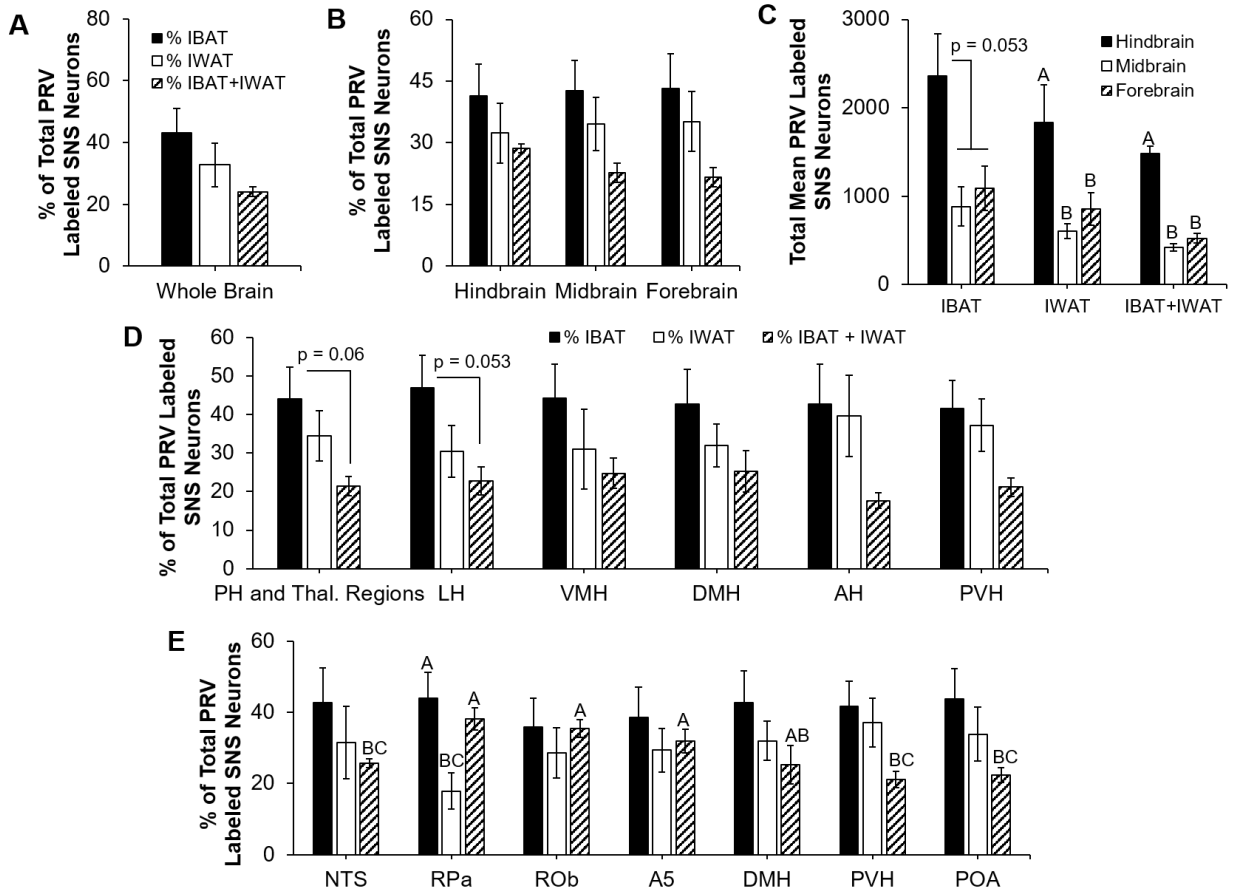

Figure 3.6 Distribution of central SNS neurons to IBAT and IWAT.
(A) Percentage of total PRV labeled SNS neurons in whole brain. (B) Percentage of total PRV labeled SNS neurons across hindbrain, midbrain, 880 and forebrain. (C) Comparison of hindbrain, midbrain, and forebrain total mean PRV labeled SNS neurons. (D) Percentage of total PRV labeled SNS neurons across hypothalamic nuclei. (E) Percentage of total PRV labeled SNS neurons across brain sites involved in SNS outflow and thermoregulation. Values that do not share a common superscript are significantly different at $p<0.05$. PH and Thal. Regions, posterior hypothalamus and thalamic regions; LH, lateral hypothalamus; VMH, ventromedial hypothalamus; DMH, dorsomedial hypothalamus; AH, anterior hypothalamus; PVH, paraventricular hypothalamus; NTS, nucleus of the solitary tract; RPa, raphe pallidus; ROb, raphe obscurus; POA, preoptic area.

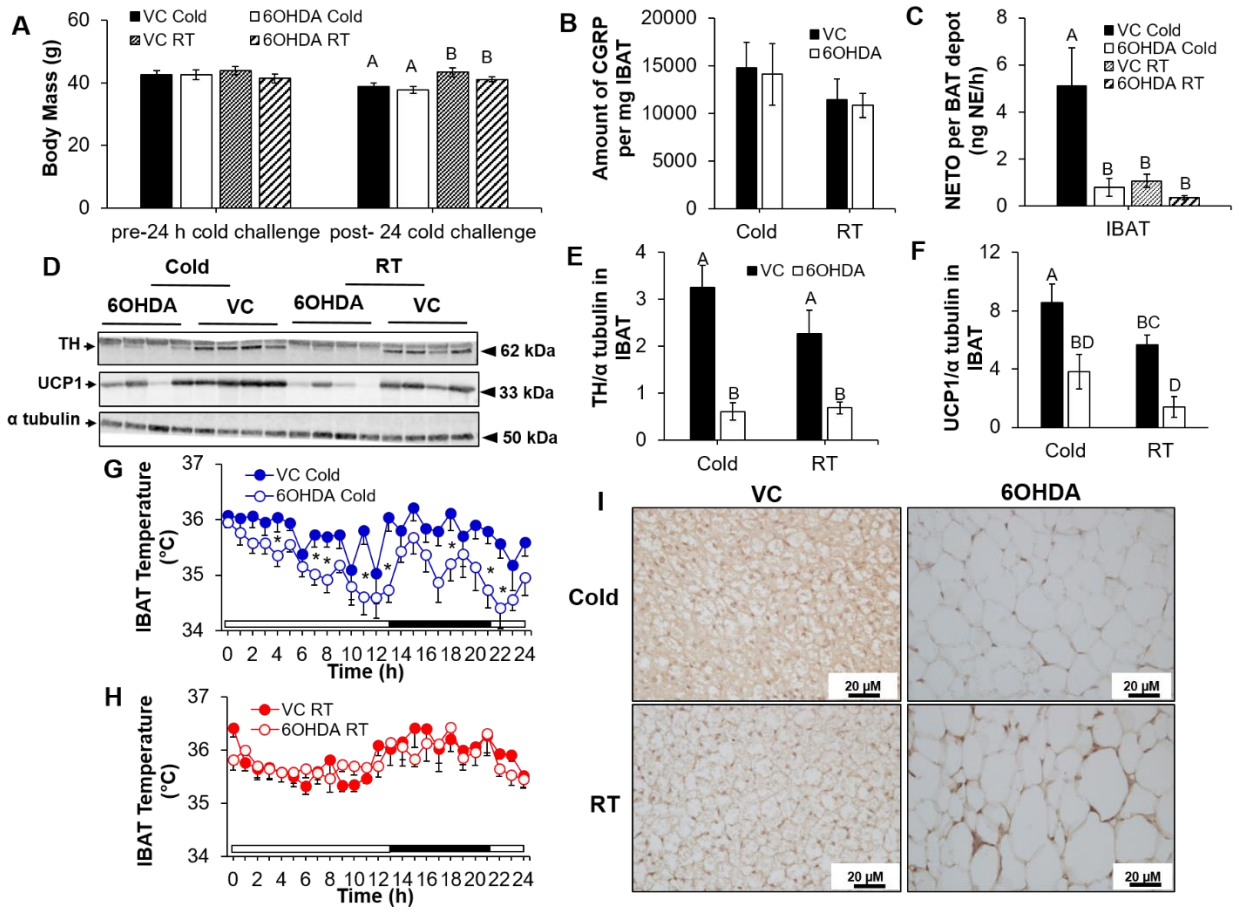

Figure 3.7 SNS denervation impairs IBAT function in 16-24 hour cold challenge. (A) Body mass decreases after cold challenge. (B) IBAT CGRP levels. (C) IBAT SNS drive measurement (NETO) during 16 hour cold exposure. (D) IBAT TH and UCP1 protein expression. Relative IBAT TH (E) and UCP1 (F) protein expression normalized to α tubulin. IBAT temperatures of cold exposed (G) and room temperature (H) hamsters. (I) UCP1 immunostained IBAT. Lights on from 0-13 and 21-24 hours (white bars) of the cold challenge; lights off from 13-21 hours (black bar). Values that do not share a common superscript are significantly different at $p<0.05$. *$p<0.05$, VC vs. 6OHDA. VC, vehicle control; RT, room temperature.

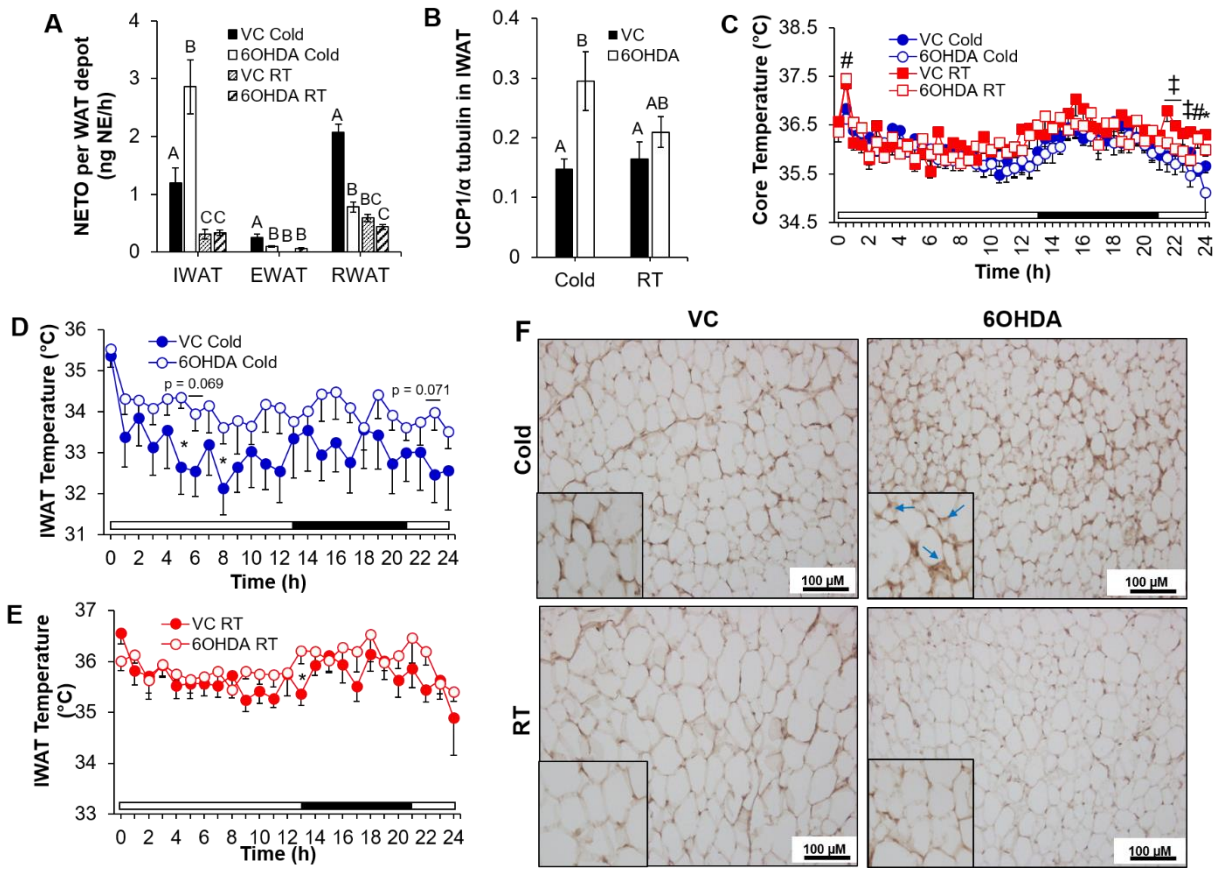

Figure 3.8 IWAT of IBAT SNS denervated hamsters increase beigeing and thermoregulatory functions during 16-24 hour cold challenge.
(A) WAT SNS drive measurement (NETO) during 16 hour cold exposure. (B) Relative IWAT UCP1 protein expression normalized to α tubulin. (C) Core body temperatures of all groups recorded every 30 minutes. IWAT temperatures of cold exposed (D) and room temperature (E) hamsters. (F) UCP1 immunostained IWAT. (G) CGRP increases in IWAT 903 of 6OHDA treated hamsters. #p<0.05, Cold vs. RT; ‡p<0.05, all vs. VC RT; *p<0.05, 6OHDA Cold vs. VC RT. Lights on from 0-13 and 21-24 h (white bars) of cold challenge; lights off from 13-21 h (black bar). Values that do not share a common superscript are significantly different at p<0.05. *p<0.05, VC vs. 6OHDA. VC, vehicle control; RT, room temperature.

Table 3.1 Percentage of total PRV labeled SNS neurons innervating IBAT, IWAT, and both fat depots.
The percentage values were averaged across hamsters (n=7) and presented in tabular form as means ± SE. Values that do not share a common superscript are significantly different at $p<0.05$.

	% of IBAT SNS Neurons	% of IWAT SNS Neurons	% of IBAT + IWAT	Total Mean of All PRV Labeled SNS Neurons
Hindbrain				
7N	37.8 ± 7.6	31.1 ± 7.3	31.1 ± 3.9	58.7 ± 11.4
10N	39.6 ± 10.1	37.9 ± 9.7	22.6 ± 2.6	95.7 ± 19.5
12N	37.6 ± 9.5^{A}	52.7 ± 12.0^{A}	9.8 ± 3.8^{B}	42.3 ± 8.3
A5	38.7 ± 8.5	29.4 ± 6.1	31.9 ± 3.4	61.4 ± 15.0
AP	40.7 ± 11.6	38.0 ± 12.2	21.3 ± 2.1	58.4 ± 8.2
Bar	33.1 ± 7.2	25.3 ± 6.2	41.6 ± 4.0	42.9 ± 9.1
Gi	37.4 ± 3.7^{A}	42.5 ± 5.2^{A}	20.1 ± 2.6^{B}	252.6 ± 45.9
DPGi	38.2 ± 2.9^{A}	35.2 ± 3.0^{A}	26.6 ± 2.3^{B}	63.6 ± 14.6
GiA	29.1 ± 7.3	25.5 ± 4.9	45.4 ± 3.8	163.0 ± 39.8
GiV	38.2 ± 6.9	27.3 ± 6.4	34.5 ± 1.7	114.1 ± 41.3
LPGi	40.4 ± 8.4	28.8 ± 8.4	30.8 ± 1.0	291.6 ± 61.0
IRt	43.4 ± 5.6^{A}	36.44 ± 5.6^{A}	20.2 ± 2.1^{B}	209.1 ± 13.9
KF	47.7 ± 11.5	19.7 ± 4.9	32.6 ± 7.8	14.6 ± 6.5
LC	26.5 ± 6.6	28.9 ± 8.3	44.6 ± 3.3	136.7 ± 23.1
Li	42.8 ± 4.9^{A}	35.3 ± 5.9^{A}	22.0 ± 2.7^{B}	36.0 ± 8.6
LRt	40.3 ± 8.6	28.0 ± 8.4	31.8 ± 1.3	486.3 ± 54.7
MdD	51.4 ± 10.3	27.4 ± 8.7	21.3 ± 2.3	220.1 ± 23.1
MdV	41.0 ± 3.3^{A}	36.8 ± 3.9^{A}	22.3 ± 1.6^{B}	176.1 ± 29.1
Mo5	51.8 ± 13.5	20.0 ± 8.9	28.3 ± 7.6	36.6 ± 14.5
NTS				
SolC	45.3 ± 10.3	32.8 ± 10.1	22.0 ± 1.0	113.1 ± 14.1
SolCE	43.2 ± 12.6	35.6 ± 15.3	21.3 ± 6.0	13.0 ± 5.3
SolDL	37.7 ± 9.4	30.2 ± 10.1	32.1 ± 4.6	101.0 ± 8.4
SolG	38.5 ± 10.6	34.6 ± 11.9	26.9 ± 1.9	74.3 ± 9.0
SolI	40.4 ± 10.0	30.5 ± 10.4	29.1 ± 4.5	22.0 ± 2.9
SolIM	39.4 ± 8.4	31.0 ± 9.4	29.6 ± 1.4	57.7 ± 6.6
SolM	42.4 ± 10.6	33.4 ± 11.1	24.2 ± 1.9	91.7 ± 14.8
SolV	43.1 ± 9.7	31.9 ± 9.5	25.0 ± 2.8	54.1 ± 5.9
SolVL	47.6 ± 11.6	28.9 ± 10.6	23.5 ± 2.5	107.3 ± 7.5
PCRt/A	45.4 ± 3.1^{A}	36.3 ± 3.3^{A}	18.3 ± 2.0^{B}	99.9 ± 18.9

Table (cont)

	% of IBAT SNS Neurons	% of IWAT SNS Neurons	% of IBAT + IWAT	Total Mean of All PRV Labeled SNS Neurons
PMn	33.1 ± 6.3	34.1 ± 3.8	32.8 ± 3.9	199.3 ± 29.6
Parabrachial Areas				
LPB	52.0 ± 18.3	27.1 ± 9.5	20.9 ± 8.9	14.0 ± 7.7
LPBC	48.6 ± 14.6	37.4 ± 18.2	14.0 ± 5.6	13.9 ± 8.2
LPBV	44.1 ± 12.8	38.9 ± 9.3	17.0 ± 6.3	25.4 ± 8.9
MPB	37.0 ± 6.7	29.8 ± 5.2	33.2 ± 4.9	54.6 ± 10.1
Doral Raphe Areas	35.6 ± 10.0	35.3 ± 12.6	29.1 ± 7.0	107.9 ± 29.0
PMnR	46.6 ± 10.7	37.2 ± 8.9	16.1 ± 5.2	13.1 ± 4.4
RC	42.3 ± 8.4	30.7 ± 8.7	27.0 ± 5.0	93.0 ± 13.3
RLi	42.4 ± 12.7	43.4 ± 18.9	20.4 ± 5.4	7.0 ± 2.4
RMg	35.2 ± 9.9	26.6 ± 6.7	38.2 ± 3.6	138.9 ± 29.9
ROb	35.9 ± 8.1	28.7 ± 7.1	35.5 ± 2.5	178.4 ± 16.6
RPa	44.0 ± 7.4^{A}	17.9 ± 5.1^{B}	38.1 ± 3.1^{A}	132.1 ± 18.3
rs	40.0 ± 8.5	30.4 ± 8.1	29.5 ± 1.3	310.9 ± 17.9
RVL/C1	34.8 ± 8.1	36.0 ± 9.7	29.2 ± 2.5	119.1 ± 33.0
SubCD	39.0 ± 7.4	28.7 ± 4.8	32.3 ± 4.5	67.7 ± 15.6
SubCV	39.9 ± 8.3	23.3 ± 7.9	36.8 ± 4.2	81.0 ± 20.0
vsc	42.2 ± 8.5	30.7 ± 7.7	27.1 ± 2.1	359.3 ± 38.1
Midbrain				
Atg	42.8 ± 19.7	41.7 ± 15.0	15.6 ± 8.6	6.3 ± 1.8
CnF	42.6 ± 8.7	35.0 ± 9.4	22.4 ± 3.8	41.4 ± 7.9
Dk	44.1 ± 8.6	28.6 ± 7.8	27.3 ± 2.8	29.3 ± 7.8
DMTg	51.3 ± 7.0^{A}	30.4 ± 7.6^{B}	18.4 ± 4.5^{B}	26.3 ± 8.3
DpMe	41.7 ± 10.8	40.9 ± 12.0	17.4 ± 3.9	55.0 ± 9.2
DPO	22.8 ± 6.1	39.1 ± 7.0	38.1 ± 2.9	38.1 ± 17.2
DpWh	47.4 ± 14.7	27.0 ± 14.8	25.6 ± 9.7	8.9 ± 2.7
EW	51.5 ± 13.3	31.3 ± 11.0	17.2 ± 4.6	12.1 ± 3.1
LDTg	41.8 ± 8.6	32.9 ± 11.0	25.3 ± 5.7	73.1 ± 25.8
LDTg/-V	51.1 ± 7.6	24.0 ± 8.9	24.9 ± 8.9	16.9 ± 6.2
MA3	43.5 ± 9.8	43.9 ± 13.2	12.6 ± 5.7	8.0 ± 2.3
mlf	46.9 ± 9.0	30.7 ± 8.5	22.4 ± 2.3	139.4 ± 14.3

Table (cont)

	% of IBAT SNS Neurons	% of IWAT SNS Neurons	% of IBAT + IWAT	Total Mean of All PRV Labeled SNS Neurons
PAG	39.7 ± 9.3	31.5 ± 9.9	28.9 ± 6.0	645.9 ± 137.2
PL	35.9 ± 10.1	23.9 ± 9.3	40.3 ± 5.5	36.9 ± 8.9
PnC	30.7 ± 4.4^{A}	49.4 ± 6.5^{B}	19.9 ± 2.5^{A}	66.6 ± 11.1
PnO	39.1 ± 6.6^{A}	42.0 ± 6.3^{A}	18.9 ± 2.9^{B}	71.0 ± 15.2
PnR	32.2 ± 6.9	39.6 ± 8.6	25.2 ± 6.0	11.3 ± 3.0
PnV	42.0 ± 4.9^{A}	36.2 ± 6.6^{AB}	21.8 ± 2.6^{B}	16.1 ± 3.6
PPTg	41.2 ± 7.8	33.5 ± 7.6	25.3 ± 3.3	141.6 ± 24.1
pv	40.4 ± 27.1	39.2 ± 27.5	20.5 ± 0.5	8.3 ± 6.2
RMC/scp	37.8 ± 7.8^{A}	46.7 ± 6.7^{A}	15.6 ± 5.2^{B}	64.1 ± 16.9
RPC/scp	32.6 ± 6.0^{A}	57.2 ± 6.3^{A}	10.2 ± 4.8^{B}	7.9 ± 3.0
RPF	38.0 ± 10.0^{A}	51.1 ± 10.5^{A}	10.9 ± 5.2^{B}	16.3 ± 5.4
RRF/A8	39.5 ± 9.5	39.2 ± 9.0	21.4 ± 2.3	35.0 ± 9.8
RtTg	22.3 ± 6.7^{A}	67.6 ± 8.7^{B}	10.1 ± 5.8^{AC}	20.3 ± 6.1
SN	43.5 ± 9.5	33.8 ± 9.3	22.7 ± 3.4	57.1 ± 4.5
Su3/C	46.4 ± 8.2^{A}	32.5 ± 5.9^{AB}	21.0 ± 3.4^{B}	138.9 ± 26.4
Su5	58.7 ± 2.9^{A}	17.1 ± 4.6^{B}	24.3 ± 3.9^{B}	31.9 ± 8.9
VLTg	37.4 ± 6.3	33.8 ± 7.4	28.8 ± 4.8	30.1 ± 10.2
VTA	45.6 ± 5.3	28.8 ± 5.8	25.6 ± 6.3	126.3 ± 31.2
Forebrain				
Hypothalamic				
AH	42.7 ± 10.4	39.7 ± 10.5	17.7 ± 2.0	101.1 ± 15.0
Arc	48.2 ± 9.4	29.9 ± 9.2	21.9 ± 3.5	55.0 ± 6.9
DM	43.6 ± 8.8	32.2 ± 4.8	24.2 ± 5.7	177.9 ± 21.9
DMC	55.1 ± 13.2	27.0 ± 9.9	18.0 ± 6.0	29.3 ± 11.3
DMD	43.8 ± 11.6	22.7 ± 6.9	33.5 ± 12.4	54.4 ± 24.2
DMV	58.4 ± 11.6	24.9 ± 11.6	16.7 ± 1.3	27.9 ± 11.6
DTM	54.8 ± 16.8	15.0 ± 10.5	30.2 ± 12.5	11.4 ± 3.8
LA	48.3 ± 17.8	36.5 ± 14.7	15.2 ± 7.8	11.0 ± 3.9
LH proper/mfb	47.1 ± 8.2	29.7 ± 6.3	23.3 ± 3.9	272.6 ± 18.1
subZI	42.4 ± 8.9	33.5 ± 6.7	24.2 ± 3.9	84.4 ± 9.9
Pe	38.1 ± 10.6	44.7 ± 11.0	17.2 ± 2.4	126.1 ± 6.7
AVPe	41.2 ± 8.9	38.3 ± 7.4	20.6 ± 4.0	17.1 ± 5.3
PH	53.6 ± 8.5^{A}	24.9 ± 7.3^{B}	21.6 ± 6.1^{B}	51.6 ± 23.6
Preoptic Areas				
LPO	42.9 ± 9.0	34.5 ± 7.3	22.6 ± 2.2	62.7 ± 6.9
MnPO	56.6 ± 0.6	26.3 ± 2.3	17.1 ± 2.9	5.6 ± 3.5

Table (cont)

	% of IBAT SNS Neurons	% of IWAT SNS Neurons	% of IBAT + IWAT	Total Mean of All PRV Labeled SNS Neurons
MPOC	42.3 ± 11.3	46.4 ± 12.7	11.3 ± 4.2	4.9 ± 0.6
MPOL	45.2 ± 12.5	35.8 ± 10.2	19.0 ± 2.5	25.3 ± 6.2
MPOM	45.1 ± 8.8	34.1 ± 7.8	20.0 ± 2.5	124.7 ± 15.9
PVH				
PaAP	51.2 ± 14.7	24.5 ± 11.1	24.3 ± 6.3	26.1 ± 11.0
PaDC	39.2 ± 8.9	37.5 ± 6.6	23.3 ± 3.9	33.1 ± 5.0
PaLM	41.0 ± 6.6	31.3 ± 6.8	27.7 ± 2.3	69.4 ± 6.3
PaMM	37.7 ± 6.5^{A}	43.5 ± 6.4^{A}	18.8 ± 2.6^{B}	88.1 ± 5.1
PaMP	36.5 ± 6.5	41.9 ± 7.8	21.6 ± 3.6	90.9 ± 3.3
PaPo	48.4 ± 8.2^{A}	32.7 ± 6.6^{AB}	18.9 ± 3.4^{B}	71.9 ± 22.3
PaV	40.2 ± 5.5^{A}	42.1 ± 7.9^{A}	17.7 ± 4.1^{B}	17.1 ± 5.8
RCh	57.3 ± 17.9	27.8 ± 14.5	14.9 ± 5.5	8.1 ± 2.6
SPa	37.0 ± 8.6^{A}	48.1 ± 7.4^{A}	15.0 ± 3.4^{B}	16.6 ± 3.4
SCh	37.0 ± 12.6	43.4 ± 13.1	19.6 ± 8.0	39.1 ± 7.4
VMH	54.7 ± 8.8^{A}	17.5 ± 9.6^{B}	27.8 ± 6.5^{AB}	13.7 ± 5.0
VMHC	47.2 ± 14.7	32.6 ± 11.7	20.2 ± 7.0	11.4 ± 3.4
VMHDM	43.1 ± 10.9	34.8 ± 11.6	22.1 ± 7.9	26.6 ± 7.5
VMHVL	38.6 ± 9.8	31.8 ± 9.3	29.6 ± 4.3	15.6 ± 2.9
Thalamic				
PF	53.1 ± 4.8	21.4 ± 10.7	25.5 ± 7.3	17.7 ± 9.2
Re	43.9 ± 8.7	35.4 ± 5.0	20.7 ± 4.7	101.4 ± 25.9
VRe	37.1 ± 7.1	35.6 ± 8.0	27.3 ± 7.4	21.3 ± 5.1
Xi	53.5 ± 12.0^{A}	35.3 ± 9.2^{AB}	11.3 ± 2.9^{B}	25.1 ± 7.4
Other forebrain areas				
BST	40.0 ± 11.9	32.2 ± 9.1	27.8 ± 7.4	123.6 ± 38.7
PeF	38.1 ± 8.7	42.2 ± 7.9	19.7 ± 3.3	30.3 ± 9.2
PMD	50.27 ± 16.9	29.9 ± 14.5	19.9 ± 5.9	13.0 ± 5.0
PMV	53.2 ± 17.4	25.5 ± 21.1	21.2 ± 4.3	8.1 ± 4.3
PR/scp	42.8 ± 9.3	33.7 ± 11.3	23.5 ± 4.4	12.7 ± 3.3
PSTh	62.2 ± 3.6^{A}	18.5 ± 5.0^{B}	17.2 ± 2.6^{B}	45.7 ± 18.2
scp	38.2 ± 9.7	42.6 ± 15.0	19.3 ± 3.5	34.9 ± 7.1
TC	31.7 ± 9.1	38.8 ± 19.4	29.5 ± 14.7	7.3 ± 2.7
VP	39.7 ± 13.7	44.3 ± 14.8	16.0 ± 6.0	13.3 ± 4.5
ZI	50.6 ± 7.8^{A}	32.8 ± 7.1^{B}	16.6 ± 1.7^{C}	101.3 ± 15.6

Hindbrain: 7N, facial nucleus; 10N, dorsal motor nucleus of vagus; 12N, hypoglossal nucleus; A5, A5 noradrenaline cells; AP, area postrema; Bar, Barrington's nucleus; Gi, gigantocellular reticular nucleus; DPGi, dorsal paragigantocellular nucleus; GiA, gigantocellular reticular nucleus, alpha part; GiV, gigantocellular reticular nucleus, ventral part; LPGi, lateral paragigantocellular nucleus; IRt, intermediate reticular nucleus; KF, Ko¨lliker-Fuse nucleus; LC, locus coeruleus; Li, linear nucleus of the medulla; LRt, lateral reticular nucleus; MdD, medullary reticular nucleus, dorsal part; MdV, medullary reticular nucleus, ventral part; Mo5, motor trigeminal nucleus; SolC, nucleus of the solitary tract, commissural part; SolCE, nucleus of the solitary tract, central part; SolDL, solitary nucleus, dorsolateral part; SolG, nucleus of the solitary tract, gelatinous part; SolI, nucleus of the solitary tract, interstitial part; SolIM, nucleus of the solitary tract, intermediate part; SolM, nucleus of the solitary tract, medial part; SolV, solitary nucleus, ventral part; SolVL, nucleus of the solitary tract, ventrolateral part; PCRt/-A, parvicellular reticular nucleus/-alpha part; PMn, paramedian reticular nucleus; LPB, lateral parabrachial nucleus; LPBC, lateral parabrachial nucleus, central part; LPBV, lateral parabrachial nucleus, ventral part; MPB, medial parabrachial nucleus; PMnR, paramedian raphe nucleus; RC, raphe cap; RLi, rostral linear nucleus of the raphe; RMg, raphe magnus nucleus; ROb, raphe obscurus nucleus; RPa, raphe pallidus nucleus; rs, rubrospinal tract; RVL/C1, rostroventrolateral reticular nucleus/C1 adrenaline cells; Sub-CD/V, subcoeruleus nucleus-dorsal/ventral parts; vsc, ventral spinocerebellar tract.

Midbrain: ATg, anterior tegmental nucleus; CnF, cuneiform nucleus; Dk, nucleus of Darkschewitsch; DMTg, dorsomedial tegmental area; DpMe, deep mesencephalic nucleus; DPO, dorsal periolivary region; DpWh, deep white layer of the superior colliculus; EW, Edinger-Westphal nucleus; LDTg/-V, laterodorsal tegmental nucleus/-ventral part; MA3, medial

accessory oculomotor nucleus; mlf, medial longitudinal fasciculus; PAG, periaqueductal gray; PL, paralemniscal nucleus; PnC, pontine reticular nucleus, caudal part; PnO, pontine reticular nucleus, oral part; PnR, pontine raphe nucleus; PnV, pontine reticular nucleus, ventral part; PPTg, pedunculopontine tegmental nucleus; pv, periventricular fiber system; RMC/scp, red nucleus, magnocellular part/superior cerebellar peduncle (brachium conjunctivum); RPC/scp, red nucleus, parvicellular part/ superior cerebellar peduncle (brachium conjunctivum); RPF, retroparafascicular nucleus; RRF/A8, retrorubral fields/A8 dopamine cells; RtTg, reticulotegmental nucleus of the pons; SN, substantia nigra; SPTg, subpedencular tegmental nucleus; Su3/C, supraoculomotor periaqueductal gray/supraoculomotor cap; VLTg, ventrolateral tegmental area; Su5, supratrigeminal nucleus; VLTg, ventrolateral tegmental area; VTA, ventral tegmental area.

Forebrain: AH, anterior hypothalamus; Arc, arcuate nucleus; DM, dorsomedial hypothalamic nucleus; DMC, dorsomedial hypothalamic nucleus, compact part; DMD, dorsomedial hypothalamic nucleus, dorsal part; DMV, dorsomedial hypothalamic nucleus, ventral part; DTM, dorsal tuberomammillary nucleus; LA, lateroanterior hypothalamic nucleus; LH, lateral hypothalamic area; LH proper, lateral hypothalamic area proper; subZI, sub-zona incerta; Pe, periventricular hypothalamic nucleus; AVPe, anteroventral periventricular nucleus; PH, posterior hypothalamic area; LPO, lateral preoptic area; MnPO, median preoptic nucleus; MPA, medial preoptic area; MPO-C/L/M, medial preoptic nucleus-central/lateral/medial parts; VLPO, ventrolateral preoptic nucleus; VMPO, ventromedial preoptic nucleus; PVH, paraventricular nucleus of the hypothalamus; PaAP, paraventricular hypothalamic nucleus, anterior parvicellular part; PaDC, paraventricular hypothalamic nucleus, dorsal cap; PaLM, paraventricular hypothalamic nucleus, lateral magnocellular part; PaMM, paraventricular hypothalamic nucleus,

medial magnocellular part; PaMP, paraventricular hypothalamic nucleus, medial parvicellular part; PaPo, paraventricular hypothalamic nucleus, posterior part; PaV, paraventricular hypothalamic nucleus, ventral part; RCh, retrochiasmatic area; SPa, subparaventricular zone of the hypothalamus; SCh, suprachiasmatic nucleus; VMH, ventromedial hypothalamic nucleus; VMHC, ventromedial hypothalamic nucleus, central part; VMHDM, ventromedial hypothalamic nucleus, dorsomedial part; VMHVL, ventromedial hypothalamic nucleus, ventrolateral part; PF, parafascicular thalamic nucleus; Re/VRe/Xi, reuniens thalamic nucleus/ventral reuniens thalamic nucleus/xiphoid thalamic nucleus; BST, bed nucleus of the stria terminalis; PeF, perifornical nucleus; PMD, premammillary nucleus, dorsal part; PMV, premammillary nucleus, ventral part; PR/scp, prerubral field/ superior cerebellar peduncle (brachium conjunctivum); PS, parastrial nucleus; PSTh, parasubthalamic nucleus; scp, superior cerebellar peduncle (brachium conjunctivum); TC, tuber cinereum area; VP, ventral pallidum; ZI, zona incerta.

3.5 Discussion

The present study characterized central SNS innervations to IWAT and IBAT for the first time using dual tract tracing with isogenic strains of PRV containing either GFP or RFP within the same animal. Throughout the brain, there was a consistent pattern of greater SNS circuitry to IBAT than IWAT, but shared SNS innervation to IWAT and IBAT was less frequent in the forebrain and midbrain compared with the hindbrain. The RPa, ROb, and A5 region had notably high percentages of doubly labeled neurons; whereas the PnC and RtTg, midbrain nuclei, had higher separate SNS circuitry to IWAT than IBAT. The shared and separate central SNS outflow to IWAT and IBAT may work together to maintain homeostasis by coordinating thermoregulation and beige adipocyte recruitment, as demonstrated by increased IWAT SNS drive, temperature and UCP1 expression during 16-24 hour cold exposure in hamsters with impaired IBAT function due to SNS denervation.

We performed an extensive characterization of IWAT and IBAT SNS circuitries across the neuroaxis and found differential SNS innervation patterns in the SNS ganglia, spinal cord, and brain. Singly labeled SNS neurons projecting to IBAT were mostly found in the thoracic region of the SNS ganglia, while singly labeled SNS neurons projecting to IWAT were mostly found in the lumbar region. These data are consistent with prior studies showing regional differences in the SNS ganglia innervating IWAT and EWAT (75) or IWAT, mesenteric WAT and RWAT (1, 50). There were no differences in SNS innervation from the intermediolateral horn (IML) of the spinal cord to IBAT and IWAT, suggesting that differences in SNS drive to IBAT and IWAT originate from the SNS ganglia. In addition, the spinal cord had low levels of doubly labeled neurons, suggesting that post ganglionic projections to peripheral tissues, such as IWAT and IBAT, are distinct. In this situation, differential SNS drive to IWAT and IBAT during

the acute cold challenge may rely on the innervation from the lumbar and thoracic regions of the SNS ganglia, respectively, but not the spinal cord.

We found divergent and convergent central SNS outflow to IWAT and IBAT across the brain. The hindbrain had a greater percentage of singly and doubly labeled SNS neurons than the midbrain and forebrain due to projections from rostral nuclei and the presence of caudal nuclei essential for integrative control of thermoregulation and potentially of beigeing. The relative sufficiency of the hindbrain for thermoregulation has been demonstrated in chronic decerebrate rats, in which the brain has been transected at the supracollicular level (49). These rats were able to maintain core body temperature when housed at 8°C and 10°C, and there were comparable increases in IBAT and WAT NETO in intact and decerebrate cold exposed rats (49). Forebrain projections, however, are still necessary for complete and stable thermoregulation, because chronic decerebrate rats, unlike intact rats, could not maintain core body temperature at 4°C (49). We found notable increases of doubly labeled neurons in the RPa, ROb, and A5 region. These nuclei regulate thermoregulatory responses and SNS outflow (2, 3, 45, 46). RPa neurons are necessary for adaptive thermoregulation during cold exposure including populations of thyrotropin releasing hormone neurons, which have been shown to be activated during 24 hour cold exposure (13, 15, 47, 52). The ROb contains serotonergic neurons that increase firing with a cold stimulus, but are inhibited by a warm one (66). The thermoregulatory role of the A5 region has not been fully tested as the raphe, but it contains noradrenergic neurons that have frequently been labeled in tract tracing studies from fat (2, 3, 44, 50, 58, 59, 63, 64). Singly labeled neurons to IWAT also contribute to IWAT thermogenic functions and beige adipocyte formation, and it has been shown that midbrain neurons in the reticular formation respond to cooling of the skin (48). We found significantly higher percentages of SNS neurons projecting to IWAT than IBAT

in the PnC and RtTg midbrain nuclei, therefore these sites may participate in both thermoregulation and beigeing of IWAT.

It is possible that some of our PRV tract tracing included SNS blood vessel innervation. The consideration of SNS input to fat vasculature is important, but it does not create interpretational issues of our virus tract tracing and denervation studies, because of the direct relation between increases in blood flow and tissue metabolic activity that includes glucose uptake into the brain and peripheral tissues such as BAT. It has been suggested that the function of SNS innervation of fat vasculature, particularly of WAT, is to increase capillary permeability so that liberated free fatty acids can leave the interstitial space and reduce their extracellular concentration in order to promote lipolysis by decreasing end product inhibition (24, 56, 57). This would enhance the function of WAT SNS as the primary driver of WAT lipolysis (5). The present neuroanatomical evidence reveals the reality of a SNS crosstalk between IWAT and IBAT for functional coordination of SNS outflow. This crosstalk is most likely mediated by sensory nerves from IWAT not IBAT, because we found increased CGRP in IWAT depots of 6OHDA treated hamsters (Fig. 3.7, B; Fig. 3.8, G). Further support of IWAT and IBAT SNS crosstalk mediated by IWAT sensory nerves is demonstrated by intra-IWAT injection of CL316,243 increases IBAT temperature, an effect that is lost when sensory nerves from IWAT are denervated (25). Thus, sensory nerves from IWAT projecting to brain sites of SNS outflow (58) can separately increase SNS drive to only IWAT or IBAT or to both fat depots via the SNS ganglia at a mechanistic level. IWAT and IBAT SNS crosstalk is not easily detected in intact hamsters due to functional IBAT depots. Intact hamsters cold exposed for 16-24 hours do, however, have increased IWAT NETO (12) and BAT-like adipocyte morphology compared with

RT controls some of which may be due to increased IWAT SNS drive. This crosstalk in intact cold exposed hamsters may be more apparent with a longer cold challenge.

The impetus for thermogenic function and beigeing in IWAT of IBAT SNS denervated hamsters most likely occurs through increased SNS outflow, as demonstrated by enhanced SNS drive in IWAT of these hamsters. A change from long day to short day photoperiod in Siberian hamsters naturally increase SNS outflow triggering beigeing in RWAT, IWAT, and EWAT and increased UCP1 expression (Ryu, Zarebidaki, Albers, Xue, and Bartness, in preparation). In addition, knockdown of DMH neuropeptide Y neurons in rats is sufficient for IWAT beigeing and when SNS nerves to IWAT were denervated there was a significant decrease in IWAT NE content (a surrogate used for SNS drive measurement, but not a replacement for NETO) and UCP1 immunostaining compared with intact contralateral control (17). Lastly, WAT of β adrenoreceptor KO mice, which do not express necessary receptors for SNS stimulation, have decreased UCP1, BAT-like appearance, and reduced peroxisome proliferator-activated receptor-gamma coactivator 1-α and CIDEA expression (4, 33, 37). These data suggest that SNS innervation and particularly increased SNS drive to WAT contribute to beigeing followed by a secondary increase in UCP1 expression and temperature (6). SNS triggering WAT UCP1 has been observed at the WAT depot level in intact mice given chronic cold exposure (10 days) (71). Those mice had increased multilocular adipocytes and UCP1 ir staining in WAT depots.

WAT SNS drive, as measured by NETO and UCP1 expression, was significantly increased in IWAT, but not in EWAT or RWAT, in 6OHDA treated hamsters. This correlation between NETO and UCP1 expression further support our hypothesis that increased SNS drive to IWAT is the driving force triggering beigeing and enhanced thermogenic function in IWAT. The presence of differential SNS drive among fat depots to a variety of energy challenges has been

previously documented (11, 12, 50) and this selective response to both energy challenges and IBAT 6OHDA treatment may reflect differential neuronal circuitries to individual fat depots (50, 75). Beigeing of all WAT depots and greater increases in UCP1 mRNA and protein expression and morphological changes are typically observed at ~7 days of chronic cold exposure in intact mice (73). We chose 16-24 hour cold exposure for our study, because it is likely that SNS coordinated control of IWAT and IBAT would occur during the early, critical period of the cold challenge, but it is possible that increased SNS drive to and beigeing of EWAT and RWAT would occur in 6OHDA treated hamsters exposed to cold for an extended period of time.

The metabolic relevance of beige adipocyte contribution to nonshivering thermogenesis has been the subject of debate. Mitochondria from IWAT of cold acclimated mice have comparable UCP1 expression to mitochondria found in IBAT, and they are functionally thermogenic (61). The thermogenic density of recruited beige adipocytes in IWAT, however, is only one fifth that of IBAT (61). A recent study exposing intact, wild type mice to 10°C for 14 days found that although cold exposure induced IWAT beigeing, it did not result in large increases in mitochondrial oxidative activity (35), suggesting that beige adipocytes did not make an appreciable contribution to thermoregulation. However, in our study, we found hamsters with impaired IBAT thermogenic function were able to maintain core body temperature during a 24 hour cold challenge with increased IWAT thermogenesis and beigeing, which implied a contribution of IWAT to maintenance of core temperature. A limitation of our model is that IBAT was the only BAT depot that was denervated, and we did not exclude the thermogenic contribution of remaining, intact BAT depots. Therefore, it is possible that intact mediastinal, axillary, perirenal, and cervical BAT contributed to the maintenance of core body temperature in the 6OHDA cold exposed hamsters in this study. This may be the reason as to why UCP1 KO

mice are cold intolerant, because all BAT depots do not express UCP1. A model of SNS impairment in all BAT depots is needed to further explore whether beige adipocyte recruitment is sufficient for long term maintenance of thermoregulation when neural activation of BAT is absent.

Here we have defined the separate and shared SNS innervations to IWAT and IBAT across the neuroaxis. We have found high percentages of doubly labeled neurons in the hindbrain (RPa, ROb, and A5 region) and significantly greater separate SNS circuitry to IWAT that IBAT in the midbrain (PnC and RtTg). We have also physiologically tested the coordinated SNS control for thermoregulation and beige adipocyte recruitment. Hamsters that had impaired IBAT function (6OHDA SNS denervation) survived 16-24 hour cold challenge and this was associated with increased SNS drive to IWAT resulting in signs of beigeing (i.e., increased IWAT temperature and UCP1 expression and immunostaining) and maintenance of body temperature.

3.6 Perspectives and Significance

Our study demonstrates a high order of SNS regulation and coordination for thermoregulation and beigeing via a functional crosstalk between IWAT and IBAT SNS most likely regulated by brain sites involved in SNS outflow and mediated, at least in part, by IWAT sensory nerves. This coordination between IWAT and IBAT is evolutionarily plausible as the maintenance of core body temperature is crucial for survival in extreme temperatures. A distributed control of body temperature has the potential to allow compensation for an event that causes BAT function to be impaired. It is clear that fat depots are not created equal, but have unique characteristics and functions. This has been demonstrated by differential SNS outflow to WAT and BAT depots during energetic challenges of cold exposure, food deprivation, and glucoprivation (12). The differential SNS drive could be attributed to crosstalk between different

fat depots and feedback from sensory nerves. At present understanding the mechanism and regulation of beigeing provides an alternative strategy for treating and reversing obesity since obese individuals have significantly decreased BAT, but excess WAT depots (67). However, the physiological contribution of WAT beigeing for maintaining body temperature and its overall contribution to whole body energy expenditure is still largely unknown and requires further investigation of WAT and BAT SNS control.

3.7 Acknowledgements

We thank Dr. Lynn Enquist for generous gift of PRV 152 (Princeton University, Princeton, NJ; Virus Center Grant P40RR018604). We also thank Drs. J. Christopher Ehlen, Xin Cui, and Emily Bruggeman for technical assistance with the chromatograph, UCP1 fat IHC, and paraffin embedding, respectively. We also thank Drs. Ruth Harris, Aaron Roseberry, and Hang Shi for insightful comments on the manuscript. Lastly, we thank Vaibhav Maheswari (an undergraduate research assistant) for help with tissue collection and GSU Department of Animal Resources for husbandry care. This research was supported by NIH R37DK035254 to T.J.B. and NIH R01DK35254 to B.X.

3.8 References

1. **Adler ES, Hollis JH, Clarke IJ, Grattan DR, and Oldfield BJ.** Neurochemical characterization and sexual dimorphism of projections from the brain to abdominal and subcutaneous white adipose tissue in the rat. JNeurosci 32: 15913-15921, 2012.

2. **Bamshad M, Aoki VT, Adkison MG, Warren WS, and Bartness TJ.** Central nervous system origins of the sympathetic nervous system outflow to white adipose tissue. AmJPhysiol 275: R291-R299, 1998.

3. **Bamshad M, Song CK, and Bartness TJ.** CNS origins of the sympathetic nervous system outflow to brown adipose tissue. Am J Physiol 276: R1569-1578, 1999.

4. **Barbatelli G, Murano I, Madsen L, Hao Q, Jimenez M, Kristiansen K, Giacobino JP, De Matteis R, and Cinti S.** The emergence of cold-induced brown adipocytes in mouse white fat

depots is determined predominantly by white to brown adipocyte transdifferentiation. American Journal of Physiology 298: E1244-1253, 2010.

5. **Bartness TJ, Liu Y, Shrestha YB, and Ryu V.** Neural innervation of white adipose tissue and the control of lipolysis. Front Neuroendocrinol 2014.

6. **Bartness TJ, and Ryu V.** Neural control of white, beige and brown adipocytes. Int J Obes Suppl 5: S35-39, 2015.

7. **Bartness TJ, Shrestha YB, Vaughan CH, Schwartz GJ, and Song CK.** Sensory and sympathetic nervous system control of white adipose tissue lipolysis. MolCell Endocrinol 318: 34-43, 2010.

8. **Bartness TJ, Vaughan CH, and Song CK.** Sympathetic and sensory innervation of brown adipose tissue. IntJ Obes(Lond) 34 Suppl 1: S36-S42, 2010.

9. **Beznak ABL, and Hasch Z.** The effect of sympathectomy on the fatty deposit in connective tissue. Quarterly Journal Experimental Physiology 27: 1-15, 1937.

10. **Bradley SP, Pattullo LM, Patel PN, and Prendergast BJ.** Photoperiodic regulation of the orexigenic effects of ghrelin in Siberian hamsters. HormBehav 2010.

11. **Brito MN, Brito NA, Baro DJ, Song CK, and Bartness TJ.** Differential activation of the sympathetic innervation of adipose tissues by melanocortin receptor stimulation. Endocrinology 148: 5339-53347, 2007.

12. **Brito NA, Brito MN, and Bartness TJ.** Differential sympathetic drive to adipose tissues after food deprivation, cold exposure or glucoprivation. AmJPhysiol RegulIntegrComp Physiol 294: R1445-R1452, 2008.

13. **Cabral A, Valdivia S, Reynaldo M, Cyr NE, Nillni EA, and Perello M.** Short-term cold exposure activates TRH neurons exclusively in the hypothalamic paraventricular nucleus and raphe pallidus. Neurosci Lett 518: 86-91, 2012.

14. **Cannon B, and Nedergaard J.** The biochemistry of an inefficient tissue: brown adipose tissue. Essays Biochem 20: 110-164, 1985.

15. **Cano G, Passerin AM, Schiltz JC, Card JP, Morrison SF, and Sved AF.** Anatomical substrates for the central control of sympathetic outflow to interscapular adipose tissue during cold exposure. J Comp Neurol 460: 303-326, 2003.

16. **Cantu RC, and Goodman HM.** Effects of denervation and fasting on white adipose tissue. American Journal Physiology 212: 207-212, 1967.

17. **Chao PT, Yang L, Aja S, Moran TH, and Bi S.** Knockdown of NPY Expression in the Dorsomedial Hypothalamus Promotes Development of Brown Adipocytes and Prevents Diet-Induced Obesity. Cell metabolism 13: 573-583, 2011.

18. **Cousin B, Cinti S, Morroni M, Raimbault S, Ricquier D, Penicaud L, and Casteilla L.** Occurrence of brown adipocytes in rat white adipose tissue: molecular and morphological characterization. J Cell Sci 103: 931-942, 1992.

19. **Cui X, Nguyen NL, Zarebidaki E, Cao Q, Li F, Zha L, Bartness T, Shi H, and Xue B.** Thermoneutrality decreases thermogenic program and promotes adiposity in high-fat diet-fed mice. Physiol Rep 4: 2016.

20. **Demas GE, and Bartness TJ.** Direct innervation of white fat and adrenal medullary catecholamines mediate photoperiodic changes in body fat. AmJPhysiol 281: R1499-R1505, 2001.

21. **Dulloo AG, and Miller DS.** Energy balance following sympathetic denervation of brown adipose tissue. Can J Physiol Pharmacol 62: 235-240, 1984.

22. **Enerback S, Jacobsson A, Simpson EM, Guerra C, Yamashita H, Harper ME, and Kozak LP.** Mice lacking mitochondrial uncoupling protein are cold-sensitive but not obese. Nature 387: 90-94, 1997.

23. **Foster MT, and Bartness TJ.** Sympathetic but not sensory denervation stimulates white adipocyte proliferation. American Journal Physiology 291: R1630-R1637, 2006.

24. **Fredholm BB, Oberg B, and Rosell S.** Effects of vasoactive drugs on circulation in canine subcutaneous adipose tissue. Acta Physiol Scand 79: 564-574, 1970.

25. **Garretson JT, Szymanski, L. A., Schwartz, G. J., Xue, B. Z., Ryu, V., & Bartness, T. J.** Lipolysis sensation by white fat afferent nerves triggers brown fat thermogenesis. Molecular metabolism 5: 2016.

26. **Giordano A, Song CK, Bowers RR, Ehlen JC, Frontini A, Cinti S, and Bartness TJ.** White adipose tissue lacks significant vagal innervation and immunohistochemical evidence of parasympathetic innervation. Am J Physiol Regul Integr Comp Physiol 291: R1243-1255, 2006.

27. **Griggio MA.** Thermogenic mechanisms in cold-acclimated animals. BrazJ MedBiolRes 21: 171-176, 1988.

28. **Hamilton JM, Bartness TJ, and Wade GN.** Effects of norepinephrine and denervation on brown adipose tissue in Syrian hamsters. AmJPhysiol 257: R396-R404, 1989.

29. **Harris RB.** Sympathetic denervation of one white fat depot changes norepinephrine content and turnover in intact white and brown fat depots. Obesity(SilverSpring) 20: 1355-1364, 2012.

30. **Heldmaier G, Steinlechner S, Ruf T, Wiesinger H, and Klingenspor M.** Photoperiod and thermoregulation in vertebrates: body temperature rhythms and thermogenic acclimation. Journal Biological Rhythms 4: 251-265, 1989.

31. **Hofmann WE, Liu X, Bearden CM, Harper ME, and Kozak LP.** Effects of genetic background on thermoregulation and fatty acid-induced uncoupling of mitochondria in UCP1-deficient mice. J Biol Chem 276: 12460-12465, 2001.

32. **Ishibashi J, and Seale P.** Medicine. Beige can be slimming. Science 328: 1113-1114, 2010.

33. **Jimenez M, Barbatelli G, Allevi R, Cinti S, Seydoux J, Giacobino JP, Muzzin P, and Preitner F.** Beta 3-adrenoceptor knockout in C57BL/6J mice depresses the occurrence of brown adipocytes in white fat. European Journal of Biochemistry 270: 699-705, 2003.

34. **Kim JS, Enquist LW, and Card JP.** Circuit-specific coinfection of neurons in the rat central nervous system with two pseudorabies virus recombinants. Journal Virology 73: 9521-9531, 1999.

35. **Labbe SM, Caron A, Chechi K, Laplante M, Lecomte R, and Richard D.** Metabolic activity of brown, "beige," and white adipose tissues in response to chronic adrenergic stimulation in male mice. Am J Physiol Endocrinol Metab 311: E260-268, 2016.

36. **Leitner C, and Bartness TJ.** Acute brown adipose tissue temperature response to cold in monosodium glutamate-treated Siberian hamsters. Brain Res 1292: 38-51, 2009.

37. **Li P, Zhu Z, Lu Y, and Granneman JG.** Metabolic and cellular plasticity in white adipose tissue II: role of peroxisome proliferator-activated receptor-alpha. American Journal of Physiology 289: E617-626, 2005.

38. **Liu X, Rossmeisl M, McClaine J, Riachi M, Harper ME, and Kozak LP.** Paradoxical resistance to diet-induced obesity in UCP1-deficient mice. J Clin Invest 111: 399-407, 2003.

39. **Loncar D, Bedrica L, Mayer J, Cannon B, Nedergaard J, Afzelius BA, and Svajger A.** The effect of intermittent cold treatment on the adipose tissue of the cat. Apparent transformation from white to brown adipose tissue. Journal Ultrastructural Molecular Structural Research 97: 119-129, 1986.

40. **Mefford IN.** Application of high performance liquid chromatography with electrochemical detection to neurochemical analysis: measurement of catecholamines, serotonin and metabolites in rat brain. Journal Neuroscience Methods 3: 207-224, 1981.

41. **Meyer CW, Willershauser M, Jastroch M, Rourke BC, Fromme T, Oelkrug R, Heldmaier G, and Klingenspor M.** Adaptive thermogenesis and thermal conductance in wild-type and UCP1-KO mice. American Journal Physiology 299: R1396-1406, 2010.

42. **Migliorini RH, Lima-Verde JS, Machado CR, Cardona GM, Garofalo MA, and Kettelhut IC.** Control of adipose tissue lipolysis in ectotherm vertebrates. Am J Physiol 263: R857-862, 1992.

43. **Minokoshi Y, Saito M, and Shimazu T.** Sympathetic denervation impairs responses of brown adipose tissue to VMH stimulation. American Journal Physiology 251: R1005-1008, 1986.

44. **Morrison SF.** Central pathways controlling brown adipose tissue thermogenesis. News Physiol Sci 19: 67-74, 2004.

45. **Morrison SF, and Madden CJ.** Central nervous system regulation of brown adipose tissue. Compr Physiol 4: 1677-1713, 2014.

46. **Morrison SF, Nakamura K, and Madden CJ.** Central control of thermogenesis in mammals. ExpPhysiol 93: 773-797, 2008.

47. **Nakamura K, and Morrison SF.** Central efferent pathways mediating skin cooling-evoked sympathetic thermogenesis in brown adipose tissue. Am J Physiol Regul Integr Comp Physiol 292: R127-136, 2007.

48. **Nakayama T, and Hardy JD.** Unit responses in the rabbit's brain stem to changes in brain and cutaneous temperature. J Appl Physiol 27: 848-857, 1969.

49. **Nautiyal KM, Dailey MJ, Brito NA, Brito MN, Harris RBS, Bartness TJ, and Grill HJ.** Energetic responses to cold temperatures in rats lacking forebrain-caudal brainstem connections. AmJPhysiol 295: R789-R798, 2008.

50. **Nguyen NL, Randall J, Banfield BW, and Bartness TJ.** Central sympathetic innervations to visceral and subcutaneous white adipose tissue. Am J Physiol Regul Integr Comp Physiol 306: R375-386, 2014.

51. **Nicholls DG, and Locke RM.** Thermogenic mechanisms in brown fat. Physiol Rev 64: 1-64, 1984.

52. **Ootsuka Y, Blessing WW, and McAllen RM.** Inhibition of rostral medullary raphe neurons prevents cold-induced activity in sympathetic nerves to rat tail and rabbit ear arteries. Neurosci Lett 357: 58-62, 2004.

53. **Paxinos G, and Franklin KBJ.** The mouse brain in stereotaxic coordinates. San Diego: Academic Press, 2001.

54. **Petrovic N, Walden TB, Shabalina IG, Timmons JA, Cannon B, and Nedergaard J.** Chronic peroxisome proliferator-activated receptor gamma (PPARgamma) activation of epididymally derived white adipocyte cultures reveals a population of thermogenically competent, UCP1-containing adipocytes molecularly distinct from classic brown adipocytes. Journal Biological Chemistry 285: 7153-7164, 2010.

55. **Rooks CR, Penn DM, Kelso E, Bowers RR, Bartness TJ, and Harris RB.** Sympathetic denervation does not prevent a reduction in fat pad size of rats or mice treated with peripherally administered leptin. American Journal Physiology 289: R92-102, 2005.

56. **Rosell S.** Neuronal control of microvessels. AnnRevPhysiol 42: 359-371, 1980.

57. **Rosell S.** Release of free fatty acids from subcutaneous adipose tissue in dogs following sympathetic nerve stimulation. Acta Physiol Scand 67: 343-351, 1966.

58. **Ryu V, and Bartness TJ.** Short and long sympathetic-sensory feedback loops in white fat. Am J Physiol Regul Integr Comp Physiol 306: R886-900, 2014.

59. **Ryu V, Garretson JT, Liu Y, Vaughan CH, and Bartness TJ.** Brown adipose tissue has sympathetic-sensory feedback circuits. J Neurosci 35: 2181-2190, 2015.

60. **Sell H, Deshaies Y, and Richard D.** The brown adipocyte: update on its metabolic role. International Journal Biochemistry Cell Biology 36: 2098-2104, 2004.

61. **Shabalina IG, Petrovic N, de Jong JMA, Kalinovich AV, Cannon B, and Nedergaard J.** UCP1 in Brite/Beige Adipose Tissue Mitochondria Is Functionally Thermogenic. Cell Reports 5: 1196-1203, 2013.

62. **Shi H, and Bartness TJ.** Neurochemical phenotype of sympathetic nervous system outflow from brain to white fat. Brain Res Bull 54: 375-385, 2001.

63. **Song CK, Jackson RM, Harris RB, Richard D, and Bartness TJ.** Melanocortin-4 receptor mRNA is expressed in sympathetic nervous system outflow neurons to white adipose tissue. American Journal Physiology 289: R1467-R1476, 2005.

64. **Song CK, Vaughan CH, Keen-Rhinehart E, Harris RB, Richard D, and Bartness TJ.** Melanocortin-4 receptor mRNA expressed in sympathetic outflow neurons to brown adipose tissue: neuroanatomical and functional evidence. Am J Physiol Regul Integr Comp Physiol 295: R417-428, 2008.

65. **Ukropec J, Anunciado RP, Ravussin Y, Hulver MW, and Kozak LP.** UCP1-independent thermogenesis in white adipose tissue of cold-acclimated Ucp1-/- mice. J Biol Chem 281: 31894-31908, 2006.

66. **Ulhoa MA, da Silva NF, Pires JG, and Futuro Neto Hde A.** Raphe obscurus neurons participate in thermoregulation in rats. Arq Neuropsiquiatr 71: 249-253, 2013.

67. **van Marken Lichtenbelt W.** Human brown fat and obesity: methodological aspects. Front Endocrinol (Lausanne) 2: 52, 2011.

68. **Vaughan CH, and Bartness TJ.** Anterograde transneuronal viral tract tracing reveals central sensory circuits from brown fat and sensory denervation alters its thermogenic responses. Am J Physiol Regul Integr Comp Physiol 302: R1049-1058, 2012.

69. **Vaughan CH, Shrestha YB, and Bartness TJ.** Characterization of a novel melanocortin receptor-containing node in the SNS outflow circuitry to brown adipose tissue involved in thermogenesis. Brain Res 1411: 17-27, 2011.

70. **Vaughan CH, Zarebidaki E, Ehlen JC, and Bartness TJ.** Analysis and measurement of the sympathetic and sensory innervation of white and brown adipose tissue. Methods Enzymol 537: 199-225, 2014.

71. **Vitali A, Murano I, Zingaretti MC, Frontini A, Ricquier D, and Cinti S.** The adipose organ of obesity-prone C57BL/6J mice is composed of mixed white and brown adipocytes. JLipid Res 53: 619-629, 2012.

72. **Wertheimer E. Stoffwechselregulationen. I.** Regulation des Fettstoffwechsels. Die zentrale Regulierung der Fettmobilisierung. Pflugers Archives gesPhysiology 213: 262-298, 1926.

73. **Xue B, Coulter A, Rim JS, Koza RA, and Kozak LP.** Transcriptional synergy and the regulation of Ucp1 during brown adipocyte induction in white fat depots. Mol Cell Biol 25: 8311-8322, 2005.

74. **Young P, Arch JR, and Ashwell M.** Brown adipose tissue in the parametrial fat pad of the mouse. FEBS Lett 167: 10-14, 1984.

75. **Youngstrom TG, and Bartness TJ.** Catecholaminergic innervation of white adipose tissue in the Siberian hamster. AmJPhysiol 268: R744-R751, 1995.

4 SENSORY DENERVATION OF INGUINAL WHITE FAT MODIFIES SYMPATHETIC OUTFLOW TO WHITE AND BROWN FAT

4.1 Abstract

White adipose tissue (WAT) and brown adipose tissue (BAT) have sympathetic nervous system (SNS) and sensory innervations. Tract tracing revealed central neuroanatomical evidence of WAT sensory and BAT SNS crosstalk with double labeling of inguinal WAT (IWAT) sensory neurons and interscapular BAT (IBAT) SNS neurons. We previously demonstrated that WAT lipolysis increases IBAT temperature, but this effect is absent when IWAT afferents are surgically denervated. It is possible that WAT sensory feedback can regulate SNS drive to itself and other WAT depots and IBAT, and thus contribute to the existence of differential SNS outflow to fat during different energy challenges. Here we selectively denervated IWAT sensory nerves in Siberian hamsters using capsaicin and measured norepinephrine turnover (NETO) *i.e.*, SNS drive to WAT and BAT depots, IBAT uncoupling protein 1 (UCP1) expression, body mass, fat mass, NE content, blood glucose, and food consumed after a 24-hour cold exposure. IWAT sensory denervation decreased IWAT and IBAT NETO in addition to reduction of IBAT UCP1 expression. IWAT sensory denervation, however, increased mesenteric WAT (MWAT) NETO and did not modify epididymal WAT (EWAT) and retroperitoneal WAT (RWAT) NETO compared with respective controls. Fat mass and NE content had differential changes due to temperature and treatment while body mass, blood glucose, and food consumed were unchanged across groups. These results functionally demonstrate the existence of IWAT sensory and IBAT SNS crosstalk and that a disruption in this sensory-SNS feedback mechanism modifies SNS drive to IWAT, IBAT, and MWAT, but not EWAT and RWAT.

4.2 Introduction

Body fat in humans and rodent models has two important functions: supplying energy and maintaining body temperature. White adipose tissue (WAT) stores excess triacylglycerols, whereas brown adipose tissue (BAT) mainly generates heat for thermoregulation during cold exposure via dissipation of the mitochondrial proton gradient by uncoupling protein 1 (UCP1) [for reviews see: (11, 24, 26, 49)]. The sympathetic nervous system (SNS) regulates WAT and BAT [for reviews see: (4, 6, 7)] by liberating stored triacylglycerols through initiating lipolysis during times of energetic demands (8, 9, 54). In brief, norepinephrine (NE) released from SNS postganglionic nerve terminal act as an agonist on β adrenergic receptors (βAR) (31) to activate downstream lipolytic enzymes (32). Non-esterified free fatty acids (NEFAs) generated from lipolysis stimulate UCP1 synthesis and activation during β oxidation for BAT nonshivering thermogenesis (33).

Studies using NE turnover (NETO), a direct neurochemical measure of SNS activity in fat, revealed differential SNS outflow to WAT depots and IBAT within the same hamsters that were given energy challenges of either cold exposure, food deprivation, or glucoprivation (8, 9, 37, 38). Subcutaneous, inguinal WAT (IWAT) consistently had increased NETO in all of the previously mentioned challenges (9, 37). NETO of intra-abdominal WAT depots such as epididymal WAT (EWAT) and retroperitoneal WAT (RWAT), however, were unaffected by glucoprivation and food deprivation, respectively (9, 37). Visceral, mesenteric WAT (MWAT) NETO remained low and unchanged during food deprivation (38). MWAT was not included in earlier NETO studies, thus its response to cold exposure and glucoprivation is unknown. Interscapular BAT (IBAT) NETO was unaffected in situations of energy deficit, food deprivation and glucoprivation, but increased during cold exposure to trigger nonshivering

thermogenesis (9, 37). Heterogeneous SNS drive has also been demonstrated in rats and mice (21, 36, 62, 63). Therefore, it is clear that SNS regulation of body fat is complex and nuanced.

Trans-synaptic, viral tract tracers, pseudorabies virus (PRV) and the H129 strain of the herpes simplex virus, have demonstrated the presence of both SNS (1, 2, 37, 38) and sensory (57, 59) innervations within fat, respectively (46-48). PRV retrogradely labels central SNS neurons (55); H129, however, labels first order sensory neurons in the dorsal root ganglia (DRG), and higher order neurons in an anterograde manner (42). Doubly labeled SNS and sensory neurons were found across many brain sites when PRV and H129 were both injected into IWAT (46). The presence of doubly labeled neurons implicates a bidirectional communication between WAT and the central nervous system (CNS) as a potential feedback mechanism to maintain energetic homeostasis.

Evidence suggests that WAT sensory nerves communicate energy availability to the CNS possibly via leptin (35), a WAT adipokine that promotes negative energy balance, or lipolytic products such as NEFA and glycerol (22). Leptin injections intra-IWAT increases IWAT sensory nerve activity and cFos labeling in the DRG (35) and central or peripheral administration of leptin selectively increases SNS drive to WAT depots (41). In addition, unilateral leptin injections into EWAT produced an increase in SNS nerve activity in the contralateral EWAT indicating an ability to stimulate the sympatho-excitatory reflex regulation between WAT sensory and SNS pathways (39, 40). This sensory and SNS crosstalk was evident when unilateral denervation of EWAT SNS nerves prevented a leptin-induced decrease in mass of the intact, contralateral EWAT (43). The notion that WAT sensory nerves most likely sense lipolysis was supported by the observation that glucoprivation not only increased SNS activity and lipolysis (9), but also WAT sensory nerve activity (57). Thus, the existence of non-uniform SNS outflow

to WAT depots during energetic challenges may be due to WAT afferents providing sensory feedback to central premotor SNS nuclei regulating fat metabolism.

Brain regions comprising the central SNS outflow circuits to WAT and BAT are relatively similar as shown by patterns of overlap in PRV labeled SNS neurons (1, 2, 37, 38). Therefore, anatomical similarities in SNS pathways along with fat sensory innervations make communication among distinct fat depots probable. For example, denervation of SNS nerves to WAT decreased SNS outflow to intact WAT depots and IBAT likely through a change in sensory input from the denervated tissues (25). The explicit role of IWAT sensory nerves in regulating SNS drive to itself and other fat depots SNS, however, has not been investigated. Injections of H129 into IWAT and PRV into IBAT revealed doubly labeled central neurons of IWAT sensory and IBAT SNS crosstalk (48). When CL316,243, a βAR agonist, was injected into IWAT to initiate lipolysis, there was an acute increase in IWAT sensory nerve activity, DRG cFos labeling, and IBAT temperature, but this response was absent when IWAT was surgically denervated (22) implying regulation of IBAT function by IWAT afferents. Because surgical denervation severs both SNS and sensory nerves (60), it is unclear whether the decreased IBAT temperature was due to loss of IWAT SNS or sensory input. Nonetheless, the influence of WAT on IBAT function was also observed when WAT lipectomy significantly decreased IBAT NETO (51).

Given the evidence that IWAT sensory nerves contribute to fat metabolism and IBAT function, it is of interest to test whether the absence of sensory feedback from IWAT, a large energy storage depot, can modify SNS outflow to WAT and IBAT depots during a cold challenge. In the present study, we selectively denervated IWAT sensory nerves in Siberian hamsters using capsaicin. We used Siberian hamsters, because they become obese, gaining 50%

fat mass relative to body mass, in response to a change in photoperiod (16), which decreases potential confounding factors associated with other obesity inducing manipulations. Furthermore, the majority of studies investigating the neural innervation of fat have been done using this species (5-7). After IWAT sensory denervation, we measured SNS drive in WAT and IBAT depots, IBAT UCP1 protein expression, body mass, food consumption, and blood glucose in response to a 24-hour cold exposure.

4.3 Materials and Methods

4.3.1 ANIMALS

Adult male Siberian hamsters (*Phodopus sungorus*, 3 months old) were singly housed under a long day photoperiod light cycle (16 hour light:8 hour dark) and an ambient temperature of 22 ± 2°C. Hamsters were given ad libitum regular rodent chow (13.4% calories from fat, 29.8% calories from protein, and 56.7% calories from carbohydrates; Purina Rodent Chow, St. Louis, MO) and tap water for the duration of the study. All procedures were approved by the Georgia State University Institutional Animal Care and Use Committee and were in accordance with Public Health Service and United States Department of Agriculture guidelines.

4.3.2 BILATERAL IWAT SENSORY DENERVATION

After one week of acclimation to single housing, weight matched hamsters (n=83) were divided into two groups, vehicle control (VC, n=43) and bilateral capsaicin (CAP, n=40) injected hamsters. Body mass was recorded before and after the surgeries, which were performed using aseptic techniques. Hamsters were anesthetized with 2-3% isoflurane in oxygen (Baxter Healthcare, Deerfield, IL), and fur around the left and right inguinal region was shaved. An incision was made to first expose the right IWAT, and hamsters were injected with the VC (1:10, 100% ethanol: olive oil) or 20 µg/µl of capsaicin (Cat. No. M2028; Sigma-Aldrich, St. Louis,

MO) with 2 µl per locus spread across the fat pad for a total of 20 loci (6, 50, 52, 60). The Hamilton syringe was held in place for 45 seconds after each injection to prevent efflux when removing the syringe. The right incision site was closed with sterile wound clips and an incision was made on the left IWAT following the same procedures for the right IWAT. Hamsters were transferred to clean cages and given daily, subcutaneous injections of Ketofen (5 mg/kg; Fort Dodge Animal Health, Fort Dodge, IA), an analgesic, for 3 days post-surgery. Wound clips were removed a week after surgeries.

4.3.3 NETO WITH 24-HOUR COLD CHALLENGE

Two weeks after surgeries, hamsters were further divided into room temperature (VC RT and CAP RT) and 4°C cold exposed (VC cold and CAP cold) groups for measurement of NETO as previously described (37, 60). Hamsters were handled daily for one week before NETO to adapt them to handling associated with the procedure and to decrease stress induced NE release. On the day that the 24-hour cold exposure began, body mass and regular rodent chow given were measured, and hamsters were placed in clean cages with food, water, and bedding, but no cotton nestlet to avoid confounding factors of hamsters warming themselves. Body mass and food consumed were recorded at the conclusion of the study. NETO was measured during the last 4 hours of the cold exposure (9, 37). At the 20th hour, RT and cold exposed hamsters in both treatment groups were injected i.p. with α-methyl-p-tyrosine (250 mg/kg α-MPT; Sigma-Aldrich, St. Louis, MO), an active competitive inhibitor for tyrosine hydroxylase (TH), the rate limiting enzyme for NE production (8, 9, 60). A supplemental dose of α-MPT (125 mg/kg) was given at the 22nd hour to ensure the inhibition of NE synthesis (8, 9, 60). Four hours after the first α-MPT injection, hamsters were weighed, and then quickly decapitated. IBAT, IWAT, EWAT, MWAT, and RWAT were quickly harvested, weighed, frozen in liquid nitrogen and stored at -80°C until

NE extraction. To obtain baseline values of NE content for NETO calculations, one-half of hamsters from each treatment and temperature groups were rapidly decapitated without receiving α-MPT injections as previously performed (8, 9, 37, 60). Since α-MPT inhibits NE production, it is likely to alter circulating metabolic fuels, thus blood glucose was measured from non-α-MPT injected hamsters immediately after rapid decapitation using blood glucose test strips (ACCU-CHEK Compact Plus meter, Roche, USA).

IWAT, EWAT, RWAT, MWAT, and IBAT were processed and extracted for NE with dihydroxybenzylamine (Sigma-Aldrich, St. Louis, MO), an internal control for extraction efficiency. NE content and NETO were measured as described previously [for review see: (60)] and following our methods and the modification of the method of Mefford (34). Calculations were made according to the following formula: $k = (\lg[NE]0 - \lg[NE]4)/(0.434 \times 4)$ and $K = k[NE]0$, where k is the constant rate of NE efflux, [NE]0 is the initial NE concentration, [NE]4 is the final NE concentration, and K = NETO.

4.3.4 CALCITONIN GENE RELATED PEPTIDE (CGRP) ENZYME IMMUNOASSAY

To validate the chemical sensory denervation technique via capsaicin injections, portions of IWAT from the same tissue samples used for NE extraction were also used to measure levels of CGRP, a marker of sensory nerves, using an enzyme linked immunosorbent assay kit (SPI Bio, Massy, France) according to the manufacturer's directions as we have previously done (37, 59, 60). The correlation coefficient was 99.9% for CGRP assays.

4.3.5 WESTERN BLOT

IBAT UCP1 protein expression, a molecular indicator of BAT nonshivering thermogenesis, was measured in IBAT as previously described (15, 37). Primary antibodies used were rabbit anti-UCP1 (1:500; Abcam, Cambridge, MA) and rabbit anti-α tubulin (1:500, Cell

Signaling, Danvers, MA) as a loading control. Membranes were blocked with 5% non-fat dry milk in tris buffered saline (TBS), and then incubated with primary antibodies at 4°C overnight. They were washed with TBS with 0.1% tween 20 followed by 2-hour incubation with goat anti-rabbit Alexa Fluor 680 nm antibody (ThermoFisher Scientific, Carlsbad, CA) at room temperature. Protein bands were visualized using Odyssey FC Imaging System (Li Cor Biotechnology, Lincoln, NE). UCP1 protein expression was normalized to α tubulin.

4.3.6 STATISTICAL ANALYSES

Results are expressed as means ± SE. Statistical analyses were carried out using Systat Software (version 11.0, San Jose, CA). CGRP levels in VC and CAP hamsters were compared by t-test. All other data were statistically analyzed by two-way ANOVA (treatment X temperature). The Holm-Sidak post hoc test was used when differences within or between groups were obtained. Differences were considered statistically significant if $p<0.05$. Exact probabilities and test values were omitted from the results section for simplicity and clarity of the presentation of results.

4.4 Results

There were no differences in body mass of the different treatment groups before or after the cold challenge (Fig. 4.1, A). Cold exposed hamsters consumed significantly less chow during the challenge compared with hamsters housed at RT regardless of capsaicin injections (Fig. 4.1, B). There was no effect of capsaicin treatment or cold exposure on blood glucose (Fig. 4.1, C). CGRP, a sensory nerve associated peptide, was measured in IWAT to validate the efficacy of sensory denervation. CGRP levels were significantly lower in IWATs of CAP injected hamsters compared with VC hamsters (Fig. 4.2, A). NE content of IWAT also was significantly decreased in CAP injected hamsters compared with VC hamsters both at RT and in the cold (Fig. 4.2, B).

EWAT NE content was significantly increased in cold exposed hamsters regardless of capsaicin injections compared with RT housed hamsters (Fig. 4.2, B). There were no significant differences in NE content of RWAT and MWAT among VC and CAP injected hamsters housed at RT or 4°C (Fig. 4.2, B).

SNS outflow varied among different fat depots across treatment groups (Fig. 4.2, C). VC cold exposed hamsters had a significant increase in IWAT, EWAT, and RWAT NETO compared with VC hamsters at RT housing (Fig. 4.2, C). CAP injected hamsters had significantly decreased IWAT NETO compared with VC hamsters at RT and cold exposure failed to increase IWAT NETO in CAP injected hamsters (Fig. 4.2, C). By contrast, IWAT sensory denervation did not affect EWAT and RWAT NETO at RT or during cold exposure (Fig. 4.2, C). Unexpectedly, cold exposure caused a significant decrease in MWAT NETO of VC hamsters, whereas MWAT NETO of CAP injected hamsters was unchanged by cold exposure compared to RT hamsters (Fig. 4.2, C).

IWAT mass was not significantly different across groups (Fig. 4.2, D) whereas EWAT and RWAT mass were significantly decreased in CAP injected hamsters (Fig. 4.2, D). Cold exposure caused a significant decrease in RWAT mass of VC hamsters, but not CAP injected hamsters. By contrast, cold exposure decreased MWAT mass in CAP injected hamsters, but not the VC controls (Fig. 4.2, D).

Cold exposure caused a three-fold increase in NE content of IBAT in VC hamsters and this was attenuated, but not prevented in CAP injected hamsters (Fig. 4.3, A). There was a significant increase in IBAT NETO and IBAT UCP1 expression of cold exposed VC hamsters, but these responses were absent in CAP injected hamsters (Fig. 4.3, B-C). IBAT mass was significantly reduced by cold exposure in both VC and CAP injected hamsters (Fig. 4.3, D).

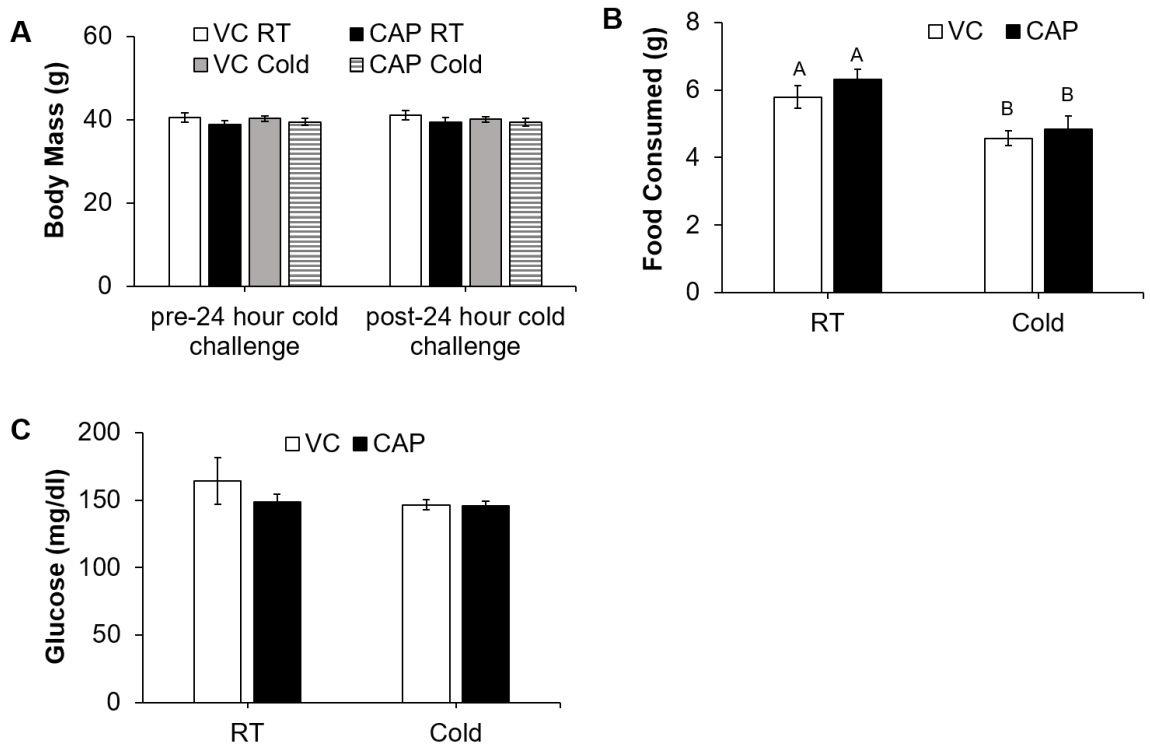

Figure 4.1 Body mass, food consumption, and glucose of control (VC) and IWAT sensory denervated (CAP) hamsters kept at room temperature (RT) or given a 24-hour cold (4°C) challenge.
(A) Body mass before and after cold challenge. (B) Food consumed during cold challenge. (C) Blood glucose after cold exposure. Within each panel, bars with different letters are significantly different from each other ($p<0.05$).

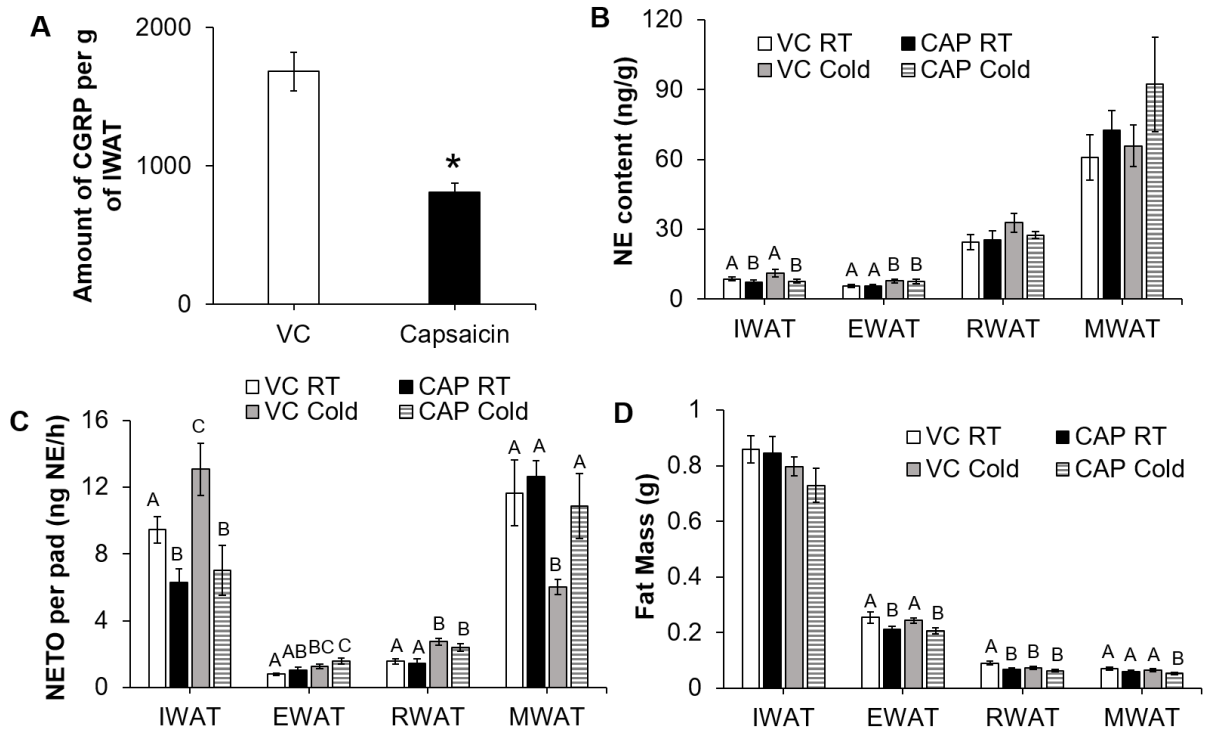

Figure 4.2 IWAT sensory denervation differentially changes SNS drive to WAT depots in hamsters given 24-hour cold (4°C) exposure.
(A) Levels of calcitonin gene related peptide (CGRP) in IWAT of controls (VC) and capsaicin injected (CAP) hamsters. (B) Norepinephrine (NE) content, (C) NE turnover (NETO), (D) and fat mass of WAT depots from VC and CAP injected hamsters kept at room temperature (RT) or 4°C. *$p<0.05$, vs. VC. Within each panel, bars with different letters are significantly different from each other ($p<0.05$).

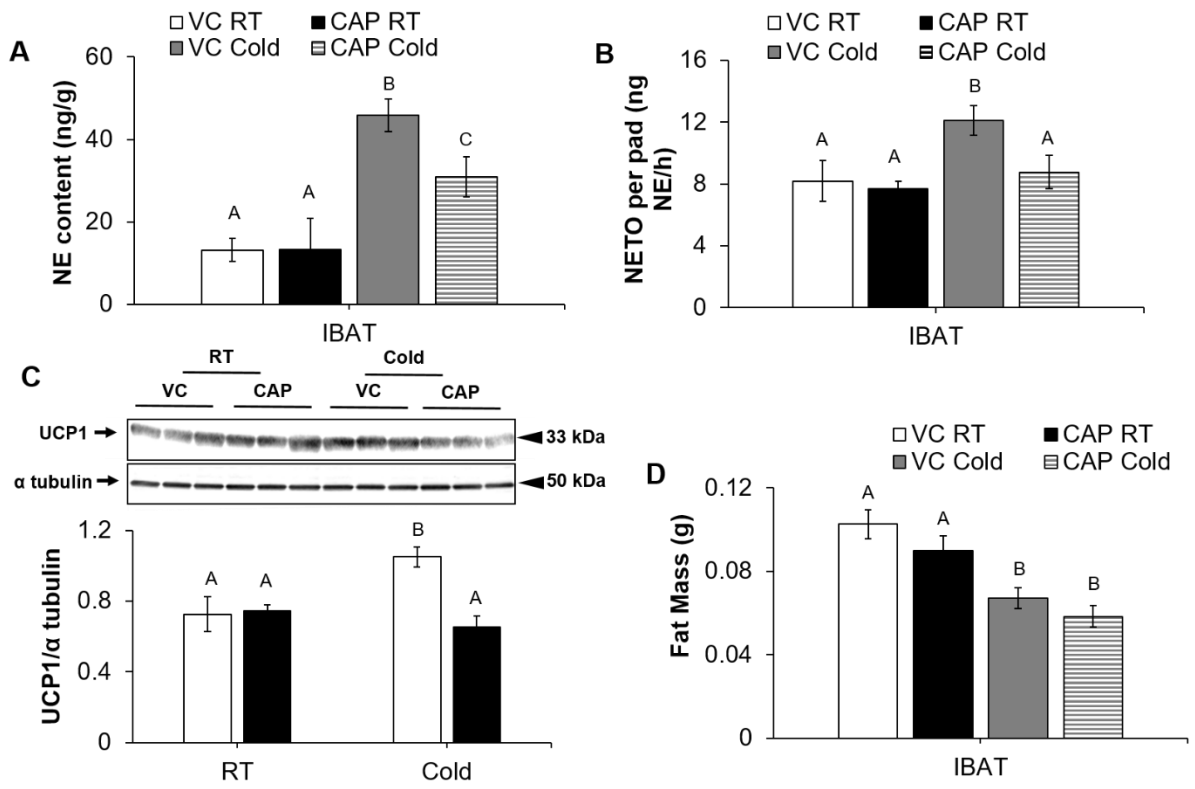

Figure 4.3 IWAT sensory denervation decreases SNS drive to IBAT in hamsters given 24-hour cold (4°C) exposure.
(A) Norepinephrine (NE) content, (B) NE turnover (NETO), (C) relative IBAT UCP1 protein expression normalized to α tubulin, and (D) IBAT mass of control (VC) and capsaicin injected (CAP) hamsters kept at room temperature (RT) or 4°C. Within each panel, bars with different letters are significantly different from each other ($p<0.05$).

4.5 Discussion

The neuroanatomy of WAT sensory innervation has been documented since the mid-1980s (17, 20, 23, 27, 39, 40), but its function in energetic homeostasis has only been studied in depth within the last decade (22, 30, 35, 46, 48, 53, 57). Here, we have functionally investigated the contribution of WAT sensory feedback to the SNS regulation of discrete fat depots. We specifically measured NETO in WAT depots and IBAT of hamsters that had IWAT sensory denervation using capsaicin. Capsaicin chemically destroys sensory nerves and is more specific than surgical denervation where both SNS and sensory nerves are likely to be severed due to their close proximity to each other (28, 29, 50, 52, 60). Unchanged TH staining in CAP injected WAT verified capsaicin's specificity for destroying afferents (18, 52). IWAT sensory denervation significantly reduced both IWAT and IBAT NETO and decreased IBAT UCP1 protein expression after a 24-hour cold challenge, which supports the necessity of IWAT sensory signaling to not only maintain function regulating its own SNS drive, but also the SNS drive to IBAT. On the other hand, with the exception of MWAT, SNS drive to other WAT depots were unaffected by IWAT sensory denervation.

As previously observed, the SNS outflow to IWAT was increased in VC cold exposed hamsters compared with RT housed hamsters (9, 37). SNS drive to IWAT in CAP injected hamsters at RT and cold exposed conditions, however, was significantly decreased likely because of the absence of IWAT sensory inflow *i.e.*, its neural signaling of energy availability to the CNS. Thus, without this sensory information central nuclei involved in the control of fat metabolism did not increase SNS drive to IWAT for lipid mobilization. Furthermore, IWAT sensory denervation significantly decreased SNS outflow to IBAT and reduced its UCP1 expression, which may also have translated into reduced IBAT temperature (37). These data

provide new evidence of WAT sensory and BAT SNS functional crosstalk and compliment a study from our lab that used surgical denervation to show that IWAT sensory nerves influence IBAT temperature in addition to IWAT lipolysis (22). Our current results from IWAT sensory chemical denervation expand upon these previous findings (22) and suggest that the decrease in IBAT temperature that was observed in animals with surgical denervation of IWAT was indeed due to sensory and not SNS denervation. Indirect evidence for this WAT and BAT sensorimotor interaction has also been documented when leptin injections into EWAT caused a steady increase in IBAT SNS nerve activity in rats (40). Furthermore, whole body capsaicin densensitization resulted in IBAT atrophy and decreased mitochondrial protein (14). The caveat to this study is that it is unclear whether IBAT atrophy was due to IWAT or IBAT sensory denervation or a non-specific side effect of systemically administered capsaicin. Nevertheless, tract tracing studies provides neuroanatomical evidence for bidirectional WAT sensory and BAT SNS feedback (48), where 50% of IWAT sensory and IBAT SNS neurons were found to colocalize across the brain (48) in nuclei that have been previously shown to be involved in SNS mediated thermogenesis and lipolysis (19, 56, 58). Thus, our functional demonstration of IWAT sensory input influencing IBAT SNS signaling is likely mediated by centrally distributed SNS nuclei involved in the regulation of fat metabolism.

Though the current study described here did not attempt to determine the molecular mechanism of WAT sensory and BAT SNS crosstalk, WAT sensory denervation may result in the absence of certain factors or molecules that might otherwise be sensed by the brain through WAT afferents as indications of WAT energy and/or metabolic status. Such candidate molecules include fatty acids (22) or leptin (35, 40). Eicosopentanoic acid (EPA) and arachidonic acid (AA) have preferential mobilization into plasma when animals are given a lipolytic challenge (13).

Independent injections of EPA or AA into IWAT and a mixture of EPA and AA significantly increased IWAT sensory nerve activity (22). Leptin is a potential candidate, because its receptors located on DRG neurons are activated by leptin injections into IWAT (35). In addition, peripheral administration of leptin selectively increase SNS drive to WAT (41). Further studies are needed in order to identify potential WAT-derived molecules that may act as WAT sensory afferent signals that regulate the IWAT sensory and IBAT SNS crosstalk.

On the other hand, SNS brain sites may sense the deficit in NEFA available for IBAT β oxidation due to decreased IWAT SNS drive in CAP injected hamsters. WAT lipolysis typically produces a large supply of NEFA that are predominantly delivered to BAT through the circulation (32), while BAT lipolysis produces a smaller NEFA supply (10). Though NEFA released from intact WAT depots can still influence IBAT SNS outflow and its residual function, the reduction in IWAT substrates for β oxidation likely has a role in attenuating IBAT activity. This has been shown when loss of NEFA source *i.e.*, removal of WAT by lipectomy significantly decreased SNS drive to IBAT (51).

Because only the sensory nerves in IWAT were destroyed and the SNS outflow to IBAT and IBAT UCP1 protein expression were significantly reduced, but not completely eliminated compared with respective controls, the contribution made by sensory nerves from IBAT and intact WAT depots to regulate IBAT thermogenic activity also need to be taken into consideration (47, 57, 59). The activation of sensory signaling from one fat tissue can plausibly increase efferent activity in other distant fat depots presumably through central sensory and SNS crosstalk. For example, leptin injections into EWAT increase EWAT afferent activity and SNS activity to IWAT and IBAT (40). Thus, remaining intact fat depots (IBAT, EWAT, RWAT, and MWAT) likely contributed sensory input to premotor SNS brain regions to support IBAT

function in CAP injected hamsters in this experiment. Prior NETO studies revealed RWAT and IWAT have the most comparable SNS drive profile compared with EWAT and MWAT during cold exposure, glucoprivation, cold exposure with food deprivation, bilateral EWAT SNS denervation, and central or peripheral leptin administration (9, 25, 41). Therefore, it is possible that sensory denervation of RWAT would also impair SNS drive to IBAT and consequently attenuate nonshivering thermogenesis.

This is the first time the SNS outflow to MWAT, the true visceral fat in rodent models, was measured during a cold challenge. By definition of visceral fat, MWAT drains into the hepatic portal vein unlike intra-abdominal WAT depots, EWAT and RWAT, which drain systemically into the inferior vena cava (12, 61). RT housed hamsters and cold exposed CAP injected hamsters had significantly higher MWAT NETO compared with cold exposed VC hamsters. *In vitro* studies have shown that primary adipocytes from MWAT have increased basal levels of free fatty acids and glycerol compared with adipocytes from EWAT (61). Thus, if the products of lipolysis are a signal to increase SNS drive to a fat pad, then the high rates of NETO in MWAT of RT housed hamsters may be accounted for by high levels of basal lipolysis. Interestingly, while cold exposure significantly reduced SNS drive to MWAT in VC injected hamsters, SNS drive to MWAT remained the same in CAP injected hamsters at RT or 4°C. Since MWAT is the most highly innervated fat depot compared with EWAT, RWAT, and IWAT (3), its high NETO values likely reflect this innervation by the SNS. This preserved SNS drive to MWAT, combined with unchanged SNS drives to EWAT and RWAT in CAP injected hamsters, may compensate for the decreased IWAT and IBAT NETO in CAP injected hamsters, and thus, may provide necessary fuels for these CAP injected hamsters to survive the cold challenge. Despite our best efforts to dissect MWAT from the viscera for NE extraction, it is possible that

some blood vessels remained in the tissue since MWAT is highly vascularized resulting in overestimation of MWAT NETO in RT housed and cold exposed CAP injected hamsters.

NE content and NETO among the fat depots did not have a consistent correlation. NE content is a static measure of SNS activity and does not imply functional changes in SNS outflow to the fat tissue (60), but rather is an indicator of potential fat depot specific differences in baseline conditions. Thus, it should not be used as an index of tissue SNS activity. In addition, EWAT, RWAT, MWAT, and IBAT mass exhibited some tendencies associated with SNS induced lipid mobilization, but also possibly non-SNS control of fat mass, which requires further studies to resolve these discrepancies. IWAT mass did not change in IWAT sensory denervated hamsters as previously observed (51), because the lack of sensory innervation promotes increased fat cell size, which is suggestive of decreased lipolysis likely because of the interrupted feedback mechanism.

After the 24-hour cold challenge, hamsters with denervated IWAT sensory nerves had similar body mass, food consumption, and blood glucose compared to intact hamsters. As reported previously (9), cold exposed hamsters most likely maintained body mass as a result of having *ad lib* access to chow and the acute duration of the cold exposure. Cold exposed hamsters regardless of CAP or VC injections ate relatively less than RT hamsters possibly because of short bouts of torpor, which is known to occur during cold exposure in an attempt to conserve energy during thermoregulatory demands (44, 45). Food intake and bouts of torpor are negatively correlated, but the causal relationship is still unclear (45). Nevertheless, IWAT sensory denervated hamsters were still able to mobilize stored fat for energy and had intact glucose control as shown by differential increases in SNS outflow to WAT depots and homogeneous blood glucose levels across groups, respectively.

Here, we have functionally demonstrated the existence of IWAT sensory and IBAT SNS crosstalk and that a disruption in this sensory-SNS feedback mechanism via IWAT sensory denervation decreases IWAT and IBAT SNS drive and attenuates IBAT UCP1 expression. IWAT sensory denervation modified SNS drive to MWAT, but not EWAT and RWAT.

4.6 Perspectives and Significance

It is becoming clear that afferent signaling from one fat depot has functional influence on other discrete and distant fat depots (22, 25, 39, 40, 43) and overall energy balance. Although the distributed control of body fat is biologically essential, it makes it difficult to develop strategies to specifically target obesity related factors contributing to fat accumulation in specific depots such as visceral fat. It also demands a holistic perspective on energy balance since there is communication among different fat depots. Further investigation will be needed to delineate the magnitude of sensory projections from individual WAT depots to central SNS nuclei projecting to IBAT. For example, one WAT depot may have more sensory projections than others may to these SNS brain sites projecting to IBAT and consequently have more influence on IBAT function and whole body energy metabolism. This is necessary to explore, because IBAT can significantly increase energy expenditure to promote a lean phenotype. Thus, it is important to understand the neural communication and crosstalk between WAT and BAT afferents and SNS nerves.

4.7 Acknowledgements

We thank Candace L. Barr (undergraduate research assistant) and Dr. J. Christopher Ehlen for technical assistance with tissue collection and chromatograph, respectively. We also thank Drs. Ruth Harris, Aaron Roseberry, Cheryl Vaughan, and Vitaly Ryu for insightful comments on the manuscript. Lastly, we thank GSU Department of Animal Resources for

husbandry care. This research was supported by NIH R37DK035254 to T.J.B. and NIH R01DK35254 and NIH R01DK107544 to B.X.

4.8 References

1. **Bamshad M, Aoki VT, Adkison MG, Warren WS, and Bartness TJ.** Central nervous system origins of the sympathetic nervous system outflow to white adipose tissue. The American journal of physiology 275: R291-299, 1998.

2. **Bamshad M, Song CK, and Bartness TJ.** CNS origins of the sympathetic nervous system outflow to brown adipose tissue. The American journal of physiology 276: R1569-1578, 1999.

3. **Bartness TJ, and Bamshad M.** Innervation of mammalian white adipose tissue: implications for the regulation of total body fat. The American journal of physiology 275: R1399-1411, 1998.

4. **Bartness TJ, Liu Y, Shrestha YB, and Ryu V.** Neural innervation of white adipose tissue and the control of lipolysis. Frontiers in Neuroendocrinology 2014.

5. **Bartness TJ, and Ryu V.** Neural control of white, beige and brown adipocytes. International journal of obesity supplements 5: S35-39, 2015.

6. **Bartness TJ, Shrestha YB, Vaughan CH, Schwartz GJ, and Song CK.** Sensory and sympathetic nervous system control of white adipose tissue lipolysis. Molecular and cellular endocrinology 318: 34-43, 2010.

7. **Bartness TJ, Vaughan CH, and Song CK.** Sympathetic and sensory innervation of brown adipose tissue. International journal of obesity 34 Suppl 1: S36-42, 2010.

8. **Brito MN, Brito NA, Baro DJ, Song CK, and Bartness TJ.** Differential activation of the sympathetic innervation of adipose tissues by melanocortin receptor stimulation. Endocrinology 148: 5339-5347, 2007.

9. **Brito NA, Brito MN, and Bartness TJ.** Differential sympathetic drive to adipose tissues after food deprivation, cold exposure or glucoprivation. American journal of physiology Regulatory, integrative and comparative physiology 294: R1445-1452, 2008.

10. **Calderon-Dominguez M, Mir JF, Fucho R, Weber M, Serra D, and Herrero L.** Fatty acid metabolism and the basis of brown adipose tissue function. Adipocyte 5: 98-118, 2016.

11. **Cannon B, and Nedergaard J.** The biochemistry of an inefficient tissue: brown adipose tissue. Essays in biochemistry 20: 110-164, 1985.

12. **Catalano KJ, Stefanovski D, and Bergman RN.** Critical role of the mesenteric depot versus other intra-abdominal adipose depots in the development of insulin resistance in young rats. Diabetes 59: 1416-1423, 2010.

13. **Conner WE, Lin DS, and Colvis C.** Differential mobilization of fatty acids from adipose tissue. J Lipid Res 37: 290-298, 1996.

14. **Cui J, and Himms-Hagen J.** Rapid but transient atrophy of brown adipose tissue in capsaicin-desensitized rats. AmJPhysiol 262: R562-R567, 1992.

15. **Cui X, Nguyen NL, Zarebidaki E, Cao Q, Li F, Zha L, Bartness T, Shi H, and Xue B.** Thermoneutrality decreases thermogenic program and promotes adiposity in high-fat diet-fed mice. Physiological reports 4: 2016.

16. **Demas GE, and Bartness TJ.** Direct innervation of white fat and adrenal medullary catecholamines mediate photoperiodic changes in body fat. American journal of physiology Regulatory, integrative and comparative physiology 281: R1499-1505, 2001.

17. **Fishman RB, and Dark J.** Sensory innervation of white adipose tissue. AmJPhysiol 253: R942-R944, 1987.

18. **Foster MT, and Bartness TJ.** Sympathetic but not sensory denervation stimulates white adipocyte proliferation. American Journal Physiology 291: R1630-R1637, 2006.

19. **Foster MT, Song CK, and Bartness TJ.** Hypothalamic paraventricular nucleus lesion involvement in the sympathetic control of lipid mobilization. Obesity 18: 682-689, 2010.

20. **Fredholm BB.** Nervous control of circulation and metabolism in white adipose tissue. In: New Perspectives in Adipose Tissue: Structure, Function and Development, edited by Cryer A, and Van RLR. Boston: Butterworth, 1985, p. 45-64.

21. **Garofalo MA, Kettelhut IC, Roselino JE, and Migliorini RH.** Effect of acute cold exposure on norepinephrine turnover rates in rat white adipose tissue. Journal of the autonomic nervous system 60: 206-208, 1996.

22. **Garretson JT, Szymanski LA, Schwartz GJ, Xue B, Ryu V, and Bartness TJ.** Lipolysis sensation by white fat afferent nerves triggers brown fat thermogenesis. Molecular metabolism 5: 626-634, 2016.

23. **Giordano A, Morroni M, Santone G, Marchesi GF, and Cinti S.** Tyrosine hydroxylase, neuropeptide Y, substance P, calcitonin gene-related peptide and vasoactive intestinal peptide in nerves of rat periovarian adipose tissue: an immunohistochemical and ultrastructural investigation. Journal of Neurocytology 25: 125-136, 1996.

24. **Griggio MA.** Thermogenic mechanisms in cold-acclimated animals. BrazJ MedBiolRes 21: 171-176, 1988.

25. **Harris RB.** Sympathetic denervation of one white fat depot changes norepinephrine content and turnover in intact white and brown fat depots. Obesity 20: 1355-1364, 2012.

26. **Heldmaier G, Steinlechner S, Ruf T, Wiesinger H, and Klingenspor M.** Photoperiod and thermoregulation in vertebrates: body temperature rhythms and thermogenic acclimation. Journal Biological Rhythms 4: 251-265, 1989.

27. **Hill B, Ralevic V, Crowe R, and Burnstock G.** Innervation and nitric oxide modulation of mesenteric arteries of the Golden hamster. European Journal of Pharmacology 317: 275-283, 1996.

28. **Jansco G, Kiraly E, and Jansco-Gabor A.** Direct evidence for an axonal site of action of capsaicin. Nauyn-Schmiedeberg's ArchPharmacol 31: 91-94, 1980.

29. **Jansco G, Kiraly E, Joo F, Such G, and Nagy A.** Selective degeneration by capsaicin of a subpopulation of primary sensory neurons in the adult rat. Neuroscience Letters 59: 209-214, 1985.

30. **Kosacka J, Nowicki M, Kacza J, Borlak J, Engele J, and Spanel-Borowski K.** Adipocyte-derived angiopoietin-1 supports neurite outgrowth and synaptogenesis of sensory neurons. Journal of neuroscience research 83: 1160-1169, 2006.

31. **Lafontan M, Barbe P, Galitzky J, Tavernier G, Langin D, Carpene C, Bousquet-Melou A, and Berlan M.** Adrenergic regulation of adipocyte metabolism. Human reproduction 12 Suppl 1: 6-20, 1997.

32. **Lass A, Zimmermann R, Oberer M, and Zechner R.** Lipolysis - a highly regulated multi-enzyme complex mediates the catabolism of cellular fat stores. Progress in lipid research 50: 14-27, 2011.

33. **Matthias A, Ohlson KB, Fredriksson JM, Jacobsson A, Nedergaard J, and Cannon B.** Thermogenic responses in brown fat cells are fully UCP1-dependent. UCP2 or UCP3 do not substitute for UCP1 in adrenergically or fatty scid-induced thermogenesis. J Biol Chem 275: 25073-25081, 2000.

34. **Mefford IN.** Application of high performance liquid chromatography with electrochemical detection to neurochemical analysis: measurement of catecholamines, serotonin and metabolites in rat brain. Journal Neuroscience Methods 3: 207-224, 1981.

35. **Murphy KT, Schwartz GJ, Nguyen NL, Mendez JM, Ryu V, and Bartness TJ.** Leptin-sensitive sensory nerves innervate white fat. American journal of physiology Endocrinology and metabolism 304: E1338-1347, 2013.

36. **Nautiyal KM, Dailey M, Brito N, Brito MN, Harris RB, Bartness TJ, and Grill HJ.** Energetic responses to cold temperatures in rats lacking forebrain-caudal brain stem

connections. American journal of physiology Regulatory, integrative and comparative physiology 295: R789-798, 2008.

37. **Nguyen NL, Barr CL, Ryu V, Cao Q, Xue B, and Bartness TJ.** Separate and shared sympathetic outflow to white and brown fat coordinately regulates thermoregulation and beige adipocyte recruitment. American journal of physiology Regulatory, integrative and comparative physiology 312: R132-R145, 2017.

38. **Nguyen NL, Randall J, Banfield BW, and Bartness TJ.** Central sympathetic innervations to visceral and subcutaneous white adipose tissue. American journal of physiology Regulatory, integrative and comparative physiology 306: R375-386, 2014.

39. **Niijima A.** Afferent signals from leptin sensors in the white adipose tissue of the epididymis, and their reflex effect in the rat. J Auton Nerv Syst 73: 19-25, 1998.

40. **Niijima A.** Reflex effects from leptin sensors in the white adipose tissue of the epididymis to the efferent activity of the sympathetic and vagus nerve in the rat. Neurosci Lett 262: 125-128, 1999.

41. **Penn DM, Jordan LC, Kelso EW, Davenport JE, and Harris RB.** Effects of central or peripheral leptin administration on norepinephrine turnover in defined fat depots. AmJ Physiol RegulIntegrComp Physiol 291: R1613-R1621, 2006.

42. **Rinaman L, and Schwartz G.** Anterograde transneuronal viral tracing of central viscerosensory pathways in rats. J Neurosci 24: 2782-2786, 2004.

43. **Rooks CR, Penn DM, Kelso E, Bowers RR, Bartness TJ, and Harris RB.** Sympathetic denervation does not prevent a reduction in fat pad size of rats or mice treated with peripherally administered leptin. American journal of physiology Regulatory, integrative and comparative physiology 289: R92-102, 2005.

44. **Ruf T, and Heldmaier G.** Reduced locomotor activity following daily torpor in the Djungarian hamster: recovery from hypothermia? Naturwissenschaften 79: 574-575, 1992.

45. **Ruf TP, Klingenspor M, Preis H, and Heldmaier G.** Daily torpor in the Djungarian hamster (Phodopus sungorus): Interactions with food intake, activity and social behavior. JCompPhysiol 160: 609-615, 1991.

46. **Ryu V, and Bartness TJ.** Short and long sympathetic-sensory feedback loops in white fat. American journal of physiology Regulatory, integrative and comparative physiology 306: R886-900, 2014.

47. **Ryu V, Garretson JT, Liu Y, Vaughan CH, and Bartness TJ.** Brown adipose tissue has sympathetic-sensory feedback circuits. The Journal of neuroscience : the official journal of the Society for Neuroscience 35: 2181-2190, 2015.

48. **Ryu V, Watts AG, Xue B, and Bartness TJ.** Bidirectional Crosstalk between the Sensory and Sympathetic Motor Systems Innervating Brown and White Adipose Tissue in Male Siberian Hamsters. American journal of physiology Regulatory, integrative and comparative physiology ajpregu 00456 02015, 2017.

49. **Sell H, Deshaies Y, and Richard D.** The brown adipocyte: update on its metabolic role. International Journal Biochemistry Cell Biology 36: 2098-2104, 2004.

50. **Shi H, and Bartness TJ.** White adipose tissue sensory nerve denervation mimics lipectomy-induced compensatory increases in adiposity. American journal of physiology Regulatory, integrative and comparative physiology 289: R514-R520, 2005.

51. **Shi H, Bowers RR, and Bartness TJ.** Norepinephrine turnover in brown and white adipose tissue after partial lipectomy. Physiol Behav 81: 535-542, 2004.

52. **Shi H, Song CK, Giordano A, Cinti S, and Bartness TJ.** Sensory or sympathetic white adipose tissue denervation differentially affects depot growth and cellularity. American journal of physiology Regulatory, integrative and comparative physiology 288: R1028-1037, 2005.

53. **Shi Z, Chen WW, Xiong XQ, Han Y, Zhou YB, Zhang F, Gao XY, and Zhu GQ.** Sympathetic activation by chemical stimulation of white adipose tissues in rats. JApplPhysiol 112: 1008-1014, 2012.

54. **Shrestha YB, Vaughan CH, Smith BJ, Jr., Song CK, Baro DJ, and Bartness TJ.** Central melanocortin stimulation increases phosphorylated perilipin A and hormone-sensitive lipase in adipose tissues. American journal of physiology Regulatory, integrative and comparative physiology 299: R140-149, 2010.

55. **Song CK, Enquist LW, and Bartness TJ.** New developments in tracing neural circuits with herpesviruses. Virus research 111: 235-249, 2005.

56. **Song CK, Jackson RM, Harris RB, Richard D, and Bartness TJ.** Melanocortin-4 receptor mRNA is expressed in sympathetic nervous system outflow neurons to white adipose tissue. American journal of physiology Regulatory, integrative and comparative physiology 289: R1467-1476, 2005.

57. **Song CK, Schwartz GJ, and Bartness TJ.** Anterograde transneuronal viral tract tracing reveals central sensory circuits from white adipose tissue. American journal of physiology Regulatory, integrative and comparative physiology 296: R501-511, 2009.

58. **Song CK, Vaughan CH, Keen-Rhinehart E, Harris RB, Richard D, and Bartness TJ.** Melanocortin-4 receptor mRNA expressed in sympathetic outflow neurons to brown adipose tissue: neuroanatomical and functional evidence. American journal of physiology Regulatory, integrative and comparative physiology 295: R417-428, 2008.

59. **Vaughan CH, and Bartness TJ.** Anterograde transneuronal viral tract tracing reveals central sensory circuits from brown fat and sensory denervation alters its thermogenic responses. American journal of physiology Regulatory, integrative and comparative physiology 302: R1049-1058, 2012.

60. **Vaughan CH, Zarebidaki E, Ehlen JC, and Bartness TJ.** Analysis and measurement of the sympathetic and sensory innervation of white and brown adipose tissue. Methods in enzymology 537: 199-225, 2014.

61. **Wueest S, Yang X, Liu J, Schoenle EJ, and Konrad D.** Inverse regulation of basal lipolysis in perigonadal and mesenteric fat depots in mice. American journal of physiology Endocrinology and metabolism 302: E153-160, 2012.

62. **Yoshida T, Kemnitz JW, and Bray GA.** Lateral hypothalamic lesions and norepinephrine turnover in rats. The Journal of clinical investigation 72: 919-927, 1983.

63. **Yoshioka K, Yoshida T, and Kondo M.** Effect of acute cold-exposure on norepinephrine turnover and thermogenesis in brown adipose tissue and metabolic rate in MSG-induced obese mice. The Japanese journal of physiology 39: 957-962, 1989.

5 CONCLUDING REMARKS

We approached the studies in this dissertation with a complementary focus on investigating the neuroanatomy and function of the neural regulation of fat in order to gain a more complete understanding into how one may influence the other. Data from the three aims provided new and vital neuroanatomical and functional information about the integrated and complex control of body fat and thermoregulation through the crosstalk of SNS circuitries to WAT depots and IBAT and the role of WAT sensory nerves for regulation of SNS drive to body fat.

The importance in outlining this neuroanatomy is to establish a structural foundation for the basis of mechanistic studies and to add to interpretation and discussion of the neural regulation of adipose biology. More specifically in accordance with our hypothesis, there are indeed groups of central SNS neurons across the brain ultimately innervating both visceral fat (MWAT) and subcutaneous fat (IWAT) and both IWAT and IBAT. We found that MWAT and IWAT have relatively separate SNS circuitries within the forebrain and midbrain, but moderately shared SNS circuitries (~20–50%) within the hindbrain. In contrast to these two WAT depots, IWAT and IBAT have substantially separate SNS circuitries throughout the brain with only ~10–40% colocalization of IWAT and IBAT SNS neurons. Overall, the overlap in SNS innervations between MWAT and IWAT and between IWAT and IBAT was not unexpected, because of the similarities in labeled brain regions across previous tract tracing studies of fat (4, 5, 108, 110). Results from our tract-tracing studies established the neuroanatomical reality of shared origins of SNS outflow among different fat depots as well as their separate SNS innervations within the same animals. These extensive neuronal quantifications of doubly labeled and singly labeled SNS neurons provide an anatomical basis and a map of sorts to conduct future functional studies

of site specific targeting to induce lipolysis, nonshivering thermogenesis, or beige adipocyte recruitment.

Furthermore, we functionally tested for the presence of a crosstalk between IWAT SNS and IBAT SNS by selectively denervating SNS nerves to IBAT and giving those hamsters a cold challenge. In agreement with our hypothesis, there was indeed SNS coordination with IWAT for thermoregulatory purposes when IBAT function was impaired, because IWAT temperature, UCP1 expression, and beige adipocyte recruitment increased in cold exposed hamsters. Furthermore, the SNS drive to IWAT was significantly increased in hamsters with IBAT SNS denervation compared with intact hamsters. Groups of central, SNS neurons shared between IWAT and IBAT may coordinate nonshivering thermogenesis and beige adipocyte recruitment. However, we did not test the necessity or sufficiency of those brain sites in doing so. An additional caveat here is that other BAT depots were functionally intact in IBAT SNS denervated hamsters, thus it is unknown whether WAT depots alone could sufficiently maintain body temperature especially through a chronic cold challenge. Using transgenic mice with whole body impairment of UCP1 protein levels or transcription factors regulating thermogenesis only in BAT depots will be useful and ideal to answering this question, but currently there are no Cre lines that will allow for this type of specificity without affecting genes in beige adipocytes.

In addition to the shared SNS circuitries between MWAT and IWAT and between IBAT and IWAT, we documented a moderate percentage of central SNS neurons singly projecting to each fat depot throughout the brain. We suspect these neurons contribute to the reality of differential SNS drive to WAT depots and IBAT, because in CHAPTER 2, only IWAT NETO was increased in hamsters given acute food deprivation challenge; whereas there was no change of NETO in other fat depots during acute food deprivation. MWAT NETO was unexpectedly

negligible in both control and food deprived hamsters. This discrepancy is likely the result of having to use different hamsters for the baseline and AMPT groups. The k value (NE constant rate of efflux) of the baseline hamsters was lower than the AMPT group, which caused the NETO value to be negative/neglible.

Lastly, we demonstrated that IWAT sensory nerves are indeed necessary to facilitate the communication among different fat depots and regulate their SNS drive. The loss of IWAT sensory nerves via sensory denervation decreased both IWAT and more importantly IBAT NETO and UCP1 protein expression during a 24-hour cold challenge. SNS drive to MWAT in these hamsters, however, was significantly increased compared with vehicle control cold exposed hamsters. SNS drive to EWAT and RWAT in IWAT sensory denervated hamsters remained unchanged. This further confirms our hypothesis that sensory afferents from WAT pads to the brain may serve as feedback coordination between sensory and SNS regulation in the fat pads and that shared and separate SNS neuronal circuits among different fat depots contribute to the differential regulation of SNS drive to these fat depot when IWAT sensory afferents are destroyed.

Overall, the studies in this dissertation provide neuroanatomical evidence of separate and shared SNS brain sites and mechanistic evidence of the roles of SNS and sensory nerves innervating fat to regulate energetic homeostasis and thermoregulation. The underlying mechanism responsible for differential SNS drive to fat in response to lipolytic challenges, however, is still a mystery. From previous studies in the literature and data from experiments in this dissertation, we speculate that shared neurons within the brain comprising SNS outflow circuits to WAT depots and IBAT receive a combination of inhibitory and excitatory signals from fat sensory nerves to coordinate the SNS outflow to these tissues. Sensory nerves

innervating WAT depots and IBAT likely provide feedback regarding energy status and changes in the fat depot milieu. IBAT afferents may also communicate changes in temperature sensed by cutaneous thermoreceptors to initiate nonshivering thermogenesis. Singly labeled SNS neurons receive signals of inhibition or excitation from fat afferents to contribute to the SNS drive exclusive to that fat tissue. A disruption in the sensory and SNS feedback mechanism can modify SNS drive to fat depots and attenuate their functions. Moving forward, future studies defining the phenotype of these central SNS and sensory neurons innervating fat are needed in order to gain insight into how and perhaps by what signaling molecule these SNS and sensory neurons are using to coordinate their function.

REFERENCES

1. **Adams KF, Schatzkin A, Harris TB, Kipnis V, Mouw T, Ballard-Barbash R, Hollenbeck A, and Leitzmann MF.** Overweight, obesity, and mortality in a large prospective cohort of persons 50 to 71 years old. The New England journal of medicine 355: 763-778, 2006.

2. **Adler ES, Hollis JH, Clarke IJ, Grattan DR, and Oldfield BJ.** Neurochemical characterization and sexual dimorphism of projections from the brain to abdominal and subcutaneous white adipose tissue in the rat. The Journal of neuroscience : the official journal of the Society for Neuroscience 32: 15913-15921, 2012.

3. **Alhadeff AL, and Grill HJ.** Hindbrain nucleus tractus solitarius glucagon-like peptide-1 receptor signaling reduces appetitive and motivational aspects of feeding. American journal of physiology Regulatory, integrative and comparative physiology 307: R465-470, 2014.

4. **Bamshad M, Aoki VT, Adkison MG, Warren WS, and Bartness TJ.** Central nervous system origins of the sympathetic nervous system outflow to white adipose tissue. The American journal of physiology 275: R291-299, 1998.

5. **Bamshad M, Song CK, and Bartness TJ.** CNS origins of the sympathetic nervous system outflow to brown adipose tissue. The American journal of physiology 276: R1569-1578, 1999.

6. **Banfield BW, Kaufman JD, Randall JA, and Pickard GE.** Development of pseudorabies virus strains expressing red fluorescent proteins: new tools for multisynaptic labeling applications. Journal of virology 77: 10106-10112, 2003.

7. **Barja-Fernandez S, Leis R, Casanueva FF, and Seoane LM.** Drug development strategies for the treatment of obesity: how to ensure efficacy, safety, and sustainable weight loss. Drug design, development and therapy 8: 2391-2400, 2014.

8. **Bartness TJ, and Bamshad M.** Innervation of mammalian white adipose tissue: implications for the regulation of total body fat. The American journal of physiology 275: R1399-1411, 1998.

9. **Bartness TJ, Kay Song C, Shi H, Bowers RR, and Foster MT.** Brain-adipose tissue cross talk. The Proceedings of the Nutrition Society 64: 53-64, 2005.

10. **Bartness TJ, Liu Y, Shrestha YB, and Ryu V.** Neural innervation of white adipose tissue and the control of lipolysis. Frontiers in neuroendocrinology 35: 473-493, 2014.

11. **Bartness TJ, and Ryu V.** Neural control of white, beige and brown adipocytes. International journal of obesity supplements 5: S35-39, 2015.

12. **Bartness TJ, and Song CK.** Thematic review series: adipocyte biology. Sympathetic and sensory innervation of white adipose tissue. Journal of lipid research 48: 1655-1672, 2007.

13. **Bartness TJ, Vaughan CH, and Song CK.** Sympathetic and sensory innervation of brown adipose tissue. International journal of obesity 34 Suppl 1: S36-42, 2010.

14. **Bartness TJ, and Wade GN**. Photoperiodic control of seasonal body weight cycles in hamsters. Neuroscience and biobehavioral reviews 9: 599-612, 1985.

15. **Bertin E, Arner P, Bolinder J, and Hagstrom-Toft E.** Action of glucagon and glucagon-like peptide-1-(7-36) amide on lipolysis in human subcutaneous adipose tissue and skeletal muscle in vivo. The Journal of clinical endocrinology and metabolism 86: 1229-1234, 2001.

16. **Boldogkoi Z, Sik A, Denes A, Reichart A, Toldi J, Gerendai I, Kovacs KJ, and Palkovits M.** Novel tracing paradigms--genetically engineered herpesviruses as tools for mapping functional circuits within the CNS: present status and future prospects. Progress in neurobiology 72: 417-445, 2004.

17. **Bowers RR, Festuccia WT, Song CK, Shi H, Migliorini RH, and Bartness TJ.** Sympathetic innervation of white adipose tissue and its regulation of fat cell number. American journal of physiology Regulatory, integrative and comparative physiology 286: R1167-1175, 2004.

18. **Brito NA, Brito MN, and Bartness TJ.** Differential sympathetic drive to adipose tissues after food deprivation, cold exposure or glucoprivation. American journal of physiology Regulatory, integrative and comparative physiology 294: R1445-1452, 2008.

19. **Cannon B, and Nedergaard J.** Brown adipose tissue: function and physiological significance. Physiological reviews 84: 277-359, 2004.

20. **Cantu RC, and Goodman HM.** Effects of denervation and fasting on white adipose tissue. The American journal of physiology 212: 207-212, 1967.

21. **Card JP, and Enquist LW.** Use and Visualization of Neuroanatomical Viral Transneuronal Tracers. In: Visualization Techniques: From Immunohistochemistry to Magnetic Resonance Imaging, edited by Badoer E. Totowa, NJ: Humana Press, 2012, p. 225-268.

22. **Catalano KJ, Stefanovski D, and Bergman RN.** Critical role of the mesenteric depot versus other intra-abdominal adipose depots in the development of insulin resistance in young rats. Diabetes 59: 1416-1423, 2010.

23. **Choquet H, and Meyre D.** Genetics of Obesity: What have we Learned? Current genomics 12: 169-179, 2011.

24. **Coimbra CC, and Migliorini RH.** Evidence for a longitudinal pathway in rat hypothalamus that controls FFA mobilization. The American journal of physiology 245: E332-337, 1983.

25. **Coimbra CC, and Migliorini RH.** Insulin-sensitive glucoreceptors in rat preoptic area that regulate FFA mobilization. The American journal of physiology 251: E703-706, 1986.

26. **Cousin B, Cinti S, Morroni M, Raimbault S, Ricquier D, Penicaud L, and Casteilla L.** Occurrence of brown adipocytes in rat white adipose tissue: molecular and morphological characterization. Journal of cell science 103 (Pt 4): 931-942, 1992.

27. **Czaja K, Kraeling R, Klimczuk M, Franke-Radowiecka A, Sienkiewicz W, and Lakomy M.** Distribution of ganglionic sympathetic neurons supplying the subcutaneous, perirenal and mesentery fat tissue depots in the pig. Acta neurobiologiae experimentalis 62: 227-234, 2002.

28. **Demas GE, and Bartness TJ.** Direct innervation of white fat and adrenal medullary catecholamines mediate photoperiodic changes in body fat. American journal of physiology Regulatory, integrative and comparative physiology 281: R1499-1505, 2001.

29. **Dib B, Rompre PP, Amir S, and Shizgal P.** Thermogenesis in brown adipose tissue is activated by electrical stimulation of the rat dorsal raphe nucleus. Brain research 650: 149-152, 1994.

30. **Diculescu I, and Stoica M.** Fluorescence histochemical investigation on the adrenergic innervation of the white adipose tissue in the rat. Journal of neuro-visceral relations 32: 25-36, 1970.

31. **Dogiel AS.** Die sensiblen Nervenedigungen im Herzen und in den Blutgefassen der Saugethiere. Arch mikr Anat 52: 44-70, 1898.

32. **Dulloo AG, and Miller DS.** Energy balance following sympathetic denervation of brown adipose tissue. Canadian journal of physiology and pharmacology 62: 235-240, 1984.

33. **Ekstrand MI, Enquist LW, and Pomeranz LE.** The alpha-herpesviruses: molecular pathfinders in nervous system circuits. Trends in molecular medicine 14: 134-140, 2008.

34. **Farooqi IS, Keogh JM, Yeo GS, Lank EJ, Cheetham T, and O'Rahilly S.** Clinical spectrum of obesity and mutations in the melanocortin 4 receptor gene. The New England journal of medicine 348: 1085-1095, 2003.

35. **Field AE, Coakley EH, Must A, Spadano JL, Laird N, Dietz WH, Rimm E, and Colditz GA.** Impact of overweight on the risk of developing common chronic diseases during a 10-year period. Archives of internal medicine 161: 1581-1586, 2001.

36. **Figala J, Hoffmann K, and Goldau G.** [The annual cycle in the Djungarian Hamster Phodopus sungorus Pallas]. Oecologia 12: 89-118, 1973.

37. **Fishman RB, and Dark J.** Sensory innervation of white adipose tissue. The American journal of physiology 253: R942-944, 1987.

38. **Flegal KM, Carroll MD, Kit BK, and Ogden CL.** Prevalence of obesity and trends in the distribution of body mass index among US adults, 1999-2010. Jama 307: 491-497, 2012.

39. **Foster MT, and Bartness TJ.** Sympathetic but not sensory denervation stimulates white adipocyte proliferation. American journal of physiology Regulatory, integrative and comparative physiology 291: R1630-1637, 2006.

40. **Foster MT, Song CK, and Bartness TJ.** Hypothalamic paraventricular nucleus lesion involvement in the sympathetic control of lipid mobilization. Obesity 18: 682-689, 2010.

41. **Fothergill E, Guo J, Howard L, Kerns JC, Knuth ND, Brychta R, Chen KY, Skarulis MC, Walter M, Walter PJ, and Hall KD.** Persistent metabolic adaptation 6 years after "The Biggest Loser" competition. Obesity 24: 1612-1619, 2016.

42. **Frayn KN.** Adipose tissue as a buffer for daily lipid flux. Diabetologia 45: 1201-1210, 2002.

43. **Friedman JM, and Halaas JL.** Leptin and the regulation of body weight in mammals. Nature 395: 763-770, 1998.

44. **Garofalo MA, Kettelhut IC, Roselino JE, and Migliorini RH.** Effect of acute cold exposure on norepinephrine turnover rates in rat white adipose tissue. Journal of the autonomic nervous system 60: 206-208, 1996.

45. **Garretson JT, Szymanski LA, Schwartz GJ, Xue B, Ryu V, and Bartness TJ.** Lipolysis sensation by white fat afferent nerves triggers brown fat thermogenesis. Molecular metabolism 5: 626-634, 2016.

46. **Gasteyger C, and Tremblay A.** Metabolic impact of body fat distribution. Journal of endocrinological investigation 25: 876-883, 2002.

47. **Gerendai I, Kocsis K, and Halasz B.** Supraspinal connections of the ovary: structural and functional aspects. Microscopy research and technique 59: 474-483, 2002.

48. **Giordano A, Morroni M, Santone G, Marchesi GF, and Cinti S.** Tyrosine hydroxylase, neuropeptide Y, substance P, calcitonin gene-related peptide and vasoactive intestinal peptide in nerves of rat periovarian adipose tissue: an immunohistochemical and ultrastructural investigation. Journal of neurocytology 25: 125-136, 1996.

49. **Giordano A, Song CK, Bowers RR, Ehlen JC, Frontini A, Cinti S, and Bartness TJ.** White adipose tissue lacks significant vagal innervation and immunohistochemical evidence of parasympathetic innervation. American journal of physiology Regulatory, integrative and comparative physiology 291: R1243-1255, 2006.

50. **Gravholt CH, Moller N, Jensen MD, Christiansen JS, and Schmitz O.** Physiological levels of glucagon do not influence lipolysis in abdominal adipose tissue as assessed by microdialysis. The Journal of clinical endocrinology and metabolism 86: 2085-2089, 2001.

51. **Hamilton JM, Bartness TJ, and Wade GN.** Effects of norepinephrine and denervation on brown adipose tissue in Syrian hamsters. The American journal of physiology 257: R396-404, 1989.

52. **Harris RB.** Sympathetic denervation of one white fat depot changes norepinephrine content and turnover in intact white and brown fat depots. Obesity 20: 1355-1364, 2012.

53. **Hedley AA, Ogden CL, Johnson CL, Carroll MD, Curtin LR, and Flegal KM.** Prevalence of overweight and obesity among US children, adolescents, and adults, 1999-2002. Jama 291: 2847-2850, 2004.

54. **Hill B, Ralevic V, Crowe R, and Burnstock G.** Innervation and nitric oxide modulation of mesenteric arteries of the golden hamster. European journal of pharmacology 317: 275-283, 1996.

55. **Ishibashi J, and Seale P.** Medicine. Beige can be slimming. Science 328: 1113-1114, 2010.

56. **Janssen I, Fortier A, Hudson R, and Ross R.** Effects of an energy-restrictive diet with or without exercise on abdominal fat, intermuscular fat, and metabolic risk factors in obese women. Diabetes care 25: 431-438, 2002.

57. **Jocken JW, and Blaak EE.** Catecholamine-induced lipolysis in adipose tissue and skeletal muscle in obesity. Physiology & behavior 94: 219-230, 2008.

58. **Kastin AJ, Redding TW, Hall R, Besser GM, and Schally AV.** Lipid mobilizing hormones of the hypothalamus and pituitary. Pharmacology, biochemistry, and behavior 3: 121-126, 1975.

59. **Lanciego JL, and Wouterlood FG.** A half century of experimental neuroanatomical tracing. Journal of chemical neuroanatomy 42: 157-183, 2011.

60. **Langin D.** Adipose tissue lipolysis as a metabolic pathway to define pharmacological strategies against obesity and the metabolic syndrome. Pharmacological research 53: 482-491, 2006.

61. **Lass A, Zimmermann R, Oberer M, and Zechner R.** Lipolysis - a highly regulated multi-enzyme complex mediates the catabolism of cellular fat stores. Progress in lipid research 50: 14-27, 2011.

62. **Leboeuf B, Flinn RB, and Cahill GF, Jr.** Effect of epinephrine on glucose uptake and glycerol release by adipose tissue in vitro. Proceedings of the Society for Experimental Biology and Medicine Society for Experimental Biology and Medicine 102: 527-529, 1959.

63. **Lee S, Miselis R, and Rivier C.** Anatomical and functional evidence for a neural hypothalamic-testicular pathway that is independent of the pituitary. Endocrinology 143: 4447-4454, 2002.

64. **Lefebvre P.** Glucagon and adipose tissue. Biochemical pharmacology 24: 1261-1266, 1975.

65. **Lefebvre P, Luyckx A, and Bacq ZM.** Effects of denervation on the metabolism and the response to glucagon of white adipose tissue of rats. Hormone and metabolic research = Hormon- und Stoffwechselforschung = Hormones et metabolisme 5: 245-250, 1973.

66. **Lefebvre PJ, and Luyckx AS.** Effect of insulin on glucagon enhanced lipolysis in vitro. Diabetologia 5: 195-197, 1969.

67. **Loewy AD, and Haxhiu MA.** CNS cell groups projecting to pancreatic parasympathetic preganglionic neurons. Brain research 620: 323-330, 1993.

68. **Loncar D, Bedrica L, Mayer J, Cannon B, Nedergaard J, Afzelius BA, and Svajger A.** The effect of intermittent cold treatment on the adipose tissue of the cat. Apparent transformation from white to brown adipose tissue. Journal of ultrastructure and molecular structure research 97: 119-129, 1986.

69. **Lutz TA, and Woods SC.** Overview of animal models of obesity. Current protocols in pharmacology Chapter 5: Unit5 61, 2012.

70. **Manolopoulos KN, Karpe F, and Frayn KN.** Gluteofemoral body fat as a determinant of metabolic health. International journal of obesity 34: 949-959, 2010.

71. **McElroy JF, Mason PW, Hamilton JM, and Wade GN.** Effects of diet and photoperiod on NE turnover and GDP binding in Siberian hamster brown adipose tissue. The American journal of physiology 250: R383-388, 1986.

72. **McQuaid SE, Humphreys SM, Hodson L, Fielding BA, Karpe F, and Frayn KN.** Femoral adipose tissue may accumulate the fat that has been recycled as VLDL and nonesterified fatty acids. Diabetes 59: 2465-2473, 2010.

73. **Minokoshi Y, Saito M, and Shimazu T.** Sympathetic denervation impairs responses of brown adipose tissue to VMH stimulation. The American journal of physiology 251: R1005-1008, 1986.

74. **Monge-Roffarello B, Labbe SM, Lenglos C, Caron A, Lanfray D, Samson P, and Richard D.** The medial preoptic nucleus as a site of the thermogenic and metabolic actions of melanotan II in male rats. American journal of physiology Regulatory, integrative and comparative physiology 307: R158-166, 2014.

75. **Morrison SF.** RVLM and raphe differentially regulate sympathetic outflows to splanchnic and brown adipose tissue. The American journal of physiology 276: R962-973, 1999.

76. **Morrison SF, and Madden CJ.** Central nervous system regulation of brown adipose tissue. Comprehensive Physiology 4: 1677-1713, 2014.

77. **Murphy KT, Schwartz GJ, Nguyen NL, Mendez JM, Ryu V, and Bartness TJ.** Leptin-sensitive sensory nerves innervate white fat. American journal of physiology Endocrinology and metabolism 304: E1338-1347, 2013.

78. **Nautiyal KM, Dailey M, Brito N, Brito MN, Harris RB, Bartness TJ, and Grill HJ.** Energetic responses to cold temperatures in rats lacking forebrain-caudal brain stem connections. American journal of physiology Regulatory, integrative and comparative physiology 295: R789-798, 2008.

79. **Nguyen DM, and El-Serag HB.** The epidemiology of obesity. Gastroenterology clinics of North America 39: 1-7, 2010.

80. **Niijima A.** Afferent signals from leptin sensors in the white adipose tissue of the epididymis, and their reflex effect in the rat. Journal of the autonomic nervous system 73: 19-25, 1998.

81. **Niijima A.** Reflex effects from leptin sensors in the white adipose tissue of the epididymis to the efferent activity of the sympathetic and vagus nerve in the rat. Neuroscience letters 262: 125-128, 1999.

82. **Nishizawa Y, and Bray GA.** Ventromedial hypothalamic lesions and the mobilization of fatty acids. The Journal of clinical investigation 61: 714-721, 1978.

83. **Ogden CL, Carroll MD, Curtin LR, Lamb MM, and Flegal KM.** Prevalence of high body mass index in US children and adolescents, 2007-2008. Jama 303: 242-249, 2010.

84. **Ogden CL, Carroll MD, Fryar CD, and Flegal KM.** Prevalence of Obesity Among Adults and Youth: United States, 2011-2014. NCHS data brief 1-8, 2015.

85. **Ouellet V, Labbe SM, Blondin DP, Phoenix S, Guerin B, Haman F, Turcotte EE, Richard D, and Carpentier AC.** Brown adipose tissue oxidative metabolism contributes to energy expenditure during acute cold exposure in humans. The Journal of clinical investigation 122: 545-552, 2012.

86. **Pasanisi F, Contaldo F, de Simone G, and Mancini M.** Benefits of sustained moderate weight loss in obesity. Nutrition, metabolism, and cardiovascular diseases : NMCD 11: 401-406, 2001.

87. **Penn DM, Jordan LC, Kelso EW, Davenport JE, and Harris RB**. Effects of central or peripheral leptin administration on norepinephrine turnover in defined fat depots. American journal of physiology Regulatory, integrative and comparative physiology 291: R1613-1621, 2006.

88. **Petrovic N, Walden TB, Shabalina IG, Timmons JA, Cannon B, and Nedergaard J.** Chronic peroxisome proliferator-activated receptor gamma (PPARgamma) activation of epididymally derived white adipocyte cultures reveals a population of thermogenically competent, UCP1-containing adipocytes molecularly distinct from classic brown adipocytes. The Journal of biological chemistry 285: 7153-7164, 2010.

89. **Preitner F, Muzzin P, Revelli JP, Seydoux J, Galitzky J, Berlan M, Lafontan M, and Giacobino JP.** Metabolic response to various beta-adrenoceptor agonists in beta3-adrenoceptor knockout mice: evidence for a new beta-adrenergic receptor in brown adipose tissue. British journal of pharmacology 124: 1684-1688, 1998.

90. **Prigge WF, and Grande F**. Effects of glucagon, epinephrine and insulin on in vitro lipolysis of adipose tissue from mammals and birds. Comparative biochemistry and physiology B, Comparative biochemistry 39: 69-82, 1971.

91. **Rebuffe-Scrive M.** Neuroregulation of adipose tissue: molecular and hormonal mechanisms. Int J Obes 15 Suppl 2: 83-86, 1991.

92. **Rinaman L, Roesch MR, and Card JP.** Retrograde transynaptic pseudorabies virus infection of central autonomic circuits in neonatal rats. Brain research Developmental brain research 114: 207-216, 1999.

93. **Rinaman L, and Schwartz G.** Anterograde transneuronal viral tracing of central viscerosensory pathways in rats. The Journal of neuroscience : the official journal of the Society for Neuroscience 24: 2782-2786, 2004.

94. **Rochon L, and Bukowiecki LJ.** Alterations in adipocyte response to lipolytic hormones during cold acclimation. The American journal of physiology 258: C835-840, 1990.

95. **Rooks CR, Penn DM, Kelso E, Bowers RR, Bartness TJ, and Harris RB.** Sympathetic denervation does not prevent a reduction in fat pad size of rats or mice treated with peripherally administered leptin. American journal of physiology Regulatory, integrative and comparative physiology 289: R92-102, 2005.

96. **Rotto-Percelay DM, Wheeler JG, Osorio FA, Platt KB, and Loewy AD.** Transneuronal labeling of spinal interneurons and sympathetic preganglionic neurons after pseudorabies virus injections in the rat medial gastrocnemius muscle. Brain research 574: 291-306, 1992.

97. **Ryu V, and Bartness TJ.** Short and long sympathetic-sensory feedback loops in white fat. American journal of physiology Regulatory, integrative and comparative physiology 306: R886-900, 2014.

98. **Ryu V, Garretson JT, Liu Y, Vaughan CH, and Bartness TJ.** Brown adipose tissue has sympathetic-sensory feedback circuits. The Journal of neuroscience : the official journal of the Society for Neuroscience 35: 2181-2190, 2015.

99. **Ryu V, Watts AG, Xue B, and Bartness TJ.** Bidirectional crosstalk between the sensory and sympathetic motor systems innervating brown and white adipose tissue in male Siberian hamsters. American journal of physiology Regulatory, integrative and comparative physiology 312: R324-R337, 2017.

100. **Schramm LP, Strack AM, Platt KB, and Loewy AD.** Peripheral and central pathways regulating the kidney: a study using pseudorabies virus. Brain research 616: 251-262, 1993.

101. **Shabalina IG, Petrovic N, de Jong JM, Kalinovich AV, Cannon B, and Nedergaard J.** UCP1 in brite/beige adipose tissue mitochondria is functionally thermogenic. Cell reports 5: 1196-1203, 2013.

102. **Shi H, Bowers RR, and Bartness TJ.** Norepinephrine turnover in brown and white adipose tissue after partial lipectomy. Physiology & behavior 81: 535-542, 2004.

103. **Shi H, Song CK, Giordano A, Cinti S, and Bartness TJ.** Sensory or sympathetic white adipose tissue denervation differentially affects depot growth and cellularity. American journal of physiology Regulatory, integrative and comparative physiology 288: R1028-1037, 2005.

104. **Slavin BG, and Ballard KW.** Morphological studies on the adrenergic innervation of white adipose tissue. The Anatomical record 191: 377-389, 1978.

105. **Smith BN, Banfield BW, Smeraski CA, Wilcox CL, Dudek FE, Enquist LW, and Pickard GE.** Pseudorabies virus expressing enhanced green fluorescent protein: A tool for in vitro electrophysiological analysis of transsynaptically labeled neurons in identified

central nervous system circuits. Proceedings of the National Academy of Sciences of the United States of America 97: 9264-9269, 2000.

106. **Song CK, and Bartness TJ.** CNS sympathetic outflow neurons to white fat that express MEL receptors may mediate seasonal adiposity. American journal of physiology Regulatory, integrative and comparative physiology 281: R666-672, 2001.

107. **Song CK, Enquist LW, and Bartness TJ.** New developments in tracing neural circuits with herpesviruses. Virus research 111: 235-249, 2005.

108. **Song CK, Jackson RM, Harris RB, Richard D, and Bartness TJ.** Melanocortin-4 receptor mRNA is expressed in sympathetic nervous system outflow neurons to white adipose tissue. American journal of physiology Regulatory, integrative and comparative physiology 289: R1467-1476, 2005.

109. **Song CK, Schwartz GJ, and Bartness TJ.** Anterograde transneuronal viral tract tracing reveals central sensory circuits from white adipose tissue. American journal of physiology Regulatory, integrative and comparative physiology 296: R501-511, 2009.

110. **Song CK, Vaughan CH, Keen-Rhinehart E, Harris RB, Richard D, and Bartness TJ.** Melanocortin-4 receptor mRNA expressed in sympathetic outflow neurons to brown adipose tissue: neuroanatomical and functional evidence. American journal of physiology Regulatory, integrative and comparative physiology 295: R417-428, 2008.

111. **Stanley S, Pinto S, Segal J, Perez CA, Viale A, DeFalco J, Cai X, Heisler LK, and Friedman JM.** Identification of neuronal subpopulations that project from hypothalamus to both liver and adipose tissue polysynaptically. Proceedings of the National Academy of Sciences of the United States of America 107: 7024-7029, 2010.

112. **Strack AM, Sawyer WB, Hughes JH, Platt KB, and Loewy AD.** A general pattern of CNS innervation of the sympathetic outflow demonstrated by transneuronal pseudorabies viral infections. Brain research 491: 156-162, 1989.

113. **Takahashi A, and Shimazu T.** Hypothalamic regulation of lipid metabolism in the rat: effect of hypothalamic stimulation on lipolysis. Journal of the autonomic nervous system 4: 195-205, 1981.

114. **Tchkonia T, Thomou T, Zhu Y, Karagiannides I, Pothoulakis C, Jensen MD, and Kirkland JL.** Mechanisms and metabolic implications of regional differences among fat depots. Cell metabolism 17: 644-656, 2013.

115. **Teixeira VL, Antunes-Rodrigues J, and Migliorini RH.** Evidence for centers in the central nervous system that selectively regulate fat mobilization in the rat. Journal of lipid research 14: 672-677, 1973.

116. **Vaill MI, Desai BN, and Harris RB.** Blockade of the cerebral aqueduct in rats provides evidence of antagonistic leptin responses in the forebrain and hindbrain. American journal of physiology Endocrinology and metabolism 306: E414-423, 2014.

117. **Vaughan CH, and Bartness TJ.** Anterograde transneuronal viral tract tracing reveals central sensory circuits from brown fat and sensory denervation alters its thermogenic responses. American journal of physiology Regulatory, integrative and comparative physiology 302: R1049-1058, 2012.

118. **Vaughan CH, Zarebidaki E, Ehlen JC, and Bartness TJ.** Analysis and measurement of the sympathetic and sensory innervation of white and brown adipose tissue. Methods in enzymology 537: 199-225, 2014.

119. **Wajchenberg BL.** Subcutaneous and visceral adipose tissue: their relation to the metabolic syndrome. Endocrine reviews 21: 697-738, 2000.

120. **Wirsen C. Studies in Lipid Mobilization.** Acta physiologica Scandinavica Supplementum SUPPL 252:251-246, 1965.

121. **Young P, Arch JR, and Ashwell M.** Brown adipose tissue in the parametrial fat pad of the mouse. FEBS letters 167: 10-14, 1984.

122. **Youngstrom TG, and Bartness TJ.** Catecholaminergic innervation of white adipose tissue in Siberian hamsters. The American journal of physiology 268: R744-751, 1995.

123. **Youngstrom TG, and Bartness TJ.** White adipose tissue sympathetic nervous system denervation increases fat pad mass and fat cell number. The American journal of physiology 275: R1488-1493, 1998.

124. **Zaborszky L, Wouterlood FG, and Lanciego JL.** Neuroanatomical tract-tracing: molecules, neurons, and systems. Springer Science & Business Media, 2006.

125. **Zaia CT, Gaziri LC, Zaia DA, Delattre E, Dolnikoff MS, and Timo-Iaria C.** Effect of chemical stimulation of the dorsomedial hypothalamic nucleus on blood plasma glucose, triglycerides and free fatty acids in rats. Brain research bulletin 42: 195-198, 1997.